POLYTECHNIC OF TURIN

Master's Degree in MATHEMATICAL ENGINEERING

Politecnico di Torino

EMBL

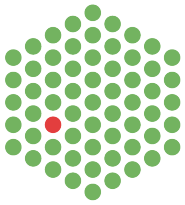

Master's Degree Thesis

Stochastic fluctuations in biophysical models of cell organization

Supervisors

Prof. Lamberto RONDONI

Dr.ssa Anna ERZBERGER

Dr. Roman BELOUSOV

Candidate

Sabrina SAVINO

A.A. 2021/2022

Summary

Self-organization of living systems is a fascinating process, interesting not only to biologists, but also to mathematicians and physicists [1, 2]. For instance, the sorting of a mixture of two types of biological cells, has been modelled by a modified version of the large-Q Potts model [3, 4]—an energy-based biophysical paradigm [5, 6] that, however, had progressed beyond being a mere proof of the concept. As dynamical aspects of this approach still lack a physical justification [7, 8], there is a growing interest in more advanced methods of modeling relevant biophysical processes. Recent developments in the theory of non-equilibrium statistical physics [9] encompass such methods [10]. The present work lays out physical foundations for a reformulated *Cellular Potts Model*, which relies on the modern framework of stochastic kinetics and thermodynamics. Our framework has multiple improvements over the traditional approaches. Among others it provides an immediate physical interpretation of the model parameters for the cell sorting phenomena, in both continuous- and discrete-time paradigms, and enables analysis of the energetics of the involved processes, including the frenetic and entropic thermodynamic properties. To test our approach we first compare its performance with the traditional *Monte-Carlo* sampling algorithm, using the paradigmatic example of the Ising chain. In this context, the framework offers a finer control over the frenetic properties of the system [9]. Finally, the approach is applied to construct a *Cellular Potts Model* for the spatial segregation between the *primitive endoderm* (PrE) and the *epiblast* (EPI) cells [11] in mouse embryogenesis.

Acknowledgements

My period at EMBL has been one of the most valuable and decisive time of my life. For this reason, I would firstly like to thank Lamberto Rondoni for giving me the opportunity to choose this project and for being such a wonderful professor, that really takes care about his students. Of course, a sincere *-thank you-* goes to Anna Erzberger and Roman Belousov for having been professionals tutors from which I have learnt a lot, as well as from all the members of the Erzberger group.

My time in Heidelberg would have not been that great without all the people I have met there; my roommates, for the funny shared dinners at the end of the day, Nikhil for being so excited by anything in life and Martin, of course, always up for a cheap weekend trip (− *who cares? There is the 9€ tickets* −) and his support and positivity.

I cannot not mention my friends from Turin. Francesca, who has shared with me these long years of university and also the months in Germany (fate wanted us to be together there too). Martina, most a friend than a roommate and all the people I met at the *Collegio Einaudi*, especially Tommaso, Roxana, Elia and Federica, who came to Heidelberg too (shall I remebeber how to share a bed in three? −*just,... let's get horizontally*−).

Of course, the −*Mexico team* − especially Pao, Ornella and Ludovica. Thank you for sharing with me one of the most exciting life experience I have ever had (−*collectivos*?− −*Let's go! It's just 20 minutes walking!*−).

Thanks sister, for bringing art and music to the sad coding days. But, especially, thank you mum, thank you dad for not making us miss anything and have supported us in all our life choices. I would not desire better parents.

Thank you all, for letting me be the person I am today.

–Ich hab mein Herz in Heidelberg verloren–

Table of Contents

List of Tables

List of Figures

Acronyms

CPM
Cellular Potts Model

MMC
Metropolis Monte-Carlo algorithm

MMA
Modified Metropolis Monte-Carlo algorithm

DT
Discrete time algorithm

CT
Continuous time algorithm

DCPM
Dynamic Cellular Potts Model

M
Medium

EPI
Epiblast

PrE
Primitive endoderm

Chapter 1

Cellular Potts Models and application in biology

1.1 Mechanical-stimuli in biology

Revealing biochemical and physical mechanisms underlying cell shapes and functions is a fascinating and long-standing problem in biology [12]. Limitations of molecular-biology methods have led researchers to look for additional tools[13]. The information carried by the genome is not sufficient to fully characterize the final cellular organization of tissues or to explain how cells specialize. However, it has been useful in identifying the connection between the cell organization level and the molecular scale. Besides biochemical signals, cells are also sensitive to *mechanical stresses*, arising from the interactions with neighboring cells and the extracellular matrix (ECM). Cells convert mechanical stimuli into an internal molecular signal, a mechanism known as *mechanotransduction* (Figure 1.1), which manifest itself into different processes [14–18]. As well as biochemical cues, mechanical forces affect cytoskeleton organization, which in turn influences cells and tissue functions by acting on a molecular level. Thereby a complex scenario emerges, in which inputs of both chemical and mechanical nature act independently to determine cell shapes and functions: same biochemical components have different effects on cells when the mechanical aspects of their environment are altered.

Exploring the principles governing multi-cellular organization helps to understand better such biological processes as cell development and collective migration [19–21], tumor growths [22, 23]. Mechanical aspects on cellular organization brings the attention to mechanical and material properties of cells, e.g. adhesion, cortical tension, stiffness and viscosity. Experimental measurements of these properties for non-isolated cells in a complex environment of a tissue are quite challenging. These limitations led to formulations of theoretical frameworks which, thus, aim

to reproduce the mechanism of cell organization and motion. Since mechanics acts at the level of cellular interactions, *agent-based models* have turned out to be particularly well-suited for this task. In contrast to continuous models, such discrete approaches treat cells as individual objects interacting with other units, allowing to capture heterogeneities on the interaction itself and differences in cellular properties. Among agent-based models are *lattice models* [24] that have been widely used in tissue mechanics simulations [25–27]. In the following, the attention will focus on a particular class of lattice models—those of which many lattice sites may be occupied by one biological cell—identifying their limitations and possible improvements.

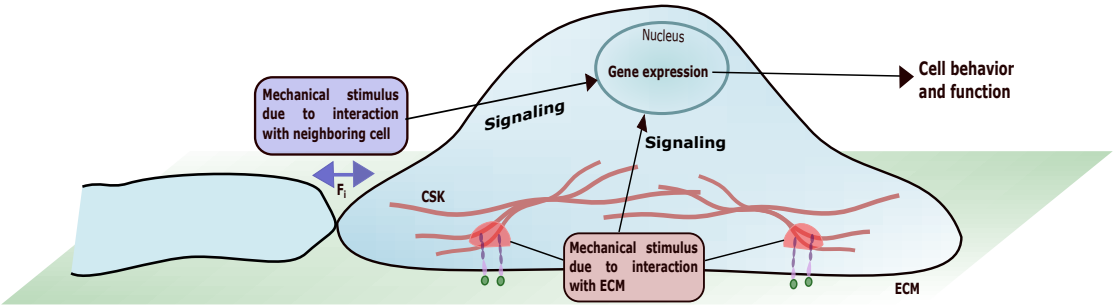

Figure 1.1: *Mechanotransduction scheme.* Mechanical forces deriving from cell-cell and cell-ECM interactions are converted into biochemical cues that act on the molecular-machine signaling of the cell itself. The altered gene expression dictates cellular functions.

1.2 The *Cellular Potts* Model

When cells' shape and size, as well as their contact area, play the key role in determining interactions, models that can accurately reproduce these properties are needed. The *Cellular Potts Model* (CPM) is indeed well-known to fulfill this request [28, 29].

Alternative approaches also exist, among which *vertex models* are worth-mentioning [30, 31]. These *off-lattice* agent-based models identify cell with a polygon, which shares vertices and edges with adjacent cells. Although vertex models are quite successful in simulations of cell-packing geometries [32], approximation of a cell by straight contours makes such a description unsuitable, e.g., for cells on micro-patterns—engineered substrates useful to study the relation between cell shape and function [28, 29].

CPMs can account for arbitrary cell shapes and do not have to neglect the intracellular space (Figure 1.2). This model class has been originally proposed by Glazier and Graner in the context of cell sorting [3], and now it is used to describe a wide range of biological processes [33–39], as well as in medical applications [40–46].

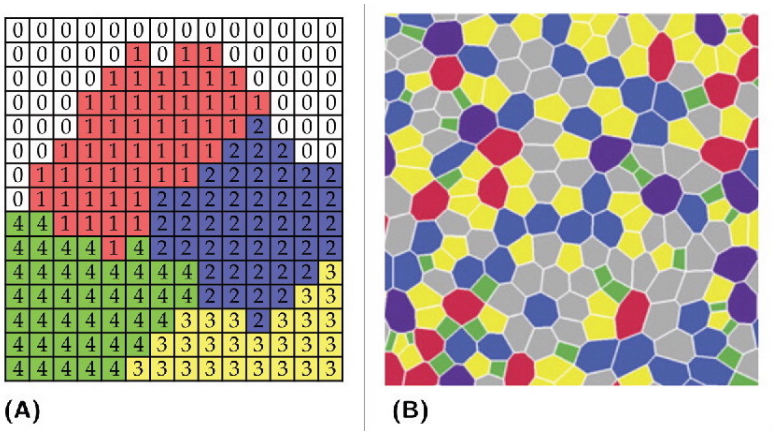

Figure 1.2: *Comparison of Cellular Potts and Vertex model* [47]. (A) Two-dimensional CPM: a set of lattice sites with the same value represents a single cell. (B) Vertex model of a compact tissue: polygons represent individual cell. The model simulate compact tissue organization.

CPMs are energy-based methods, which generalize the Potts model [48]. As a spatial lattice-based formalism, a CPM is characterized by a countable set S representing a discretized space, which is usually a two- or three-dimensional regular lattice with fixed or periodic boundary conditions, and by a set of *cell indices* $\Gamma = \{0, \ldots, n\}$, where n is the total number of cells considered in the simulation. The function $\xi : S \to \Gamma$ assigns at each site $x \in S$ a value $\gamma \in \Gamma$ and a *cell* is identified by a set of all the sites $x \in S$ with the same cell index *i.e.* $cell_\gamma = \{x \in S : \xi(x) = \gamma\}, \gamma \in \Gamma \setminus \{0\}$. The *zero* cell index is assigned to the sites x occupied by the medium—not by any of the cells. The state of the whole system is defined as a configuration $\boldsymbol{\gamma} \in \Gamma^S$. To depict the different mechanical properties of cells and their interactions, the model uses a parameter referred as *cell type* σ. Denoting by $\Lambda \subset \mathbb{N}^0$ the set of all possible cell types, the map $\tau : \Gamma \to \Lambda$ assigns to each cell its type. The value zero of σ indicates the medium, whereas cells with the same value of σ belong to the same type. The model's structure is thus able to represent different cells of the same type (Figure 1.3).

In the context of the CPMs, the concept of a neighbourhood of a given lattice site is of central importance. One should distinguish between its *coupling* and *target* neighborhoods, denoted respectively by N_C and N_T respectively. The first

represents the set of lattice sites involved in the evaluation of the interfacial energy. The value of a given site may only be replaced by one, which is present in the set of sites forming the target neighbourhood. Standard choices of the coupling neighborhood are *Moore* or IV-order neighborhoods, whereas *Moore* neighborhood is the most common choice of the target set (Figure 1.4).

In three-dimension the *Hamiltonian* $H : \Gamma^S \to \mathbb{R}$ has a general form

$$H = \frac{1}{2} \sum_{\substack{x \in S \\ x' \in N_C(x)}} J\Big(\tau(\xi(x)), \tau(\xi(x'))\Big)\Big(1 - \delta_{\xi(x),\xi(x')}\Big) + \sum_{\gamma \in \Gamma} \lambda_{\tau(\gamma)}\Big(V_\gamma(\boldsymbol{\gamma}) - V_{\tau(\gamma)}\Big)^2,$$

$$V_\gamma(\boldsymbol{\gamma}) = \sum_{x \in S} \delta(\gamma, \xi(x)), \quad \boldsymbol{\gamma} \in \Gamma^S \tag{1.1}$$

which accounts for both the intracellular interactions and the preferred shape of a single cell. The first term describes the surface energy, e.g. cell-cell and cell-ECM adhesion, through a symmetric coefficient $J : \Lambda \text{ x } \Lambda \to \mathbb{R}$. According to the Steinberg's *differential adhesion hypothesis* [49] difference of energy costs per interface area between two cells gives rise to their sorting. The second term of the Hamiltonian is a *volume constraint* which only depends on the cell-type, through the target volume and the penalty coefficient $\lambda_{\tau(\gamma)}$ (volume elasticity). In two dimensions the volume constraint is replaced by an *area constraint*.

Formally, a CPM is a discrete-time Markov chain with the state space Γ^S, where the transition probabilities are specified with the help of the Hamiltonian, the target neighbourhood and the temperature parameter; each lattice site is authorized to change its index only into the value of a site belonging to the set of its neighbours, with a Monte Carlo probability. Such constraint aims to avoid the presence of value sites different from the ones belonging to the target neighbourhood, favouring the simulation of compact aggregate patterns and finally defining a modified version of the Metropolis algorithm (MMA, Algorithm 1) of which unit of time is a *Monte Carlo step*, that generally correspond to a number of trial lattice updates, usually equal to the total number of lattice sites.

The CPM interprets patterns present at the tissue level as a result of interactions at cellular level, accounting for a description at different spatio-temporal scales. Cells' shape is determined by respecting the volume constrains, while cells' motility is intrinsic in the modified Monte Carlo Algorithm: at each step, a cell can acquire or lose a lattice site, resulting in a shift of its center of mass and such displacement represents the movement of the cell. A more realistic picture might be achieved by taking into account non-equilibrium phenomena such as cell *death, division* and *growth*, not present in the original formulation of the CPM [3]. A possible approach for including these natural processes in the model, is to consider them as stochastic jump-processes. As described in chapter 4, growth is modeled by updating the

target volume of the cell at each time step, while the division occurs when the volume of the cell reach a pre-determined *division volume*. Death of the cell is usually modeled by setting a *death probability* and sampling a value from a uniform distribution; if the latter is lower than the death probability, the simulation will kill the cell. An example simulation involving non-equilibrium processes is shown in Figure 1.5.

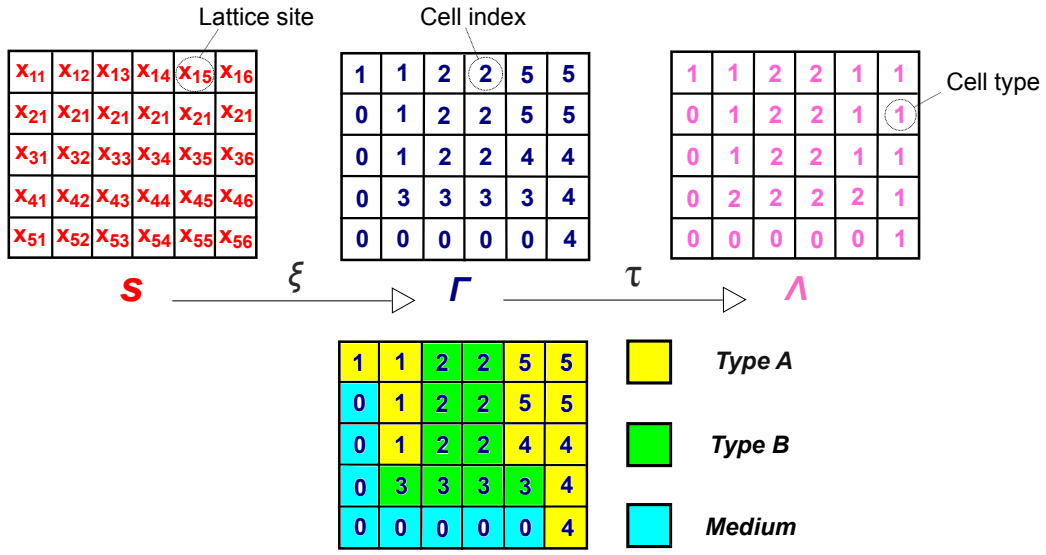

Figure 1.3: *Space representation of 2D CPM.* Five cells with cell indices 1, 2, 3, 4 and 5. Cells 1, 4 and 5 are of type A (yellow). Cells 2 and 3 are of type B (green). Cells with index and type equal zero are assigned to the medium sites.

Algorithm 1 Monte Carlo Modified Algorithm (MMA)

1: Select at random a lattice site x with uniform distribution on S
2: Select at random a lattice site x' with uniform distribution in $N_T(x)$
3: Evaluate the energy difference $\Delta H = H(\xi_x^{x'}) - H(\xi(x)) = H(\xi(x')) - H(\xi(x))$
4: Accept the transition with probability $p(\Delta H) = \min(1, \mathrm{e}^{-\Delta H/T})$
5: Increment the number of copy attempts
6: **if** number of copy attempts $\neq$ number of lattice sites go to step (1) **else** increment time step and repeat.

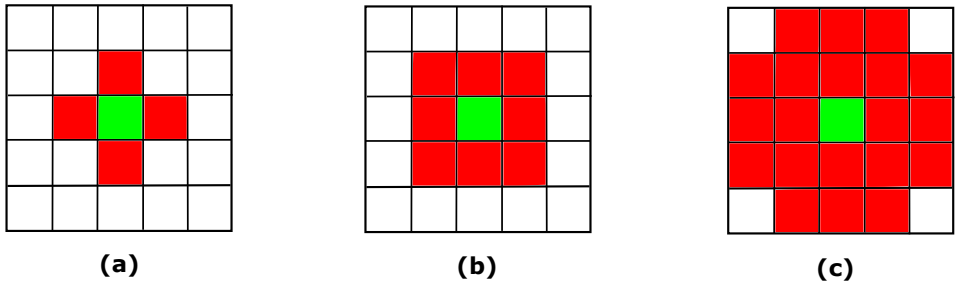

Figure 1.4: *Illustration of neighborhood.* (a) order I or Von Neumann; (b) order II or Moore; (c) order IV.

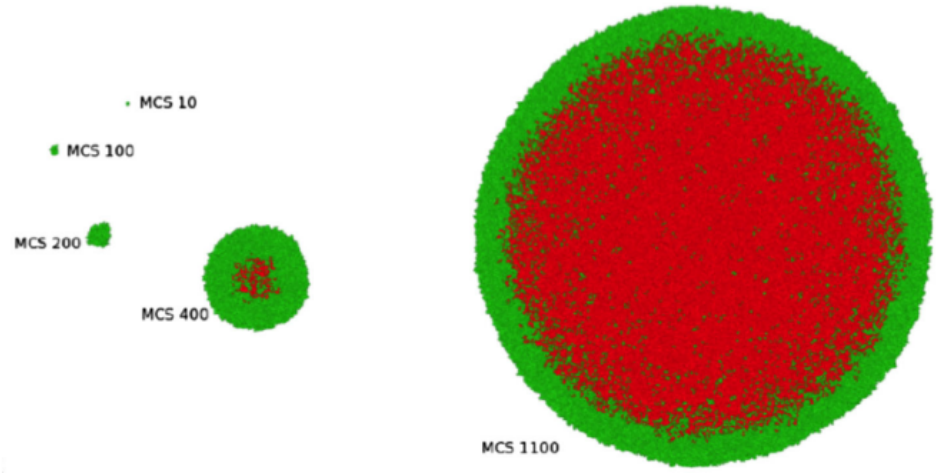

Figure 1.5: Simulation of the CPM with growth, division and death [50].

1.2.1 Limitations of the *Cellular Potts Model*

Cellular Potts Models, despite their success in reproducing geometry and dynamics of cell shapes, have been criticized for the lack of interpretation of the model parameters in terms of commonly used biological and physical quantities[51]. Though the *target volume* which depends on the cell type can be inferred from experiments, as well as the *division volume*, the quantities $J_{\tau[\xi(x)],\tau[\xi(x')]}$, $\lambda_{\tau(\gamma)}$ and the temperature T present some issues. Although the *surface energy* coefficient $J_{\tau(\xi(x)),\tau(\xi(x'))}$ resembles intracellular interactions, its value is quite challenging to determine. Furthermore, such a value is homogeneous over the whole perimeter of a cell and, thus, it neglects variations of adhesion which might be present along the cell's membrane. Instead, the *penalty coefficient* resembles cells' elasticity, indeed in the Hamiltonian defines the impact of the volume or surface constrains. However, it is generally treated as a static parameter during the simulation, which it is not very realistic since biological elements adapt their properties in response to internal and external stimuli. The temperature T is a merely technical parameter, related the membrane fluctuations [52]. A rigorous protocol to adjust the model parameters is not present yet and their values can only be determined by intuitions and experiences of the modeler.

Because motion of a cell in CPMs emerges as the displacement of the center of mass through volume expansion and contraction, such an approach cannot describe dynamics of incompressible, but flexible cells. Indeed, it has been shown that in the case of $\lambda_{\tau(\gamma)} \to \infty$ the simulation freezes when the cells acquire their target volume. The energy penalty of a volume change then blocks any further progress.

Also the choice of the *target neighborhood* have not negligible effects on the realism of the model. Usually, the set is chosen as a Moore neighborhood, while in reality cells present a substantial number of neighbours, thus the simplification adopted distorts the time scale of the interactions phenomena.
One of the major CPM's issue is the violation of the detailed balance condition not only with respect to the Gibbs measure, but any measure due to the modified Metropolis method [53]. Intuitively, the MMA has been defined with the purpose to avoid the *spontaneous nucleation*, an effect where a site assumes a value different from the ones of its neighbours. Thereby, when evaluating the probabilities of a site to change its value to ones of its neighbors, such probabilities are weighted according to the number of sites that have the same value. This also mean that a cell covering only one site has non-zero probability to disappear during a transition and zero probability to reappear (Figure 1.6). Therefore, the Markov Chain underlying the modified algorithm presents absorbing states (characterized by all lattice sites having same type/cell-index *i.e.* only one cell covering the whole lattice) where the chain will be trapped in the long-time behavior (Appendix A). Imposing a condition on which values a lattice site may change to, influences the impact of

the Hamiltonian in the transition itself; besides the Hamiltonian, also the set of neighbours of a lattice site controls the model kinetics. Although the model fixes the target neighbourhood a priori, the chosen site x' to which the current site x is going to change to, it is unpredictable. The topology of cells on the lattice uncontrollably changes over the simulation steps and such a property influences the transition probabilities, as well does the Hamiltonian of which structure and parameters are instead set by the modeler. It emerges a conflict between a controlled and an uncontrolled term affecting the CPM's dynamic, which becomes extreme in the long-time run, where the unpredictable part wins over the Hamiltonian role [53]. In the case of high temperature, $T \to \infty$ the influence of the Hamiltonian vanishes completely and the lattice sites are continuously replaced by the value of a random chosen neighbour, while in a standard Metropolis algorithm the evolution of one lattice site becomes independent from the other ones. As a consequence, in this regime, the connectivity of the cells is not guaranteed and *fragments* may appear: small portions of the lattice (usually a single lattice site) detach from the original cell, acquiring an index/type value of a random nearby cell (Figure 1.7). Besides being unrealistic, these fragmentation events overestimate the number of cell's boundaries, complicating the evaluation of the interfacial energies, fact that slow down the simulation and set a limit on the maximum simulation temperature, lowering the overall performances of the algorithm itself. Computational issues are also present in three-dimensional framework where the maximum number of simulation cells is around 10^5 when, in order to properly simulate morphogenetic processes, are usually needed $10^6 - 10^8$ cells [54].

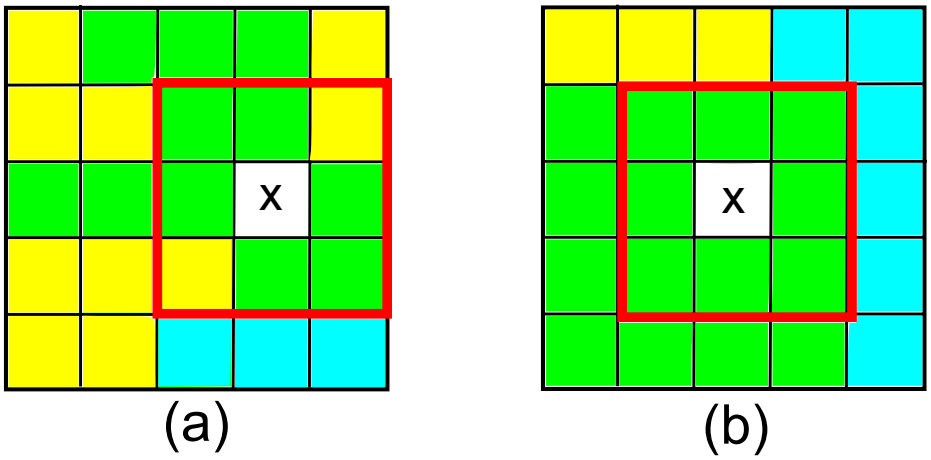

Figure 1.6: *Detailed balance in CPM.* Two cell types (yellow and green) and medium (light blue). The target neighborhood N_T is of order II (Moore).
(a) Detailed balance is not respected: $\mathbb{P}(x : y \to g) = \frac{6}{8N} \neq \mathbb{P}(x : g \to y) = \frac{2}{8N}$
(b) Spontaneous nucleation is forbidden: $\mathbb{P}(x : y \to g) = \frac{8}{8N} \neq \mathbb{P}(x : g \to y) = \frac{0}{8N}$

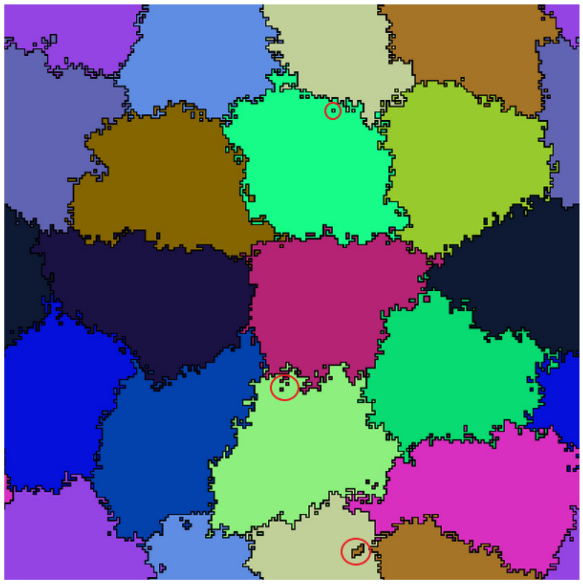

Figure 1.7: *Fragments* [55]. Red circles highlight some of the fragments present in the simulation.

From a mechanical point of view, a further limitation of the model is the impossibility of controlling the properties of a cell (cell motility, shape flexibility, intercellular adhesion etc.) individually, since the assumption of the CPM relies on the idea that such cellular characteristics are embedded in the cells' surface fluctuations, dependent on the simulation temperature T which indeed simulates membrane fluctuations caused by cell activity [52]. Moreover, the original Hamiltonian includes only static properties of the cell, thus to incorporate some dynamical characteristics it can be possible to either add new terms in the expression of the Hamiltonian or act on the acceptance rates *(kinetic approaches)*.

A schematic representation of CPM's pro and cons is shown below.

+ Each cell is an individual object
+ Bound and unbound regions of the cell membrane is distinct
+ Cell shape is realistically represented
+ Cell motility is incorporated
+ Flexibility of the model which can be easily extended. Non-equilibrium phenomena can be included

- Lack of physical and biological meaning of the model parameters. Difficulty on properly fit them
- Impossibility to simulate incompressible but flexible cell
- Detailed balance condition is not respected
- Fragments are possible
- Properties of the cell are static and it is not possible to control them individually

1.2.2 Modified versions of the *Cellular Potts Model*

Thanks to its high flexibility, the *Cellular Potts Model* has been subjected to a wide range of modifications and extensions. For instance, if one succeeds to express a given biological process in form of a generalized potential, a straightforward procedure consists of just adding this term (denoted by $H_{process}$) to the standard Hamiltonian, which then takes the expression of Equation 1.2.

$$\begin{aligned} H &= H_{adhesion} + H_{volume} + H_{process} \\ H_{adhesion} &= \frac{1}{2} \sum_{\substack{x \in S \\ x' \in N_C(x)}} J\Big(\tau(\xi(x)), \tau(\xi(x'))\Big)\Big(1 - \delta_{\xi(x),\xi(x')}\Big) \\ H_{volume} &= \sum_{\gamma \in \Gamma} \lambda_{\tau(\gamma)}\Big(V_\gamma(\boldsymbol{\gamma}) - V_{\tau(\gamma)}\Big)^2 \end{aligned} \tag{1.2}$$

One of the most common modification of the CPM's Hamiltonian provides that the additional term is related to the *chemotaxis*, phenomenon of crucial importance in the long-range signaling during morphogenesis [56]. Therefore, in this case, the addend $H_{process}$ will coincide with

$$H_{chemotaxis} = \sum_{\gamma \in \Gamma \setminus \{0\}} \sum_{x \in \text{cell}_\gamma} \lambda_{chemotaxis}(\gamma) c(x)$$

where $c : S \to [0, \infty)$ is interpreted as the chemical potential, while $\lambda_{chemotaxis}(\gamma)$ as the chemotactic response parameter of the cell, which may depend on its type. Another way of integrating chemotaxis in the model is using a *kinetic* approach as it is done in [57].

Biological phenomena are physically interpreted as *multi-scale* processes since they act in mainly three different temporal and spatial scales: molecular or subcellular (microscopic), cellular (mesoscopic) and at tissue level (macroscopic). The CPM works on the mesoscopic scale, interpreting the cell as a spatially extended but internally structureless object. In this way any intrinsic inhomogeneities of the cell and information about the molecular-level processes influencing its behavior and morphology, are lost. Therefore, it arises the need of new frameworks able to capture the different biological scales [58–60]. Models that integrate the standard CPM description with a microscopic one have been developed by using, for example, a *compartmentalization* technique according to which parts of the CPM unit objects are reasonably organized in clusters representing cell subunits like nucleus, cytosol, organelles etc. [5, 61].
Furthermore, the CPM suffers for a limitation on the total number of simulation

cells and the high computational cost of simulating three-dimensional lattices. The sequential algorithm has thus been substituted by different parallelized approaches that improve the performances at three-dimensional scale and increase the total number of possible simulation cells [62–67].
The unrealistic formation of *fragments* inside a cell of the CPM, has been addressed through the so-called *connectivity algorithm* (CA, [55]) which modifies further the MMA (Algorithm 1). The fragments break the *connectivity* of the cell *i.e.* they break the *path* that links every couple of lattice sites belonging to a cell, where a path is a list of lattice sites having same value and each of which is a neighbour of the preceding one. Thereby, an algorithm that aims to forbid cells' fragmentation, before changing cell site's value, has to check the connectivity of the two cells involved at each simulation step *i.e.* the cell of which a site value might change and the cell that provide the alternative value. However, verifying the existence of a path for every couple of cells' lattice sites is computational expensive, thus a new notion of connectivity to be checked, might be useful. The CA algorithm defines the *local connectivity* on a *connected domain* $D_c(x)$, because it has been proven that if the initial configuration is connected, the test of such local connectivity will ensure cells' connectivity during the simulation. By introducing the concept of *adjacency neighborhood* N_A as the list of different site values that are neighbours of a given cell's lattice site, it is possible to define the connected domain $D_c(x)$ as the set of lattice sites containing the adjacency neighborhood of x, but not x itself. Therefore, the local connectivity at site x^* manifests itself if all the cell sites belonging to the adjacency neighborhood of x^* are connected through paths included in $D_c(x^*)$. The choices of $D_c(x)$, N_A and N_T are of crucial importance for the performances of the algorithm. The adjacency neighborhood N_A is set to be as small as possible (usually *Von Neumann*) to not overestimate the number of different values around a site, while the target neighbourhood verifies the condition $N_T \subseteq N_A$ so that detailed balance is restored (Figure 1.8). The most common choice is to take N_T coinciding with N_A, while the typical choice of the *connectivity domain* is defining it as a domain containing the lattice sites of the adjacency neighborhood N_A plus the shortest paths that connect them. The connectivity algorithm can be then formalized as in Algorithm 2.

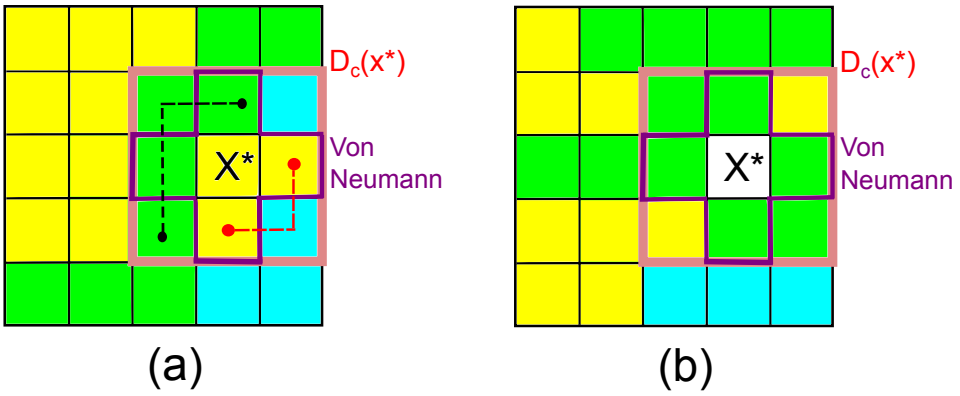

Figure 1.8: *Illustration of CA.* The neighborhood of site x^* is Von Neumann (purple contour) and the connectivity domain $D_c(x^*)$ is Moore (pink contour). (a) Local Connectivity: the green cell in $D_c(x^*)$ respects local connectivity (black path) while the yellow cell does not (red path). (b) Detailed balance: given the Von Neumann target neighborhood, the possible value type are yellow and green *i.e.* $N_A = \{yellow,\ green\}$. The choice $N_T \equiv N_A$ ensures $\mathbb{P}(x^* : y \to g) = \mathbb{P}(x^* : g \to y) = \frac{1}{2N}$

Algorithm 2 Connectivity Algorithm (CA)

1: Select at random a lattice site x with uniform distribution on S
2: Select at random a lattice site x' with uniform distribution in $N_T(c)$
3: Check the local connectivity at x on $D_c(x)$
4: Check the local connectivity at x' on $D_c(x')$
5: Evaluate the energy difference $\Delta H = H(\xi_x^{x'}) - H(\xi(x)) = H(\xi(x')) - H(\xi(x))$
6: Accept the transition with probability $p(\Delta H) = \min(1, \mathrm{e}^{-\Delta H/T})$
7: Increment the number of copy attempts
8: **if** number of copy attempts $\neq$ number of lattice sites go to step (1) **else** increment time step and repeat.

The *Cellular Potts Model* does not allow to treat single cell's property individually since they are all interpreted in terms of surface fluctuations which depends on temperature. However, one of the main feature characterizing various biological processes is the *cellular motility* [68, 69] which generally depends on other mechanisms and parameters, rather than temperature [70]. In the CPM, the motility is interpreted as the sequential movement of the cells' center of mass and such dynamic is intrinsic in the expression of the probability computed in the modified metropolis algorithm which depends on energy difference and the temperature. The latter formulation does not give any insights for a rigorous mechanical construction of the CPM, thus it emerges a substantial need to model better the motion of cells. One attempt has been made and it consists on adding an Hamiltonian term related to the inertia of the cells [54]. However, the resistance to motion that cells experience when moving through a fluid, due to dissipation and viscosity, needs to be described more realistically. Furthermore, living matter is a composite material made of a combination of materials with different physical and chemical properties, thus a theoretical formulation also capable of taking track of such heterogeneities will be useful. In the following contents it will be presented a *kinetic framework* that tries to satisfy these needs. First, the approach is introduced on a paradigmatic case of the Ising spin-dynamic, then it will be extended at the Cellular Potts Model.

Chapter 2

A paradigmatic example

The CPM is a generalization of the Potts Model and the Ising model is a particular case of the latter. Therefore, on the following sections, the basis of the kinetic framework, subject of this work, will be introduced in the case of the one-dimensional Ising model.

2.1 The *Ising Model*

The *Ising model* was originally formulated for studying the phenomenon of *spontaneous magnetization*, occurring at a certain *critical temperature* T_c in ferromagnetic systems. If a magnetic material is held at a constant temperature and it is placed in a magnetic field, the latter will create a tendency for the magnetic moments of the material to point in its same direction. If the external field is slowly turned off, the behavior of the magnetic material is different according to the temperatures it is kept; for high temperatures the material is in an unmagnetized condition, while for low temperatures the material retains a degree of magnetism. Thus, there exist a critical temperature at which the system is subject to a phase transition *i.e.* at which the spontaneous magnetization occurs. The interest of the Ising model relies indeed in the explanation of such phase transitions: the study of the mechanism according to which short-range interactions between molecules (elementary units of the model) propagate over the long-range will give insights on the prediction of the phase transition. Physical-chemical and biophysical systems can be formalized by a lattice arrangements of molecules, with interactions on a small and defined range. Therefore, the Ising model represents the simplest theory to study such large systems where cooperative behavior occurs. These extensions to different fields than the physics of ferromagnetism are possible thanks to the mathematical formulation characterizing the Ising model, as well as its generalizations.

The lattice is usually in one, two or three d dimension (Figure 2.1), where each

line segment connects two lattices, thus called *nearest neighbors*. Each lattice site not at the boundary has $2d$ neighbors, but periodic boundary conditions are usually adopted so that differences between lattice sites at boundary and those which are not, do not longer exist. At each lattice site i is assigned a variable assuming only two values $\sigma_i = \pm 1$, commonly called *states*. In the model of ferromagnetism the values ± 1 indicate if the spin points *"up"* or *"down"*, but this couple of values can be used in any model where its variables can assume only two possible states.
Given the configuration $\boldsymbol{\sigma} = (\sigma_1, \sigma_2, ..., \sigma_N)$, the total energy of the system is the *Hamiltonian* in Equation 2.1, where h is the external field and $J_{i,j}$ is a coefficient weighting the interaction between spin i and spin j. If each coefficient $J_{i,j}$ is positive for all the couples (i, j), the preferred configuration is that of spins having parallel moments (*ferromagnetic*), while anti-parallel configurations (*antiferromagnetic*) are favoured if the coupling coefficients are negative.

$$H = H(\boldsymbol{\sigma}) = -h \sum_{i}^{N} \sigma_{i=1} - \sum_{(i,j)} J_{i,j} \sigma_i \sigma_j \tag{2.1}$$

The focus will be on the case of a one-dimensional lattice, imposing periodic boundary conditions so that the lattice will form a ring. Usually the *Hamiltonian* of such system is given by the relation:

$$H = H(\boldsymbol{\sigma}) = -h \sum_{i=1}^{N} \sigma_i - \sum_{i=1}^{N} J_{i,j} \sigma_i \sigma_{i+1}, \quad \sigma_{N+1} = \sigma_1 \tag{2.2}$$

Denoting by N the number of spins in the lattice, the total number of configurations is 2^N and the *partition function* Z is given by summing the exponential of the Hamiltonian over all the possible configurations:

$$Z = \sum_{\boldsymbol{\sigma}} \mathrm{e}^{-\frac{H(\boldsymbol{\sigma})}{k_B T}} = \sum_{\boldsymbol{\sigma}} \mathrm{e}^{-\beta H(\boldsymbol{\sigma})}$$

The probability that the system at equilibrium will be in a particular configuration $\boldsymbol{\sigma}^*$, is given by the *Gibbs* measure:

$$\mathbb{P}(\boldsymbol{\sigma}^*) = \frac{\mathrm{e}^{-\beta H(\boldsymbol{\sigma}^*)}}{Z} \tag{2.3}$$

The average magnetization of the system, when it is in the configuration $\boldsymbol{\sigma}$, is given by

$$M(\boldsymbol{\sigma}) = \frac{1}{N} \sum_{i}^{N} \sigma_i \tag{2.4}$$

and by rewriting it as

$$M = -\frac{1}{N}\frac{\partial F}{\partial h}$$

where $F = -k_B T ln Z$ is the *Helmotz free energy*, one can show that the Ising model in one-dimension fails to predict the spontaneous magnetization (Appendix B). However, it has been proven that the model in higher dimensions shows a phase transition [71–74] and that, the behaviour of physical quantities (such as magnetization density) near phase transition are described by power low with *critical exponents* that are considered universal *i.e.* dependent only on general features of the system, like the lattice dimension and the range of interactions, where the latter is consider to be at the *nearest neighbours* level in the Ising model. Furthermore, for dimension $d > 2$ analytical results for the determination of the critical exponents are provided by the *mean field theory* (MFT) and the *renormalization group* (RF) framework [75, 76].

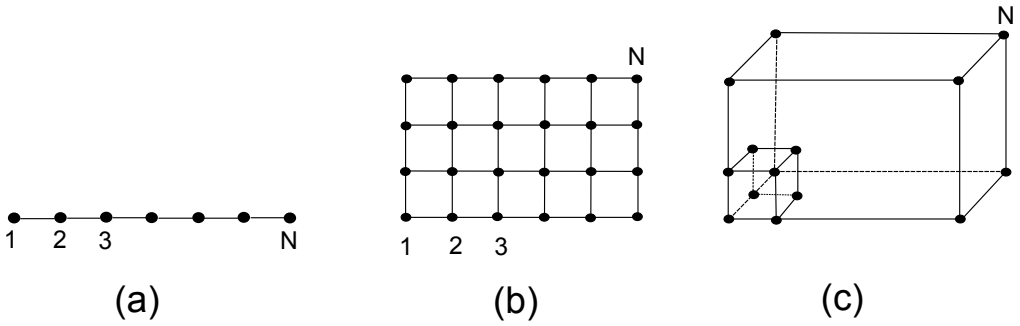

Figure 2.1: *Lattice models.* (a) One-dimensional lattice where repeating units are point and lines. (b) Two-dimensional lattice where the units are squares.
(c) Three-dimensional lattice whose repeating units are cubes.

2.2 Microscopic Stochastic Kinetics

In the context of phase transitions, there exist an interesting class of problems studying the dynamical evolution of a system subject to a rapid change of some of its parameters; the system will go from an initial equilibrium state to a final equilibrium state on a certain timescale, but the knowledge about the dynamic of these relaxation process (through non-equilibrium states) is still of main interest. These problems are categorized under the framework of the *kinetic of phase transitions* and, since the Ising models were initially formulated with the purpose of studying phase transitions, one can define the so-called *kinetics Ising models*. Phase transitions

are ubiquitous in biology [77–80] and in such field of research it has been done a wide use of Ising models and its generalization. The Ising spin variables do not have any intrinsic dynamic, thus there is a significant freedom in formulating the kinetic rules of such systems. For instance, the *"spin-change"* events can occur one at the time or in correlated blocks, a spin may flip its value (*Glauber dynamic*) or exchange its position with a neighbouring one (*Kawasaki dynamic*) as shown in Figure 2.2. In the following section, the focus will be on the *single spin-flip dynamic* in the case of the one dimensional Ising model, even tough it is know that the latter does not show phase transition. The interest is to compare the already formulated *Glauber* dynamic with a new one following different kinetics rules and that will be applied in the context of the *Cellular Potts Model*.

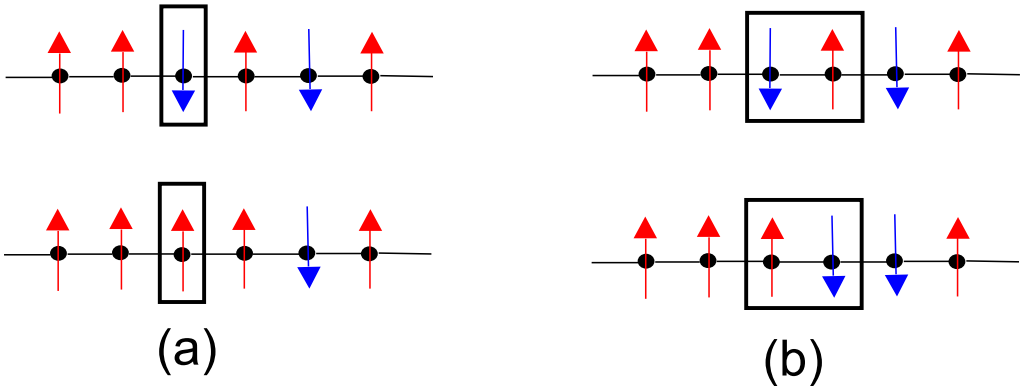

Figure 2.2: *Kinetics Ising models.* (a) Glauber dynamic: one spin flips at the time. (b) Kawasaki dynamic: two spins exchange their position

The *Glauber dynamic* assumes that each spin of the chain can randomly change its value due to the interactions with neighbouring spins and an heat bath at a certain temperature. Thus, the spin particles may be represented as stochastic functions $\sigma_i(t)$, $i = 1, \dots, N$ restricted between ± 1 and the random transitions between these two values happen at a certain rate $w_i(\sigma_i)$. Denoting by $\boldsymbol{\sigma}$ the configuration of the Ising chain at time t and considering that only one spin can flip at the time, the configuration may change from the one of type $\boldsymbol{\sigma} = (\sigma_1, \dots, \sigma_i, \cdots, \sigma_N)$ to $\boldsymbol{\sigma}_{-i} = (\sigma_1, \dots, -\sigma_i, \cdots, \sigma_N)$ and one can study the time evolution of the probability function $\mathbb{P}(\boldsymbol{\sigma}, t)$ which express the probability of being in configuration $\boldsymbol{\sigma}$ at time t. Since the total number of possible configuration is 2^N, there will be 2^N probability functions. The model is describing a Markov process where the states are given by configurations with a spin value different from the previous one and the transition between one state to another happens with rate of the spin that flips. Thus, we

can write the following *master equation*:

$$\frac{d}{dt}\mathbb{P}(\boldsymbol{\sigma},t) = \sum_i r_i(\sigma_i)\mathbb{P}(\boldsymbol{\sigma}_i,t) - \sum_i r_i(\sigma_{-i})\mathbb{P}(\boldsymbol{\sigma}_{-i},t) \tag{2.5}$$

which expresses the fact that any configuration $\boldsymbol{\sigma}$ can be destroyed by a flip of any of its spin, but it can be created by the flip of any spins in the configuration $\boldsymbol{\sigma}_{-i}$. At equilibrium, a stationary distribution is reached and one may write

$$\frac{d}{dt}\mathbb{P}(\boldsymbol{\sigma},t) = 0 = \sum_i r_i(\sigma_i)\mathbb{P}(\boldsymbol{\sigma}_i,t) - \sum_i r_i(-\sigma_i)\mathbb{P}(\boldsymbol{\sigma}_{-i},t)$$

from where, the *detailed balance condition* can be derived:

$$r_i(\sigma_i)\mathbb{P}(\boldsymbol{\sigma}_i,t) = r_i(-\sigma_i)\mathbb{P}(\boldsymbol{\sigma}_{-i},t) \tag{2.6}$$

Since at equilibrium, the probability of being in a certain configuration is given by Equation 2.3 one can write:

$$\begin{aligned} \frac{r_i(\sigma_i)}{r_i(-\sigma_i)} &= \frac{\mathbb{P}(\boldsymbol{\sigma}_{-i},t)}{\mathbb{P}(\boldsymbol{\sigma}_i,t)} = \\ &= \frac{\mathrm{e}^{-\beta H(\boldsymbol{\sigma}_{-i})}}{\mathrm{e}^{-\beta H(\boldsymbol{\sigma})}} = \mathrm{e}^{-\beta\left[H(\boldsymbol{\sigma}_{-i})-H(\boldsymbol{\sigma})\right]} = \mathrm{e}^{-\beta\Delta H(\sigma_i)} \\ \Rightarrow \frac{r_i(\sigma_i)}{r_i(-\sigma_i)} &= \mathrm{e}^{-\beta\Delta H(\sigma_i)} \end{aligned} \tag{2.7}$$

where $\Delta H(\sigma_i)$ is the difference on the Hamiltonian when only the spin i^{th} flips and it is equal to

$$\Delta H(\sigma_i) = 2\sigma_i[h + J_{i-1,i}\sigma_{i-1} + J_{i,i+1}\sigma_{i,i+1}]$$

If $J_{i-1,i} = J_{i,i+1} = J$ then

$$\Delta H(\sigma_i) = 2\sigma_i[h + J(\sigma_{i-1} + \sigma_{i+1})]$$

One may notice that the ratio of the transition rates solely depends on the difference of the energy, according with the fact that the kinetics has been formulated considering only the interactions between nearby spins and the heat bath, information stored in the Hamiltonian. It is also possible to find an explicit form of the transition rates as following, where by semplicity it has been considered $J_{i-1,i} = J_{i,i+1} = J$:

$$\begin{aligned}
\frac{r_i(\sigma_i)}{r_i(-\sigma_i)} &= \frac{\mathrm{e}^{-\beta H(\boldsymbol{\sigma}_{-i})}}{\mathrm{e}^{-\beta H(\boldsymbol{\sigma})}} = \frac{\mathrm{e}^{\beta\sigma_i[h+J(\sigma_{i-1}+\sigma_{i+1})]}}{\mathrm{e}^{-\beta\sigma_i[h+J(\sigma_{i-1}+\sigma_{i+1})]}}\frac{2}{2} = \\
&= \frac{(1+\sigma_i)\mathrm{e}^{-\beta[h+J(\sigma_{i-1}+\sigma_{i+1})]} + (1-\sigma_i)\mathrm{e}^{\beta[h+J(\sigma_{i-1}+\sigma_{i+1})]}}{(1+\sigma_i)\mathrm{e}^{\beta[h+J(\sigma_{i-1}+\sigma_{i+1})]} + (1-\sigma_i)\mathrm{e}^{-\beta[h+J(\sigma_{i-1}+\sigma_{i+1})]}} = \\
&= \frac{2\cosh\Big(\beta[h+J(\sigma_{i-1}+\sigma_{i+1})]\Big) - 2\sigma_i\mathrm{senh}\Big([h+J(\sigma_{i-1}+\sigma_{i+1})]\Big)}{2\cosh\Big(\beta[h+J(\sigma_{i-1}+\sigma_{i+1})]\Big) + 2\sigma_i\mathrm{senh}\Big([h+J(\sigma_{i-1}+\sigma_{i+1})]\Big)} = \\
&= \frac{1-\sigma_i\tanh\Big(\beta[h+J(\sigma_{i-1}+\sigma_{i+1})]\Big)}{1+\sigma_i\tanh\Big(\beta[h+J(\sigma_{i-1}+\sigma_{i+1})]\Big)} \\
\Rightarrow r_i(\sigma_i) &= \frac{1}{2}\Big\{1-\sigma_i\tanh\Big(\beta[h+J(\sigma_{i-1}+\sigma_{i+1})]\Big)\Big\}
\end{aligned}$$

where the factor two is due to normalization.

Since the dynamical rules can be arbitrarily fixed, one may define an alternative kinetics in which each spin makes an attempt to flip with a certain rate $\alpha_i(\sigma_i)$ that may depend on the value of the spin itself. Once the attempt has been made, the spin can succeed in changing its value or not. Following the same framework of [81], it is possible to express the latter conditional probability in terms of the *directing functions* $L(\pm\sigma_i)$ as:

$$\mathbb{P}(\sigma_i \to -\sigma_i|\text{attempt}) \propto \mathrm{e}^{L(-\sigma_i)} \qquad \mathbb{P}(-\sigma_i \to \sigma_i|\text{attempt}) \propto \mathrm{e}^{L(\sigma_i)}$$

By defining the normalization factor as $Z = \mathrm{e}^{L(\sigma_i)} + \mathrm{e}^{L(-\sigma_i)}$, the probabilities take the form:

$$\begin{aligned}
\mathbb{P}(\sigma_i \to -\sigma_i|\text{attempt}) &= \frac{\mathrm{e}^{L(-\sigma_i)}}{\mathrm{e}^{L(\sigma_i)} + \mathrm{e}^{L(-\sigma_i)}} = \frac{\mathrm{e}^{L(-\sigma_i)}}{\mathrm{e}^{L(\sigma_i)}(1+\mathrm{e}^{L(-\sigma_i)-L(\sigma_i)})} = \\
&= \frac{\mathrm{e}^{\overbrace{L(-\sigma_i)-L(\sigma_i)}^{\Delta L(\sigma_i)}}}{1+\mathrm{e}^{\overbrace{L(-\sigma_i)-L(\sigma_i)}^{\Delta L(\sigma_i)}}} = \frac{\mathrm{e}^{\Delta L(\sigma_i)}}{1+\mathrm{e}^{\Delta L(\sigma_i)}} = \\
&= \frac{w_i}{1+w_i}
\end{aligned} \tag{2.8}$$

and likewise:

$$\mathbb{P}(-\sigma_i \to \sigma_i|\text{attempt}) = \frac{\mathrm{e}^{-\Delta L(\sigma_i)}}{1+\mathrm{e}^{-\Delta L(\sigma_i)}} = \frac{1}{1+w_i} \tag{2.9}$$

The unconditional probabilities of making a flip can thus be written as:

$$\begin{aligned}\mathbb{P}(\sigma_i \to -\sigma_i) = \underbrace{\alpha_i(\sigma_i)dt}_{\substack{\text{probability of}\\ \text{making an}\\ \text{attempt}}} \mathbb{P}(\sigma_i \to -\sigma_i|\text{attempt}) = \\ = \alpha_i(\sigma_i)dt\frac{\mathrm{e}^{L(-\sigma_i)}}{Z} = \alpha_i(\sigma_i)\frac{\mathrm{e}^{\Delta L(\sigma_i)}}{1+\mathrm{e}^{\Delta L(\sigma_i)}}dt = \\ = \alpha_i(\sigma_i)\frac{w_i}{1+w_i}dt\end{aligned} \tag{2.10}$$

and likewise:

$$\begin{aligned}\mathbb{P}(-\sigma_i \to \sigma_i) = \alpha_i(-\sigma_i)dt\mathbb{P}(-\sigma_i \to \sigma_i|\text{attempt}) = \\ = \alpha_i(-\sigma_i)\frac{\mathrm{e}^{-\Delta L(\sigma_i)}}{1+\mathrm{e}^{-\Delta L(\sigma_i)}}dt = \alpha_i(-\sigma_i)\frac{1}{1+w_i}dt\end{aligned} \tag{2.11}$$

where the *escape rates* $\kappa(\pm\sigma_i)$ are:

$$\kappa(\sigma_i) = \alpha_i(\sigma_i)\frac{w_i}{1+w_i}, \qquad \kappa(-\sigma_i) = \alpha_i(-\sigma_i)\frac{1}{1+w_i} \tag{2.12}$$

However, the probabilities introduced are still dependent on the *directing function* which expression can be found considering the system at equilibrium and imposing *detailed balance conditions*, obtaining:

$$\begin{aligned}&\mathbb{P}(\sigma_i)\mathbb{P}(\sigma_i \to -\sigma_i) = \mathbb{P}(-\sigma_i)\mathbb{P}(-\sigma_i \to \sigma_i) \\ &\mathrm{e}^{-\beta H(\sigma_i)}\alpha_i(\sigma_i)dt\mathrm{e}^{L(-\sigma_i)} = \mathrm{e}^{-\beta H(-\sigma_i)}\alpha_i(-\sigma_i)dt\mathrm{e}^{L(\sigma_i)} \\ &\mathrm{e}^{\overbrace{L(-\sigma_i) - L(\sigma_i)}^{\Delta L(\sigma_i)}} = \frac{\alpha_i(-\sigma_i)}{\alpha_i(\sigma_i)}\mathrm{e}^{-\beta[\overbrace{H(-\sigma_i) - H(\sigma_i)}^{\Delta H(\sigma_i)}]} \\ &\Rightarrow \mathrm{e}^{\Delta L(\sigma_i)} = w_i = \frac{\alpha_i(-\sigma_i)}{\alpha_i(\sigma_i)}\mathrm{e}^{-\beta\Delta H(\sigma_i)}\end{aligned} \tag{2.13}$$

At this point, it is possible to find an explicit expression of the equations 2.8-2.12, using Equation 2.13.

2.2.1 *Entropy-Frenesy decomposition* formalism

Microscopic kinetics has been motivated from the need of studying the dynamic of physical systems subject to a statistical description. Since the dynamic is the centre of interest, it turns out to be useful formulating frameworks within *dynamical ensembles i.e.* ensembles in which it is considered the time evolution of the stochastic physical system (Figure 2.3). This kind of formulation is quite interesting when studying non-equilibrium physics in which time-reversability is broken at some level, also considering the fact that such processes are widely spread in biological systems [82, 83]. Historically, the intrinsic irreversibility of a system has been characterized introducing the *entropy production*, a thermodynamic quantity expressing the additional entropy increase due to irreversible processes inside the system. However, nowadays new techniques, as the optical ones [84, 85] have been developed, allowing to acquire non-thermodynamic information like micro-fluctuations [86] or jump events in multilevel system [87]. These new advances in the study of non-equilibrium physics give the right to introduce new theoretical features, not of thermodynamic nature. To this purpose and considering dynamical ensembles, it is possible to develop frameworks in the context of the *Lagrangian statistical mechanics*'s view. Under this prospective, one may make use of the functional *action* A, defined as the integral over a time interval of the Lagrangian and, by imposing the stationary condition of such functional, it is possible to derive the *Euler-Lagrange* equations of motion- which solutions are stationary points of the action functional and represent the trajectories the physical system will follow, from a starting point to a final one. It thus results that the action A assigns a value at each possible path the system might follow in the space-time window. For all the possible paths or trajectories ω characteristic of a stochastic physical system, one can think of weighting them with an action functional made of two components: an anti-symmetric (in time) part which is the total entropy $S(\omega)$ associated to a path, made of all the entropy

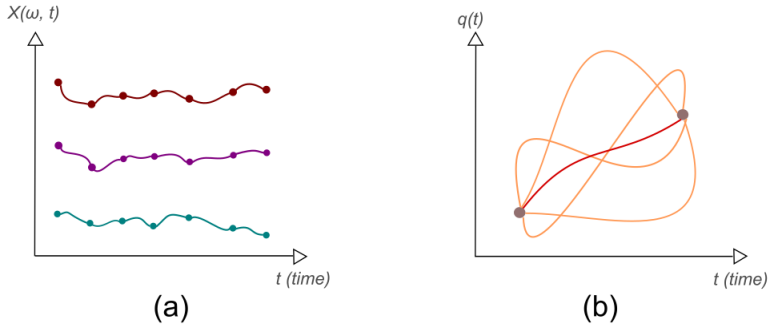

Figure 2.3: (a) *Dynamical ensemble:* possible trajectories of a stochastic process. (b) *Lagrangian mechanics:* all the possible trajectories the system can take between two point in the configuration space. The chosen trajectory (red) is a stationary point of the action.

changes $s(x, y)$ when passing from state x to state y and a time-symmetric part called *frenesy*, a kinetic rather than a thermodynamic quantity [9]. A trajectory is the sequence of states the physical system passes through, where the jump and the quiescence of the system itself is determined by kinetic features and constrains so that the system may wait for a certain amount of time in the same state and jump to another one with certain rates, defined by its kinetics rules. The *frenesy* $D(\omega)$ wishes to evaluate the level of *traffic* and *persistence* of a given trajectory.
The trajectory weight might then be defined as:

$$\mathbb{P}(\omega) \sim \mathrm{e}^{-D(\omega)+\frac{1}{2}S(\omega)}$$

In order to get an exact evaluation of the probability of a given trajectory, it must be defined a reference process that also allow to evaluate entroy and frenesy with respect to it (Equation 2.14).

$$\begin{aligned} \frac{\mathbb{P}(\omega)}{\mathbb{P}_{\mathrm{ref}}(\omega)} &= \mathrm{e}^{-A(\omega)} \\ A(\omega) &= \Delta D(\omega) - \frac{1}{2}\Delta S(\omega) \end{aligned} \tag{2.14}$$

Considering a trajectory ω and another one ω' which is the trajectory ω traveled in reverse, one may write:

$$\begin{aligned} ln[\mathbb{P}(\omega)] - ln[\mathbb{P}(\omega')] &= ln\left[\frac{\mathbb{P}(\omega)}{\mathbb{P}(\omega')}\right] = \\ &= -\Delta D(\omega) + \frac{1}{2}\Delta S(\omega) + \Delta D(\omega') - \frac{1}{2}\Delta S(\omega') = \\ &= \Delta S(\omega) = S(\omega) - S(\omega') \\ \Rightarrow \Delta S(\omega) &= ln[\mathbb{P}(\omega)] - ln[\mathbb{P}(\omega')] = ln\left[\frac{\mathbb{P}(\omega)}{\mathbb{P}(\omega')}\right] \end{aligned} \tag{2.15}$$

$$\begin{aligned} ln[\mathbb{P}(\omega)] + ln[\mathbb{P}(\omega')] &= ln\Big[\mathbb{P}(\omega)\cdot\mathbb{P}(\omega')\Big] = \\ &= -\Delta D(\omega) + \frac{1}{2}\Delta S(\omega) - \Delta D(\omega') + \frac{1}{2}\Delta S(\omega') = \\ &= -2\Delta D(\omega) \\ \Rightarrow \Delta D(\omega) &= -\frac{1}{2}\Big(ln[\mathbb{P}(\omega)] + ln[\mathbb{P}(\omega')]\Big) = -\frac{1}{2}ln\Big[\mathbb{P}(\omega)\cdot\mathbb{P}(\omega')\Big] \end{aligned} \tag{2.16}$$

Since the probability of the whole trajectory can be expressed as a product of probabilities of starting in an initial configuration, making a transition and possibly remain in the final state (idle), the entropy and the frenesy at equilibrium can be rewritten as:

$$\begin{aligned}\Delta S(\omega) &= ln\left[\frac{\mathbb{P}[\boldsymbol{\sigma}_0]\cdot\prod_{k=1}^{n_{trans}}\mathbb{P}_k\cdot\mathbb{P}_{\text{idle}}}{\mathbb{P}[\boldsymbol{\sigma}_\tau]\cdot\prod_{k=1}^{n_{trans}}\mathbb{P}'_k\cdot\mathbb{P}'_{\text{idle}}}\right] = \\ &= \underbrace{-\beta[H(\boldsymbol{\sigma}_0)-H(\boldsymbol{\sigma}_\tau)]+ln\left[\frac{\mathbb{P}_{idle}}{\mathbb{P}'_{idle}}\right]}_{\text{boundary terms B.T}}+\sum_{k=0}^{n_{trans-1}}\underbrace{ln\left[\frac{\mathbb{P}_k}{\mathbb{P}'_k}\right]}_{S_k\text{ elementary entropy}} \\ &= B.T.+\sum_{k=0}^{n_{trans-1}}S_k\end{aligned}$$

$$\begin{aligned}\Delta D(\omega) &= -\frac{1}{2}ln\left[\left(\mathbb{P}[\boldsymbol{\sigma}_0]\cdot\prod_{k=1}^{n_{trans}}\mathbb{P}_k\cdot\mathbb{P}_{\text{idle}}\right)\left(\mathbb{P}[\boldsymbol{\sigma}_\tau]\cdot\prod_{k=1}^{n_{trans}}\mathbb{P}'_k\cdot\mathbb{P}'_{\text{idle}}\right)\right] = \\ &= \underbrace{\frac{\beta}{2}[H(\boldsymbol{\sigma}_0)-H(\boldsymbol{\sigma}_\tau)]-\frac{1}{2}ln\left[\mathbb{P}_{idle}\cdot\mathbb{P}'_{idle}\right]}_{\text{boundary terms B.T.}}+\sum_{k=0}^{n_{trans-1}}\underbrace{-\frac{1}{2}ln\left[\mathbb{P}_k\cdot\mathbb{P}'_k\right]}_{D_k\text{ elementary frenesy}} = \\ &= B.T.+\sum_{k=0}^{n_{trans-1}}D_k\end{aligned}$$

Focusing the attention only in one transition k and considering the case of the single spin-flip dynamic, the elementary frenesy is:

$$D_k = -\frac{1}{2}ln\left[\mathbb{P}(\sigma\to-\sigma)\mathbb{P}(-\sigma\to\sigma)\right]$$

Recalling Equation 2.3 of *Glauber* dynamic

$$\mathbb{P}(\sigma\to-\sigma)\propto \mathrm{e}^{-\beta\Delta H(\sigma_i)} \qquad \mathbb{P}(-\sigma\to\sigma)\propto \mathrm{e}^{\beta\Delta H(\sigma_i)}$$

and Equation 2.10 - 2.11

$$\mathbb{P}(\sigma\to-\sigma)\propto \alpha_i(\sigma_i)\mathrm{e}^{\Delta L(\sigma_i)} \qquad \mathbb{P}(-\sigma\to\sigma)\propto \alpha_i(-\sigma_i)\mathrm{e}^{-\Delta L(\sigma_i)}$$

one may evaluate the elementary frenesy in both the dynamics, obtaining:

$$D_{k,\text{Glauber}} = -\frac{1}{2} ln\Big[c_1 \mathrm{e}^{-\beta \Delta H(\sigma_i)} c_2 \mathrm{e}^{\beta \Delta H(\sigma_i)}\Big] = const$$

$$\begin{aligned} D_{k,\text{Directing}} &= -\frac{1}{2} ln\Big[c_1' \alpha_i(\sigma_i) \mathrm{e}^{-\Delta L(\sigma_i)} c_2' \alpha_i(-\sigma_i) \mathrm{e}^{\Delta L(\sigma_i)}\Big] = \\ &= const \cdot ln[\alpha_i(\sigma_i)\alpha_i(-\sigma_i)] \end{aligned}$$

$$\Rightarrow D_{k,\text{Glauber}} = const \qquad D_{k,\text{Directing}} = const \cdot ln[\alpha_i(\sigma_i)\alpha_i(-\sigma_i)]$$

The above results show that, in the case of the *Glauber* dynamic, the frenesy is a constant; its kinetic does not contain any parameters giving a direct information about how "fast" or "slower" the spins are to make a transition, but it is indirectly contained in the Hamiltonian of the system and in the factor β which depends on the temperature. Instead, by defining the *action rates* for each spin, that can also depend on the value the spin assumes, the frenesy is not anymore a constant, but its value change with the variation of these rates. The new dynamical rules allow to set parameters that directly control how frequently a transition may occur, thus impacting the value of the frenesy that actually aims to assess the level of "lingering and trafficking" of a trajectory.

2.2.2 Entropy and Frenesy in the single spin-flip dynamics

In the case of the *single spin-flip* dynamics, the states are characterized by configurations that differ from the previous state only on the value of one spin. The process is Morkovian with transition rates given by Equation 2.12.
Thereby, the probability of a given trajectory from time zero to time τ can be defined as follow:

$$\begin{aligned}\mathbb{P}[\boldsymbol{\sigma}(0)\to\boldsymbol{\sigma}(\tau)] &= \mathbb{P}[\boldsymbol{\sigma}(\tau)=\boldsymbol{\sigma}_\tau,\boldsymbol{\sigma}(\tau-dt)=\boldsymbol{\sigma}_{\tau-dt},\dots,\boldsymbol{\sigma}(0)=\boldsymbol{\sigma}_0] = \\ &= \mathbb{P}[\boldsymbol{\sigma}(\tau)=\boldsymbol{\sigma}_\tau|\boldsymbol{\sigma}(\tau-dt)=\boldsymbol{\sigma}_{\tau-dt},\dots,\boldsymbol{\sigma}(0)=\boldsymbol{\sigma}_0]\cdot \\ &\quad\cdot\mathbb{P}[\boldsymbol{\sigma}(\tau-dt)=\boldsymbol{\sigma}_{\tau-dt},\dots,\boldsymbol{\sigma}(0)=\boldsymbol{\sigma}_0] = \\ &= \mathbb{P}[\boldsymbol{\sigma}(\tau)=\boldsymbol{\sigma}_\tau|\boldsymbol{\sigma}(\tau-dt)=\boldsymbol{\sigma}_{\tau-dt}]\cdot \\ &\quad\cdot\mathbb{P}[\boldsymbol{\sigma}(\tau-dt)=\boldsymbol{\sigma}_{\tau-dt}|\boldsymbol{\sigma}(\tau-2dt)=\boldsymbol{\sigma}_{\tau-2dt}]\cdots\mathbb{P}[\boldsymbol{\sigma}(0)=\boldsymbol{\sigma}_0]\end{aligned}$$

As it is shown in Figure 2.4, a trajectory for the spin-flip dynamics may includes a number n_k of steps in which nothing happens *i.e.* none of the spin in the configuration $\boldsymbol{\sigma}_k$ will flip and there will be a number of step n_{flips} in which only one spin will flip. Moreover, when the system will arrive at the final configuration, it may remain in such configuration for a certain number of time steps with probability $\mathbb{P}_{idle}$. Thus, the trajectory's probability may be evaluated as:

$$\begin{aligned}\mathbb{P}[\boldsymbol{\sigma}(0)\to\boldsymbol{\sigma}(\tau)] = \mathbb{P}[\boldsymbol{\sigma}(0)=\boldsymbol{\sigma}_0]\cdot\left(\prod_{k=0}^{n_{flips}-1}\underbrace{\mathbb{P}^{n_k}(\text{no flips}|\boldsymbol{\sigma}_k)\mathbb{P}_i(1\text{ flip}|\boldsymbol{\sigma}_k)}_{\mathbb{P}_k\text{ elementary probability}}\right)\cdot\mathbb{P}_{\text{idle}} = \\ = \mathbb{P}[\boldsymbol{\sigma}(0)=\boldsymbol{\sigma}_0]\cdot\left(\prod_{k=0}^{n_{flips}-1}\mathbb{P}_k\right)\cdot\mathbb{P}_{\text{idle}} \\ \Rightarrow\mathbb{P}[\boldsymbol{\sigma}(0)\to\boldsymbol{\sigma}(\tau)] = \mathbb{P}[\boldsymbol{\sigma}(0)=\boldsymbol{\sigma}_0]\cdot\left(\prod_{k=0}^{n_{flips}-1}\mathbb{P}_k\right)\cdot\mathbb{P}_{\text{idle}}\end{aligned} \tag{2.17}$$

Likewise, for the time-reverse trajectory:

$$\mathbb{P}[\boldsymbol{\sigma}(\tau)\to\boldsymbol{\sigma}(0)] = \mathbb{P}[\boldsymbol{\sigma}(\tau)=\boldsymbol{\sigma}_\tau]\cdot\left(\prod_{k=0}^{n_{flips}-1}\mathbb{P}'_k\right)\cdot\mathbb{P}'_{\text{idle}} \tag{2.18}$$

However, it results that $\mathbb{P}_{\text{idle}} = \mathbb{P}'_{\text{idle}}$ and that, when no flip occurs at all, the configuration of the forward and backward trajectory will coincide, as well as the number of steps $n_k = n'_k$, meaning that $\mathbb{P}^{n_k}(\text{no flip}|\boldsymbol{\sigma_k}) = \mathbb{P}'^{n_k}(\text{no flip}|\boldsymbol{\sigma_k})$. Furthermore, in the case of the flip of only one spin, the same spin will flip in the forward and backward trajectory with a different probability, but the probability of the other spins of not even trying to flip will be the same: if spin i makes the

flip, for all the $j \neq i$, it holds that the term $\mathbb{P}(\sigma_j \text{ no flip}|\sigma_i \text{ flips})$ is the same in the two trajectories. With these premises, it is now possible to find an explicit formula for the probability $\mathbb{P}_k$ of Equation 2.17:

$$\begin{aligned}
\mathbb{P}(1 \text{ flip}|\boldsymbol{\sigma}_k) &= \mathbb{P}(\sigma_i \text{ flips}) \prod_{j=0, j\neq i}^{L-1} \mathbb{P}(\sigma_j \text{ no flip}|\sigma_i \text{ flips}) = \\
&= \underbrace{\alpha_i(\sigma_i)\frac{w_i}{1+w_i}}_{\kappa(\sigma_i)} dt \cdot \underbrace{\prod_{j=0, j\neq i}^{L-1} \Big[1 - \alpha_j(\sigma_j)dt\Big]}_{\substack{\text{probability that all the spins} \\ j\neq i \text{ do not even make} \\ \text{an attempt to flip}}} = \\
&= \kappa(\sigma_i)dt \cdot \prod_{j=0, j\neq i}^{L-1} \Big[1 - \alpha_j(\sigma_j)dt\Big] \\
\mathbb{P}(\text{no flip}|\boldsymbol{\sigma}_k) &= \prod_{j=0}^{L-1} \mathbb{P}(\sigma_j \text{ no attempt}) + \\
&\quad + \sum_{i=0}^{L-1} \mathbb{P}(\sigma_i \text{ tries but fails}) \prod_{j=0, j\neq i}^{L-1} \mathbb{P}(\sigma_j \text{ no attempt}) = \\
&= \prod_{j=0}^{L-1} [1 - \alpha_j(\sigma_j)dt] + \\
&\quad + \sum_{i=0}^{L-1} \alpha_i(\sigma_i)dt \frac{1}{1+w_i} \prod_{\substack{j=0 \\ j\neq i}}^{L-1} [1 - \alpha_j(\sigma_j)dt] \frac{1 - \alpha_i(\sigma_i)dt}{1 - \alpha_i(\sigma_i)dt} = \\
&= \prod_{j=0}^{L-1} [1 - \alpha_j(\sigma_j)dt] + \prod_{j=0}^{L-1} [1 - \alpha_j(\sigma_j)dt] \sum_{i=0}^{L-1} \frac{\alpha_i(\sigma_i)dt}{1 - \alpha_i(\sigma_i)dt} \frac{1}{1+w_i} = \\
&= \prod_{j=0}^{L-1} [1 - \alpha_j(\sigma_j)dt] \left(1 + dt \sum_{i=0}^{L-1} \frac{\alpha_i(\sigma_i)}{1 - \alpha_i(\sigma_i)dt} \frac{1}{1+w_i}\right)
\end{aligned}$$

For the case of the reverse trajectory, the term expressing the probability that the spin i is going to flip is changing since in this trajectory its value is opposite to the one of the forward. Therefore, the probability $\mathbb{P}'(\sigma_i \text{ flips})$ is:

$$\begin{aligned}\mathbb{P}'(\sigma_i \text{ flips}) &= \underbrace{\alpha_i(\sigma_i')\frac{w_i'}{1+w_i'}dt}_{\kappa(\sigma_i')} \\ &= \alpha_i(-\sigma_i)\frac{1}{1+w_i}dt \\ \sigma_i' = -\sigma_i \Rightarrow \alpha_i(\sigma_i') = \alpha_i(-\sigma_i) \qquad & w_i' = \frac{1}{w_i}\end{aligned}$$

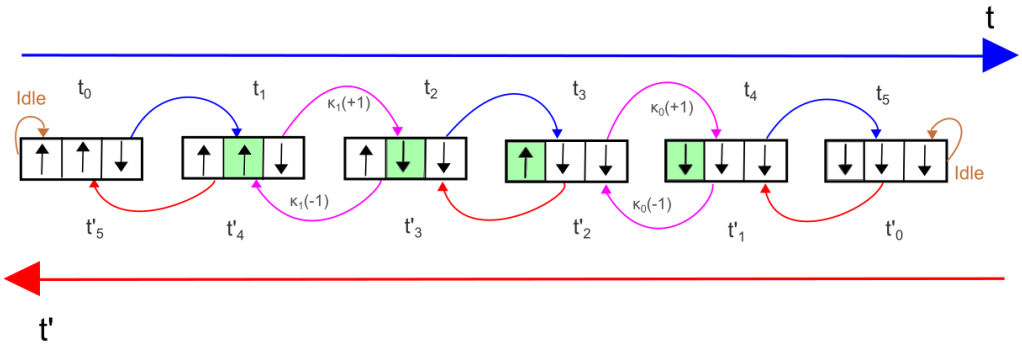

Figure 2.4: *Sigle spin-flip dynamic in a 3-spins Ising chain.* The blue and red arrows indicate respectively the forward and backward direction of time. In each transition a spin may make an attempt to change and the flip can occur or not. The number of transitions in which no spin flips is the same in forward and backward trajectory (red and blue arrows). The number of flip occurrences is also the same (pink arrows), but the rates are different in the two trajectories.

Thus:

$$ln[\mathbb{P}_k] = ln\Big[\mathbb{P}^{n_k}(\text{no flips}|\boldsymbol{\sigma}_k)\mathbb{P}(1 \text{ flip}|\boldsymbol{\sigma}_k)\Big] =$$
$$= n_k ln\Big[\mathbb{P}(\text{no flips}|\boldsymbol{\sigma}_k)\Big] + ln\Big[\mathbb{P}(\sigma_i \text{ flips}) \prod_{j=0,j\neq i}^{L-1} \mathbb{P}(\sigma_j \text{ no flip}|\sigma_i \text{ flips})\Big] =$$
$$= n_k ln\Big[\mathbb{P}(\text{no flips}|\boldsymbol{\sigma}_k)\Big] + \sum_{j=0,j\neq i}^{L-1} ln\Big[\mathbb{P}(\sigma_j \text{ no flip}|\sigma_i \text{ flips})\Big] + ln\Big[\mathbb{P}(\sigma_i \text{ flips})\Big]$$

$$ln[\mathbb{P}'_k] = ln\Big[\mathbb{P}'^{n_k}(\text{no flips}|\boldsymbol{\sigma}_k)\mathbb{P}'(1 \text{ flip}|\boldsymbol{\sigma}_k)\Big] =$$
$$= ln\Big[\mathbb{P}^{n_k}(\text{no flips}|\boldsymbol{\sigma}_k)] + ln\Big[\mathbb{P}'(\sigma_i \text{ flips}) \prod_{j=0,j\neq i}^{L-1} \mathbb{P}(\sigma_j \text{ no flip}|\sigma_i \text{ flips})\Big] =$$

$$= n_k ln\Big[\mathbb{P}(\text{no flips}|\boldsymbol{\sigma}_k)\Big] + \sum_{j=0,j\neq i}^{L-1} ln\Big[\mathbb{P}(\sigma_j \text{ no flip}|\sigma_i \text{ flips})\Big] + ln\Big[\mathbb{P}'(\sigma_i \text{ flips})\Big]$$

$$\Rightarrow ln[\mathbb{P}_k] - ln[\mathbb{P}'_k] = ln\left[\frac{\mathbb{P}(\sigma_i \text{ flips})}{\mathbb{P}'(\sigma_i \text{ flips})}\right] = ln\left[\frac{\alpha_i(\sigma_i)\frac{w_i}{1+w_i}}{\alpha_i(-\sigma_i)\frac{1}{1+w_i}}\right] =$$
$$= ln\left[\frac{\alpha_i(\sigma_i)}{\alpha_i(-\sigma_i)} w_i\right] = -\beta\Delta H(\sigma_i)$$

The elementary entropy is:

$$S_k = ln\left[\frac{\mathbb{P}_k}{\mathbb{P}'_k}\right] = -\beta\Delta H(\sigma_i)$$

with spin i being the spin that flips at transition k.
Instead, for the calculus of the elementary frenesy the sum $ln[\mathbb{P}_k] + ln[\mathbb{P}'_k]$ shall be evaluated:

$$\Rightarrow ln[\mathbb{P}_k] + ln[\mathbb{P}'_k] = 2n_k ln\Big[\mathbb{P}(\text{no flips}|\boldsymbol{\sigma}_k)\Big] + 2\sum_{j=0,j\neq i}^{L-1} ln\Big[\mathbb{P}(\sigma_j \text{ no flip}|\sigma_i \text{ flips})\Big] +$$
$$+ ln\Big[\mathbb{P}(\sigma_i \text{ flips})\Big] + ln\Big[\mathbb{P}'(\sigma_i \text{ flips})\Big] =$$
$$= 2n_k \underbrace{ln\left\{\prod_{j=0}^{L-1}[1-\alpha_j(\sigma_j)dt]\left(1 + dt\sum_{i=0}^{L-1}\frac{\alpha_i(\sigma_i)}{1-\alpha_i(\sigma_i)dt}\frac{1}{1+w_i}\right)\right\}}_{A} +$$
$$+ 2\sum_{j=0,j\neq i}^{L-1} ln\Big[1-\alpha_j(\sigma_j)dt\Big] + ln[\kappa(\sigma_i)dt] + ln[\kappa(\sigma'_i)dt]$$

The term A is:

$$A = \sum_{j=0}^{L-1} ln\Big[1-\alpha_j(\sigma_j)dt\Big] + ln\left(1+dt\sum_{i=0}^{L-1}\frac{\alpha_i(\sigma_i)}{1-\alpha_i(\sigma_i)dt}\frac{1}{1+w_i}\right) \overset{\text{small dt}}{\simeq}$$

$$\simeq \sum_{j=0}^{L-1} ln[\mathrm{e}^{-\alpha_j(\sigma_j)dt}] + ln\left(\mathrm{e}^{dt\sum_{i=0}^{L-1}\frac{\alpha_i(\sigma_i)}{1-\alpha_i(\sigma_i)dt}\frac{1}{1+w_i}}\right) =$$

$$= -\sum_{j=0}^{L-1}\alpha_j(\sigma_j)dt + \sum_{i=0}^{L-1}\frac{\alpha_i(\sigma_i)dt}{1-\alpha_i(\sigma_i)dt}\frac{1}{1+w_i} =$$

$$\overset{i=j}{=} \sum_{j=0}^{L-1}\left(-\alpha_j(\sigma_j)dt + \frac{\alpha_j(\sigma_j)dt}{1-\alpha_j(\sigma_j)dt}\frac{1}{1+w_j}\right) =$$

since $\alpha_j(\sigma_j) = \kappa(\sigma_j)\dfrac{1+w_j}{w_j}$

$$= \sum_{j=0}^{L-1}\left(-\kappa(\sigma_j)dt\frac{1+w_j}{w_j} + \frac{\kappa(\sigma_j)dt\frac{1+w_j}{w_j}}{1-\kappa(\sigma_j)dt\frac{1+w_j}{w_j}}\frac{1}{1+w_j}\right) =$$

$$= \sum_{j=0}^{L-1}\left(-\kappa(\sigma_j)dt\frac{1+w_j}{w_j} + \frac{\kappa(\sigma_j)dt}{w_j-\kappa(\sigma_j)dt(1+w_j)}\right) =$$

$$= -\sum_{j=0}^{L-1}\kappa(\sigma_j)dt\left(\frac{1+w_j}{w_j} - \frac{1}{w_j-\kappa(\sigma_j)dt(1+w_j)}\right) =$$

$$= -\sum_{j=0}^{L-1}\kappa(\sigma_j)dt\left(\frac{[1+w_j][w_j-\kappa(\sigma_j)dt(1+w_j)]-w_j}{w_i[w_j-\kappa(\sigma_j)dt(1+w_j)]}\right) =$$

$$= -\sum_{j=0}^{L-1}\kappa(\sigma_j)dt\left(\frac{w_j-\kappa(\sigma_j)dt(1+w_j)+w_j^2-w_j\kappa(\sigma_j)dt(1+w_j)-w_j}{w_j^2-w_j\kappa(\sigma_j)dt(1+w_j)}\right) =$$

$$= -\sum_{j=0}^{L-1}\kappa(\sigma_j)dt\left(1-\frac{\kappa(\sigma_j)dt(1+w_j)}{w_j^2-w_j\kappa(\sigma_j)dt(1+w_j)}\right) =$$

$$= -\sum_{j=0}^{L-1}\kappa(\sigma_j)dt + \sum_{j=0}^{L-1}\frac{\kappa^2(\sigma_j)dt^2(1+w_j)}{w_j^2-w_j\kappa(\sigma_j)dt(1+w_j)} \overset{dt^2\to 0}{\simeq}$$

$$\simeq -\sum_{j=0}^{L-1}\kappa(\sigma_j)dt$$

$$\Rightarrow A \simeq -\sum_{j=0}^{L-1}\kappa(\sigma_j)dt$$

So the term $ln[\mathbb{P}_k] + ln[\mathbb{P}'_k]$ will become:

$$\begin{aligned}
ln[\mathbb{P}_k] + ln[\mathbb{P}'_k] =& -2n_k \sum_{j=0}^{L-1} \kappa(\sigma_j)dt + 2 \sum_{j=0, j\neq i}^{L-1} ln\Big[1 - \alpha_j(\sigma_j)dt\Big] + \\
&+ ln[\kappa(\sigma_i)dt] + ln[\kappa(\sigma'_i)dt] \overset{\text{for small dt}}{\simeq} \\
\simeq& -2n_k \sum_{j=0}^{L-1} \kappa(\sigma_j)dt + 2 \sum_{j=0, j\neq i}^{L-1} ln\Big[\mathrm{e}^{-\alpha_j(\sigma_i)dt}\Big] + \\
&+ ln[\kappa(\sigma_i)dt] + ln[\kappa(\sigma'_i)dt] \overset{\text{for small dt}}{\simeq} \\
\simeq& -2n_k \sum_{j=0}^{L-1} [\kappa(\sigma_j)dt] - 2 \sum_{j=0, j\neq i}^{L-1} [\alpha_j(\sigma_i)dt] + \\
&+ ln[\kappa(\sigma_i)dt] + ln[\kappa(\sigma'_i)dt] = \\
=& -2n_k \sum_{j=0}^{L-1} [\kappa(\sigma_j)dt] - 2 \sum_{j=0, j\neq i}^{L-1} \left[\kappa(\sigma_j)\frac{1+w_j}{w_j}dt\right] + \\
&+ ln[\kappa(\sigma_i)dt] + ln[\kappa(\sigma'_i)dt] = \\
=& -2n_k \sum_{j=0}^{L-1} [\kappa(\sigma_j)dt] - 2 \sum_{j=0, j\neq i}^{L-1} \left[\kappa(\sigma_j)\frac{1+w_j}{w_j}dt\right] + \\
&+ ln[\kappa(\sigma_i)dt] + ln[\kappa(-\sigma_i)dt]
\end{aligned} \tag{2.19}$$

since $ln[\kappa(-\sigma_i)dt] = ln[\kappa(\sigma_i)dt] + \Delta ln[\kappa(\sigma_i)dt]$

$$\begin{aligned}
ln[\mathbb{P}_k] + ln[\mathbb{P}'_k] =& -2n_k \sum_{j=0}^{L-1} [\kappa(\sigma_j)dt] - 2 \sum_{j=0, j\neq i}^{L-1} \left[\kappa(\sigma_j)\frac{1+w_j}{w_j}dt\right] + \\
&+ 2ln[\kappa(\sigma_i)dt] + \Delta ln[\kappa(\sigma_i)dt]
\end{aligned}$$

Finally, the elementary frenesy D_k is:

$$\begin{aligned} D_k = &-\frac{1}{2} ln\Big[\mathbb{P}_k \cdot \mathbb{P}'_k\Big] = \\ = &\underbrace{n_k \sum_{j=0}^{L-1} \kappa(\sigma_j) dt}_{\substack{\text{contribution of the cases when} \\ \text{no spins flip}}} + \underbrace{\sum_{\substack{j=0 \\ j\neq i}}^{L-1} \kappa(\sigma_j) \frac{1+w_j}{w_j} dt}_{\substack{\text{contribution of the spins} \\ \text{that do not flip when one} \\ \text{spin has flipped}}} + \\ &- \underbrace{ln[\kappa(\sigma_i)dt]}_{\substack{\text{contribution of} \\ \text{the spin that} \\ \text{has flipped} \\ \text{on the forward} \\ \text{trajectory}}} - \frac{1}{2} \underbrace{\Delta ln[\kappa(\sigma_i)dt]}_{\substack{\text{contribution of} \\ \text{the spin that} \\ \text{has flipped} \\ \text{on the backward} \\ \text{trajectory w.r.t} \\ \text{the forward trajectory}}} \end{aligned} \tag{2.20}$$

Thus, the entropy and frenesy of a trajectory following the single spin-flip dynamics as in section 2.2 are:

$$\begin{aligned} S(\omega) =& B.T. - \beta \sum_{k=0}^{n_{flips}-1} \Delta H(\sigma_{i|\boldsymbol{\sigma}_k}) = \\ =& -\beta[H(\boldsymbol{\sigma}_0) - H(\boldsymbol{\sigma}_\tau)] + ln\left[\frac{\mathbb{P}_{\text{idle}}}{\mathbb{P}'_{\text{idle}}}\right] - \beta \sum_{k=0}^{n_{flips}-1} \Delta H(\sigma_{i|\boldsymbol{\sigma}_k}) = \\ \overset{\mathbb{P}_{\text{idle}} \equiv \mathbb{P}'_{\text{idle}}}{=}& -\beta[H(\boldsymbol{\sigma}_0) - H(\boldsymbol{\sigma}_\tau)] - \beta \sum_{k=0}^{n_{flips}-1} \Delta H(\sigma_{i|\boldsymbol{\sigma}_k}) \end{aligned}$$

Since the entropy's contribution is given only by those states in which a flip has happened, one can rewrite the entropy of the trajectory as a sum over consecutive states of the system where the configuration change by only one spin, thus rewriting:

$$\begin{aligned} S(\omega) &= -\beta[H(\boldsymbol{\sigma}_0) - H(\boldsymbol{\sigma}_\tau)] - \beta \sum_{k=0}^{n_{flips}-1} \Delta H(\sigma_{i|\boldsymbol{\sigma}_k}) = \\ &= -\sum_{k=0}^{n_{\text{flips}}} s(\boldsymbol{\sigma}_k, \boldsymbol{\sigma}_{k+1}) = \end{aligned} \tag{2.21}$$

$$\text{with, } s(\boldsymbol{\sigma}_k, \boldsymbol{\sigma}_{k+1}) = -\beta[H(\boldsymbol{\sigma}_k) - H(\boldsymbol{\sigma}_{k+1})] = -\beta \Delta H(\boldsymbol{\sigma}_k)$$

$$\begin{aligned} D(\omega) =& B.T. + \sum_{k=0}^{n_{flips}-1} n_k \sum_{j=0}^{L-1} \kappa(\sigma_{j|\boldsymbol{\sigma}_k}) dt + \sum_{k=0}^{n_{flips}-1} \sum_{\substack{j=0 \\ j\neq i}}^{L-1} \kappa(\sigma_{j|\boldsymbol{\sigma}_k}) \frac{1 + w_{j|\boldsymbol{\sigma}_k}}{w_{j|\boldsymbol{\sigma}_k}} dt + \\ &- \sum_{k=0}^{n_{flips}-1} ln[\kappa(\sigma_{i|\boldsymbol{\sigma}_k}) dt] - \frac{1}{2} \sum_{k=0}^{n_{flips}-1} \Delta ln[\kappa(\sigma_{i|\boldsymbol{\sigma}_k}) dt] \end{aligned} \tag{2.22}$$

According to the present entropy-frenesy decomposition formalism, the total entropy and frenesy of the path are expressed in function of the sum of elementary entropy and frenesy (S_k and D_k respectively), where the latter depend on the *action rates* that resemble the *active* part of the system *i.e.* the tendency of the spins to change their values. Therefore, one could think of parametrizing the transition rates $\kappa(\sigma_i)$ of Equation 2.12 as:

$$\kappa(\boldsymbol{\sigma}_x, \boldsymbol{\sigma}_y) = \underbrace{a(\boldsymbol{\sigma}_x, \boldsymbol{\sigma}_y)}_{\substack{\text{activity} \\ \text{parameter}}} \mathrm{e}^{-\overbrace{s(\boldsymbol{\sigma}_x, \boldsymbol{\sigma}_y)}^{\text{entropy change}}/2}$$

with the *entropy change* being anti-symmetric and equal to:

$$\begin{aligned} s(\boldsymbol{\sigma}, \boldsymbol{\sigma}_{-i}) = -s(\boldsymbol{\sigma}_{-i}, \boldsymbol{\sigma}) &= ln\left[\frac{\kappa(\boldsymbol{\sigma}, \boldsymbol{\sigma}_{-i})}{\kappa(\boldsymbol{\sigma}_{-i}, \boldsymbol{\sigma})}\right] = \\ &= ln\left[\frac{\alpha(\sigma_i)\frac{\mathrm{e}^{L(-\sigma_i)}}{Z}}{\alpha(-\sigma_i)\frac{\mathrm{e}^{L(\sigma_i)}}{Z}}\right] = \Delta L(\sigma_i) + ln\left[\frac{\alpha(\sigma_i)}{\alpha(-\sigma_i)}\right] = \\ &= -\beta \Delta H(\sigma_i) \end{aligned}$$

where in the last equality it has been used the result of Equation 2.13. Instead, the *activity parameter* is the symmetric part and it is equal to:

$$\begin{aligned} a(\boldsymbol{\sigma}, \boldsymbol{\sigma}_{-i}) = a(\boldsymbol{\sigma}_{-i}, \boldsymbol{\sigma}) &= \sqrt{\kappa(\boldsymbol{\sigma}, \boldsymbol{\sigma}_{-i})\kappa(\boldsymbol{\sigma}_{-i}, \boldsymbol{\sigma})} = \\ &= \sqrt{\alpha_i(\sigma_i)\frac{w_i}{1+w_i}\alpha_i(-\sigma_i)\frac{1}{1+w_i}} = \\ &= \frac{1}{1+w_i}\sqrt{\alpha_i(\sigma_i)\alpha_i(-\sigma_i)\frac{\alpha_i(-\sigma_i)}{\alpha_i(\sigma_i)}\mathrm{e}^{-\beta\Delta H(\sigma_i)}} = \frac{\alpha_i(-\sigma_i)}{1+w_i}\mathrm{e}^{-\frac{\beta}{2}\Delta H(\sigma_i)} = \\ &= \frac{\alpha_i(\sigma_i)\alpha_i(-\sigma_i)\mathrm{e}^{-\frac{\beta}{2}\Delta H(\sigma_i)}}{\alpha_i(\sigma_i) + \alpha_i(-\sigma_i)\mathrm{e}^{-\beta\Delta H(\sigma_i)}} = \frac{\alpha_i(\sigma_i)\alpha_i(-\sigma_i)}{\alpha_i(\sigma_i)\mathrm{e}^{\frac{\beta}{2}\Delta H(\sigma_i)} + \alpha_i(-\sigma_i)\mathrm{e}^{-\frac{\beta}{2}\Delta H(\sigma_i)}} \end{aligned}$$

From Equation 2.19 the terms related to the contributions of a spin i that flip in the forward and backward trajectory, can be reformulated as following:

$$
\begin{aligned}
ln[\kappa(\sigma_i)dt] + ln[\kappa(-\sigma_i)dt] =& ln[\alpha_i(\sigma_i)dt] + ln[\alpha_i(-\sigma_i)dt] + ln[w_i] - 2ln[1+w_i] = \\
=& ln[\alpha_i(\sigma_i)dt] + ln[\alpha_i(-\sigma_i)dt] + ln\left[\frac{\alpha(-\sigma_i)}{\alpha(\sigma_i)}\mathrm{e}^{-\beta\Delta H(\sigma_i)}\right] + \\
& - 2ln\left[\frac{\alpha_i(\sigma_i) + \alpha_i(-\sigma_i)\mathrm{e}^{-\beta\Delta H(\sigma_i)}}{\alpha_i(\sigma_i)}\right] = \\
=& ln[\alpha_i(\sigma_i)] + 2ln[dt] + ln[\alpha_i(-\sigma_i)] + ln[\alpha_i(-\sigma_i)] + \\
& - ln[\alpha_i(\sigma_i)] - \beta\Delta H(\sigma_i) + 2ln[\alpha_i(\sigma_i)] + \\
& - 2ln\left[\alpha_i(\sigma_i) + \alpha_i(-\sigma_i)\mathrm{e}^{-\beta\Delta H(\sigma_i)}\right] = \\
=& 2ln[\alpha_i(\sigma_i)\alpha_i(-\sigma_i)dt] - \beta\Delta H(\sigma_i) + \\
& - 2ln\left[\alpha_i(\sigma_i) + \alpha_i(-\sigma_i)\mathrm{e}^{-\beta\Delta H(\sigma_i)}\right] = \\
=& 2ln[\alpha_i(\sigma_i)\alpha_i(-\sigma_i)dt] - 2ln\left[\mathrm{e}^{\frac{\beta}{2}\Delta H(\sigma_i)}\right] + \\
& - 2ln\left[\alpha_i(\sigma_i) + \alpha_i(-\sigma_i)\mathrm{e}^{-\beta\Delta H(\sigma_i)}\right] = \\
=& 2ln\left[\underbrace{\frac{\alpha_i(\sigma_i)\alpha_i(-\sigma_i)}{\alpha_i(\sigma_i)\mathrm{e}^{\frac{\beta}{2}\Delta H(\sigma_i)} + \alpha_i(-\sigma_i)\mathrm{e}^{-\frac{\beta}{2}\Delta H(\sigma_i)}}}_{a(\boldsymbol{\sigma},\boldsymbol{\sigma}_{-i}) = a(\boldsymbol{\sigma}_{-i},\boldsymbol{\sigma})} dt\right]
\end{aligned}
$$

The final term is expressed in term of the *activity parameter* which indeed indicates the level of activity of the trajectory when considering both the directions of time.

2.3 Response to perturbation

In the previous section it has been adopted a perspective in which the system (the $d-dimensional$ lattice) evolves in time visiting the possible states *i.e.* changing its configuration, according to stochastic kinetic rules. This point of view has been useful to evaluate the frenesy of a trajectory, revealing the importance also of kinetic quantities, besides thermodynamic ones. However, the Ising model still relies in an Hamiltonian formalism, useful to model particle systems whose the study of the response to perturbations is a matter of interest. Such response is identified as a variation of a macroscopic quantity called *observable*, measurable at macroscopic scale and associated to the system of interest which is kept at fixed (thermodynamic) conditions. Due to the fact that the observable is measurable, its value is determined by the act of measurement that takes a certain time t at the macroscopic scale. During this time, a large number of events happen at the microscopic scale, which then can be described by the evolution of an initial microstate during the time interval t. Therefore, the time of the measurement at macroscopic scale is infinitely larger from the point of view of the microstate's evolution, thus it is possible to assume that the measurement coincides with the average in time of the observable:

$$\bar{O}(x) = \lim_{t\to\infty} \frac{1}{t} \int_0^t O(\Phi^s x) ds \tag{2.23}$$

x is a *microstate* of the *phase space* M
Φ^t is the *time evolution operator*, $\Phi : M \to M$

Given a system under certain fixed conditions (e.g. temperature, volume), the macroscopic state is the ensemble of all the microstates that realize it. In the interval of time t, if the system is *"fast enough"* [88] in visiting all the microscopic states representative of its macroscopic state, the Equation 2.23 coincides with the measure actually made and the system is at equilibrium. The main issues of the expression in Equation 2.23 are its dependence on the initial condition x and the interval of time t; the starting point $x \in M$ is unknown and the time t for the meseaurament of the same observable O may change with the experiment, thus influencing its average value. However, in the limit $t \to \infty$ one can assume that the system is indeed fast enough, so that the observable explores many times its range of values with proper frequencies and it results that the initial condition x is irrelevant. Thus, instead of integrate in time one can assume that there exists a probability measure u such that:

$$\bar{O}(x) = \lim_{t\to\infty} \frac{1}{t} \int_0^t O(\Phi^s x) ds = \int_M O du = \langle O \rangle_u \quad u\text{-q.o. } x \in M \tag{2.24}$$

When the system reaches equilibrium, a stationary probability density f over the states x of the phase space M exists and it is such that:

$$du(x) = f(x)dx \quad \forall x \in M$$

Using this result one may express the Equation 2.24 as:

$$\bar{O}(x) = \lim_{t\to\infty} \frac{1}{t} \int_0^t O(\Phi^s x) ds = \int_M O(x) f(x) dx \tag{2.25}$$

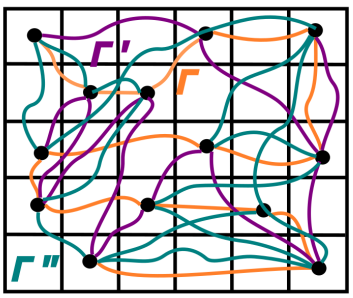

The Equation 2.24-2.25 are expressions of the well-known relation named *Ergodic Hypothesis* which commonly states that the phase space M, representative of all the possible microstates, is densely explored by almost all the possible trajectories (Figure 2.5).

Figure 2.5: *Ergodicity, schematic representation.* The phase space M is densely explored by the trajectories.

The context of the canonical ensemble is a special case, where the statements above are valid and the equilibrium has to be taken in the sense of thermal equilibrium. In equilibrium statistical mechanics, it is possible to evaluate the dynamics of the many particles system in terms of the Hamiltonian $H = H(\Gamma)$, with $\Gamma = (\boldsymbol{q}, \boldsymbol{p}) \in M$ and expressing the probability density function f (Appendix C) as:

$$\begin{aligned} f &= \frac{\mathrm{e}^{-\beta H(\Gamma)}}{Z} \\ Z &= \int \mathrm{e}^{-\beta H(\Gamma)} d\Gamma \\ \beta &= \frac{1}{k_B T}, \ k_B \text{ Boltzmann constant, } T \text{ temperature} \end{aligned} \tag{2.26}$$

Now, supposing the system is in an initial condition with energy $H_0(\Gamma)$ and probability density f_0. If a perturbation of the kind $\lambda A(\Gamma)$ with $\lambda \in \mathbb{R}$ is applied, the system will evolve in a state whose energy can be written as $H(\Gamma) = H_0(\Gamma) + \lambda A(\Gamma)$. Supposing the new state is an equilibrium one, it is possible to write the new probability density f as [89, 90]:

$$f = \frac{\mathrm{e}^{-\beta H(\Gamma)}}{\int \mathrm{e}^{-\beta H(\Gamma)} d\Gamma} = \frac{\mathrm{e}^{-\beta[H_0(\Gamma)+\lambda A(\Gamma)]}}{\int \mathrm{e}^{-\beta[H_0(\Gamma)+\lambda A(\Gamma)]} d\Gamma} = \frac{\mathrm{e}^{-\beta H_0(\Gamma)} \mathrm{e}^{-\beta\lambda A(\Gamma)}}{\int \mathrm{e}^{-\beta H_0(\Gamma)} \mathrm{e}^{-\beta\lambda A(\Gamma)} d\Gamma}$$

In the case of small λ it is possible to use the approximation $\mathrm{e}^{-x} \simeq 1 - x + O(x^2)$ and write:

$$f = \frac{\mathrm{e}^{-\beta H_0(\Gamma)} \mathrm{e}^{-\beta\lambda A(\Gamma)}}{\int \mathrm{e}^{-\beta H_0(\Gamma)} \mathrm{e}^{-\beta\lambda} d\Gamma} \simeq \frac{\mathrm{e}^{-\beta H_0(\Gamma)}[1 - \beta\lambda A(\Gamma) + O(\lambda^2)]}{\int \mathrm{e}^{-\beta H_0(\Gamma)}[1 - \beta\lambda A(\Gamma) + O(\lambda^2)] d\Gamma} \frac{\int \mathrm{e}^{-\beta H_0(\Gamma)} d\Gamma}{\int \mathrm{e}^{-\beta H_0(\Gamma)} d\Gamma} =$$

$$= \frac{\mathrm{e}^{-\beta H_0(\Gamma)}}{\int \mathrm{e}^{-\beta H_0(\Gamma)} d\Gamma} \cdot \frac{[1 - \beta\lambda A(\Gamma) + O(\lambda^2)]}{\int \frac{\mathrm{e}^{-\beta H_0(\Gamma)}}{\int \mathrm{e}^{-\beta H_0(\Gamma)} d\Gamma} [1 - \beta\lambda A(\Gamma) + O(\lambda^2)] d\Gamma} =$$

$$= f_0 \cdot \frac{[1 - \beta\lambda A(\Gamma) + O(\lambda^2)]}{\int f_0 [1 - \beta\lambda A(\Gamma) + O(\lambda^2)] d\Gamma} = f_0 \cdot \frac{1 - \beta\lambda A(\Gamma) + O(\lambda^2)}{1 - \beta\lambda \langle A(\Gamma) \rangle_0 + O(\lambda^2)} \simeq$$

$$\simeq f_0 [1 - \beta\lambda A(\Gamma) + O(\lambda^2)][1 + \beta\lambda \langle A(\Gamma) \rangle_0 + O(\lambda^2)] \simeq$$

$$\simeq f_0 \Big[1 - \beta\lambda \{A(\Gamma) - \langle A(\Gamma) \rangle_0\}\Big]$$

$$\Rightarrow f = f_0\Big[1 - \beta\lambda\{A(\Gamma) - \langle A(\Gamma)\rangle_0\}\Big] \tag{2.27}$$

Using Equation 2.25-2.27 one can evaluates the difference on the value of the observable O before and after the perturbation as follow:

$$\begin{aligned}\langle \Delta O\rangle_0 &= \int_M O[f - f_0]d\Gamma \simeq \int_M O f_0\Big[1 - \beta\lambda\{A - \langle A\rangle_0\} - 1\Big]d\Gamma = \\ &= -\beta\lambda \int_M O f_0\Big[A - \langle A\rangle_0\Big]d\Gamma = -\beta\lambda\left[\int_M (OA) f_0 d\Gamma - \langle A\rangle_0 \int_M O f_0 d\Gamma\right] = \\ &= -\beta\lambda\Big[\langle OA\rangle_0 - \langle A\rangle_0\langle O\rangle_0\Big]\end{aligned}$$

$$\Rightarrow \langle \Delta O\rangle_0 \simeq -\beta\lambda\Big[\langle OA\rangle_0 - \langle A\rangle_0\langle O\rangle_0\Big] \tag{2.28}$$

2.3.1 Temperature perturbation

With the Ising model formalism, it has been supposed that the physical system described is held at certain temperature T_0 so that there exists a probability equilibrium density f_0 over the states given by Equation 2.26 where $\beta = 1/k_B T_0$. If at a certain time the temperature is suddenly changed to a value $T = T_0 + \Delta T$, such system will reach an equilibrium state where the probability density is now f, different form f_0 since the coefficient β has been changed. One may be interested in the response of the system's energy at the variation of the temperature, thus evaluating the quantity:

$$\langle (H_0|T) - (H_0|T_0)\rangle = \int H_0(f - f_0)du \tag{2.29}$$

where H_0 is the energy of the system before and after the perturbation. In order to find a more informative expression of the above integral, it is useful to exploit the relation between f and f_0:

$$\begin{aligned}f &= \frac{\mathrm{e}^{-\frac{H_0}{k_B T}}}{\int \mathrm{e}^{-\frac{H_0}{k_B T}}du} = \frac{\mathrm{e}^{-\frac{H_0}{k_B(T_0+\Delta T)}}}{\int \mathrm{e}^{-\frac{H_0}{k_B(T_0+\Delta T)}}du} = \frac{\mathrm{e}^{-\frac{H_0}{k_B(T_0+\Delta T)}\frac{T_0}{T_0}}}{\int \mathrm{e}^{-\frac{H_0}{k_B(T_0+\Delta T)}\frac{T_0}{T_0}}du} = \\ &= \frac{\mathrm{e}^{-\frac{H_0}{k_B T_0}\cdot\frac{T_0}{T_0+\Delta T}}}{\int \mathrm{e}^{-\frac{H_0}{k_B T_0}\cdot\frac{T_0}{T_0+\Delta T}}du} = \frac{\mathrm{e}^{-\frac{H_0}{k_B T_0}\cdot\frac{1}{1+\frac{\Delta T}{T_0}}}}{\int \mathrm{e}^{-\frac{H_0}{k_B T_0}\cdot\frac{1}{1+\frac{\Delta T}{T_0}}}du}\end{aligned}$$

For small changes of temperature *i.e.* for small ΔT, one can write $\frac{1}{1+\frac{\Delta T}{T_0}} \simeq 1 - \frac{\Delta T}{T_0} + O(\frac{\Delta T}{T_0})$, so that:

$$
\begin{aligned}
f &= \frac{\mathrm{e}^{-\frac{H_0}{k_B T_0}\cdot\frac{1}{1+\frac{\Delta T}{T_0}}}}{\int \mathrm{e}^{-\frac{H_0}{k_B T_0}\cdot\frac{1}{1+\frac{\Delta T}{T_0}}} du} \simeq \frac{\mathrm{e}^{-\frac{H_0}{k_B T_0}\left(1-\frac{\Delta T}{T_0}\right)}}{\int \mathrm{e}^{-\frac{H_0}{k_B T_0}\left(1-\frac{\Delta T}{T_0}\right)} du} = \frac{\mathrm{e}^{-\frac{H_0}{k_B T_0}\left(1-\frac{\Delta T}{T_0}\right)}}{\int \mathrm{e}^{-\frac{H_0}{k_B T_0}\left(1-\frac{\Delta T}{T_0}\right)} du} = \\
&= \frac{\mathrm{e}^{-\frac{H_0}{k_B T_0}}\mathrm{e}^{\frac{H_0 \Delta T}{k_B T_0^2}}}{\int \mathrm{e}^{-\frac{H_0}{k_B T_0}}\mathrm{e}^{\frac{H_0 \Delta T}{k_B T_0^2}} du} \simeq \frac{\mathrm{e}^{-\frac{H_0}{k_B T_0}}\left(1+\frac{H_0\Delta T}{k_B T_0^2}\right)}{\int \mathrm{e}^{-\frac{H_0}{k_B T_0}}\left(1+\frac{H_0\Delta T}{k_B T_0^2}\right) du}\frac{Z_0}{Z_0} = \\
&= \frac{\mathrm{e}^{-\frac{H_0}{k_B T_0}}}{Z_0} \cdot \frac{1+\frac{H_0\Delta T}{k_B T_0^2}}{\int \frac{\mathrm{e}^{-\frac{H_0}{k_B T_0}}}{Z_0}\left(1+\frac{H_0\Delta T}{k_B T_0^2}\right) du} = f_0 \cdot \frac{1+\frac{H_0\Delta T}{k_B T_0^2}}{\int f_0 \left(1+\frac{H_0\Delta T}{k_B T_0^2}\right) du} = \\
&= f_0 \frac{1+\frac{H_0\Delta T}{k_B T_0^2}}{1+\langle\frac{H_0\Delta T}{k_B T_0^2}\rangle_0} \simeq f_0 \cdot \left[\left(1+\frac{H_0\Delta T}{k_B T_0^2}\right)\left(1-\langle\frac{H_0\Delta T}{k_B T_0^2}\rangle_0\right)\right] \simeq \\
&\simeq f_0 \left[1+\frac{H_0\Delta T}{k_B T_0^2} - \langle\frac{H_0\Delta T}{k_B T_0^2}\rangle_0\right] = f_0\left[1-\frac{\Delta T}{k_B T_0^2}\left(\langle H_0\rangle_0 - H_0\right)\right] \\
&\Rightarrow f = f_0\left[1-\frac{\Delta T}{k_B T_0^2}\left(\langle H_0\rangle_0 - H_0\right)\right]
\end{aligned}
$$

It is then possible to express Equation 2.29 as:

$$
\begin{aligned}
\langle (H_0|T) - (H_0|T_0)\rangle &= \int H_0 (f - f_0) du = \\
&= \int H_0 \cdot f_0 \left[1-\frac{\Delta T}{k_B T_0^2}\left(\langle H_0\rangle_0 - H_0\right) - 1\right] du = \\
&= -\frac{\Delta T}{k_B T_0^2}\int H_0 \cdot \left(\langle H_0\rangle_0 - H_0\right) f_0 du = \\
&= -\frac{\Delta T}{k_B T_0^2}\left[\langle H_0\rangle_0 \int H_0 \cdot f_0 du - \int H_0^2 \cdot f_0 du\right] = \\
&= -\frac{\Delta T}{k_B T_0^2}\left[\langle H_0\rangle_0^2 - \langle H_0^2\rangle_0\right] = \frac{\Delta T}{k_B T_0^2}\mathrm{var}(H_0) \\
\Rightarrow \langle (H_0|T) - (H_0|T_0)\rangle &= \frac{\Delta T}{k_B T_0^2}\mathrm{var}(H_0)
\end{aligned}
\tag{2.30}
$$

Chapter 3

Numerical simulations and results - Ising chain

3.1 *Metropolis-Hastings* algorithm

The *Markov Chain Monte Carlo* (MCMC) techniques were first introduced in the context of statistical mechanics [91] and, as of today, they are one of the most powerful methods used to solve the problem of Bayesian inference. Indeed, there exists a close similarity between statistical mechanics and parametric Bayesian inference: suppose to parameterize the energy associated to a certain state in the canonical ensemble as $E_s(\boldsymbol{\theta}) = -k_B T ln[f(\boldsymbol{x}|\boldsymbol{\theta})f(\boldsymbol{\theta})]$. The partition function Z will be:

$$Z = \int d\boldsymbol{\theta} \mathrm{e}^{-\beta E_s(\boldsymbol{\theta})} = \int d\boldsymbol{\theta} f(\boldsymbol{x}|\boldsymbol{\theta}) f(\boldsymbol{\theta}) = f(\boldsymbol{x})$$

The canonical distribution is given by:

$$\frac{\mathrm{e}^{-\beta E_s(\boldsymbol{\theta})}}{Z} = \frac{f(\boldsymbol{x}|\boldsymbol{\theta}) f(\boldsymbol{\theta})}{f(\boldsymbol{x})} = f(\boldsymbol{\theta}|\boldsymbol{x}) \tag{3.1}$$

i.e. the canonical distribution coincides with the bayesian *posterior*, where $\boldsymbol{\theta}$ is the set of parameters of which a *prior* probability density $f(\boldsymbol{\theta})$ is defined, while $f(\boldsymbol{x}|\boldsymbol{\theta})$ is called *likelihood*. In order to correct the assumption made on the *prior* and make it converges to the *posterior*, one should be able to evaluate the likelihood $f(\boldsymbol{x}|\boldsymbol{\theta})$. However, unless some special case, solving Equation 3.1 is not trivial or it is even impossible to find an analytical solution; the MCMC algorithms offer a numerical solution to this problem by generating a sequence (chain) of values in the parameters space, where the value (state) $\boldsymbol{\theta}_i$ is updated with $\boldsymbol{\theta}_{i+1}$ in a way that the final distribution over the chain follows the desired one (*posterior*). The chain is supposed to be a Markov one and the probability of going from a state $\boldsymbol{\theta}_i$ to $\boldsymbol{\theta}_{i+1}$

is encoded in the *transition matrix* T which is supposed to be homogeneous *i.e.* it depends only on the state of the system and not on the number of steps that have been made ($T_i[\boldsymbol{\theta}_i, \boldsymbol{\theta}_{i+1}] = T[\boldsymbol{\theta}_i, \boldsymbol{\theta}_{i+1}]$). The homogeneity of T allows the chain to be completely specified once it has been given the transition matrix T and the initial distribution $\boldsymbol{\pi}_0$ over the states. If the chain is *ergodic i.e.* $\lim_{i\to\infty} \boldsymbol{\pi}_i = \boldsymbol{\pi}$, it holds that it has a unique and *invariant* distribution (*equilibrium* distribution), where invariance means that $\boldsymbol{\pi}(\boldsymbol{\theta}) = \sum_{\boldsymbol{\theta'}} \boldsymbol{\pi}(\boldsymbol{\theta'})T(\boldsymbol{\theta'}, \boldsymbol{\theta})$. The *equilibrium* distribution satisfies detailed balance condition:

$$\boldsymbol{\pi}(\boldsymbol{\theta}_i)T(\boldsymbol{\theta}_i, \boldsymbol{\theta}_{i+1}) = \boldsymbol{\pi}(\boldsymbol{\theta}_{i+1})T(\boldsymbol{\theta}_{i+1}, \boldsymbol{\theta}_i)$$

The *Metropolis-Hasting* algorithm is a MCMC method that builds a chain of states $\boldsymbol{\theta}_i$ where a new state is accepted with probability

$$\alpha_{i,i+1} = min\left[1, \frac{p_{i+1,i}\boldsymbol{\pi}(\boldsymbol{\theta}_{i+1})}{p_{i,i+1}\boldsymbol{\pi}(\boldsymbol{\theta}_i)}\right]$$

where $p_{j,k}$ is a proposal transition probability between states i and j so that the actual transition matrix of the chain will be $T(\boldsymbol{\theta}_j, \boldsymbol{\theta}_k) = \alpha_{j,k}p_{j,k}$. However, since the choice of $p_{j,k}$ is arbitrary, one can also assume that such probabilities are symmetric ($p_{j,k} = p_{k,j}$) so that the *Metropolis-ratio* $\alpha_{i,i+1}$ is equal to:

$$\alpha_{i,i+1} = min\left[1, \frac{\boldsymbol{\pi}(\boldsymbol{\theta}_{i+1})}{\boldsymbol{\pi}(\boldsymbol{\theta}_i)}\right]$$

The latter construction still allows to satisfy the detailed balance condition and $\boldsymbol{\pi}$ is an *equilibrium* distribution:

$$\begin{aligned}\boldsymbol{\pi}(\boldsymbol{\theta}_{i+1})T(\boldsymbol{\theta}_{i+1}, \boldsymbol{\theta}_i) &= \boldsymbol{\pi}(\boldsymbol{\theta}_{i+1})\alpha_{i+1,i}p_{i+1,i} = min[\boldsymbol{\pi}(\boldsymbol{\theta}_{i+1}), \boldsymbol{\pi}(\boldsymbol{\theta}_i)]p_{i+1,i} = \\ &= min[\boldsymbol{\pi}(\boldsymbol{\theta}_i), \boldsymbol{\pi}(\boldsymbol{\theta}_{i+1})]p_{i,i+1} = \boldsymbol{\pi}(\boldsymbol{\theta}_i)\alpha_{i,i+1}p_{i,i+1} = \\ &= \boldsymbol{\pi}(\boldsymbol{\theta}_i)T(\boldsymbol{\theta}_i, \boldsymbol{\theta}_{i+1})\end{aligned}$$

In the case of the Ising chain, the energy is defined by the Hamiltonian $H(\boldsymbol{\sigma})$ and the set of parameters coincides with the spins of the chain *i.e.* $\boldsymbol{\theta} = \boldsymbol{\sigma}$, where $\boldsymbol{\sigma}$ is a configuration. The *equilibrium* distribution is given by Equation 2.3 so that the *Metropolis ratio* is defined as:

$$\alpha_{i,i+1} = min\left[1, \frac{\mathrm{e}^{-\beta H(\boldsymbol{\sigma}_{i+1})}}{\mathrm{e}^{-\beta H(\boldsymbol{\sigma}_i)}}\right] = min\left[1, \mathrm{e}^{-\beta\Delta H(\sigma_i)}\right] \tag{3.2}$$

where the last equality is due to the fact that only one spin can change its value at each transition.

One issue concerning the *Monte-Carlo* methods consist in the number of steps that the simulation needs to reach the equilibrium distribution, since the initial state $\boldsymbol{\theta}_0$ is usually defined randomly. This imply that, at the beginning of the simulation, the latter will create states not still representative of the equilibrium distribution, against the purpose of the method which instead, aims to store samples that comes more likely from the chosen target distribution. To prevent such disadvantage, one should define how many number of steps are needed to reach the equilibrium distribution and to start storing the samples. Such number of step is a parameter that has to be set a priori, known as *burn-in time*.
The other problem is about the nature of the Markov chain itself: since each state of the chain directly depend on the previous one, the risk is that subsequent samples might be highly correlated. To decrease the impact of this issue, it is useful to set rules that allow to define a number of steps the simulation has to wait for, before storing a sample. In the algorithm presented in this section, it has been chosen to consider a new sample after having tried to evaluate the probability of changing a value of all the spins of the chain, in a random order, as described in Algorithm 3. To summarize, the algorithm generates a random initial configuration $\boldsymbol{\sigma}_0$, it will wait a *burn-in* number of steps after which the first state of the chain will be taken into account. Then, until the total number of simulation step, for each spin of the chain it will be evaluated if it actually changes its value and, at the end, a new state will be generate. In order to decrease further the correlation between the samples, at each fixed *frame step* the energy and the magnetizaion, whose value is determined according to Equation 2.2-2.4, will be calculated over the respective configuration and stored.

Algorithm 3 Metropolis-Hastings Algorithm (MMC) - Ising Chain

Initialize a random configuration $\boldsymbol{\sigma}_0$ of the chain ▷ $\boldsymbol{\sigma}_0$ is *state* of the chain
while $t < \tau_0$ **do** ▷ τ_0 is the *burn-in* time
  for i **in** random_indices(L) ▷ L is the length of the chain
    generate $u \sim U(0,1)$
    evaluate $\Delta H(\sigma_i)$
    if $\alpha \geq u$ accept change ▷ α is given by Equation 3.2
    else do not accept
  end for
  $t \leftarrow t + 1$
end while
$\boldsymbol{\sigma}_0 \leftarrow \boldsymbol{\sigma}_{burn-in}$
while $t < \tau$ **do** ▷ τ is the total number of simulation-steps
  for i **in** random_indices(L) ▷ L is the length of the chain
    generate $u \sim U(0,1)$
    evaluate $\Delta H(\sigma_i)$
    if $\alpha \geq u$ accept change ▷ α is given by Equation 3.2
    else do not accept
  end for
  if t % $n = 0$ ▷ n is the frame step
    Store energy $H(\boldsymbol{\sigma}_t)$
    Store magnetizaion $M(\boldsymbol{\sigma}_t)$
  end if
  $t \leftarrow t + 1$
end while

3.2 *Discrete time dynamic* algorithm

Unlike the *Monte Carlo* algorithm that try to find samples from a defined equilibrium distribution and that assumes the symmetry on the proposed transition probabilities, the *discrete time algorithm* (DT) bases the choice of the samples meanly by evaluating if the probability of flipping the value of the spin (given by Equation 2.10) is bigger than a random variable generated from a uniform distribution. In this way, the algorithm still generates a series of configurations representative of a given probability distribution over the states of the system, but the chosen state of the chain has been selected on the basis of the transition probability $p(\sigma_i \rightarrow -\sigma_i)$, rather than using rules depending on the equilibrium distribution. Since the state space admits an equilibrium distribution and the algorithm fixes a random initial configuration $\boldsymbol{\sigma}_0$, it will still be necessary to wait a certain number of steps (*i.e.* set a *burn-in* time) before the algorithm will provide a sample representative of the equilibrium distribution. After this initial relaxation time, the algorithm will

create the chain with states obtained after that all the spins of the chain have tried to change their signs, with the purpose to decrease the correlation between the samples. To further avoid correlation, the energy and magnetizaion will be evaluated and stored after that a number of time steps (equal to the fixed *frame step*) is passed. A summary is given in Algorithm 4.

The main aspect characterizing the discrete algorithm is the presence of the parameter dt, which explicitly appear in the transition probability $p(\sigma_i \to -\sigma_i)$ and thus in the simulation. If in the Metropolis algorithm the time coincides with the Monte-Carlo step, in the discrete algorithm the time has to be seen equal to the product between the simulation step and the parameter dt. How to properly define the value of dt is not obvious. Considering that the *action rates* $\alpha_i(\sigma_i)$ have been fixed, the parameter dt still depends on the simulation temperature and the reasons is mainly physical: for higher temperatures the spins will try to change their values more frequently with respect to lower temperatures, due to thermal agitation. Indeed, the probability of flipping is expressed through the term $e^{\Delta L}$, which in turn is proportional to $e^{-\beta \Delta H}$ that is larger at higher temperature, with the result that $p(\sigma \to -\sigma)$ is also larger. This, finally implies that the number of times in which the condition $p(\sigma \to -\sigma) > u, u \sim U(0,1)$ is verified is higher, so that the spins will flip more likely in the high temperature case than in the low one. Since the algorithm has been built with the assumption that only one spin will flip at the time, when the flipping events happen more frequently, the dt has to be choosen small enough to guarantee that at each time step there will be only one flip-occurrence. Therefore, the parameter dt will become smaller with the increasing of the temperature, causing instead a rise of the total number of simulation step, with the result that for higher temperatures the computational cost of the algorithm will increase. Since the value of dt has to be fixed in advance, in order to set it in a reasonable way, a possibility is to compare the *autocorrelation function* of the discrete time algorithm with the one of the continuous case, as it is done in Figure 3.2.

Algorithm 4 Discrete time Algorithm (DT) - Ising Chain

Initialize a random configuration $\boldsymbol{\sigma}_0$ of the chain ▷ $\boldsymbol{\sigma}_0$ is *state* of the chain
while $t < \tau_0$ **do** ▷ τ_0 is the *burn-in* time
  for $i < L$: ▷ L is the length of the chain
    generate $u \sim U(0,1)$
    if $p(\sigma_i \to -\sigma_i) \geq u$ accept change ▷ $p(\sigma_i \to -\sigma_i)$ is given by Equation 2.10
    else do not accept change
  end for
  $t \leftarrow t + 1$
end while
$\boldsymbol{\sigma}_0 \leftarrow \boldsymbol{\sigma}_{\tau_0}$
while $t < \tau$ **do** ▷ τ is the total number of simulation-steps
  for $i < L$: ▷ L is the length of the chain
    generate $u \sim U(0,1)$
    if $p(\sigma_i \to -\sigma_i) \geq u$ accept change ▷ $p(\sigma_i \to -\sigma_i)$ is given by Equation 2.10
    else do not accept change
  end for
  if t % $n = 0$ ▷ n is the frame step
    Store energy $H(\boldsymbol{\sigma}_t)$
    Store magnetizaion M
  end if
  $t \leftarrow t + 1$
end while

3.3 *Continuous time dynamic* algorithm

The kinetics rules, described in section 2.2, state that each spin will make an attempt to flip with probability $\alpha_i(\sigma_i)dt$ and after that, the flip might actually occur or it might not, with a certain probability. In the case of the DT algorithm a particular attention has been given on the parameter dt. However, an alternative approach may be formulated by directly sampling the random time at which the spins try to flip. By identifying the number of flips that may happen along the chain during an interval of time $I = [0, t]$ as a *Poisson process N(t)*, the random times τ_i at which the spin-flip will occur are exponential random variable with parameter $\alpha_i(\sigma_i)$. In order to get samples of such random times a particular stochastic simulation algorithm, referred as *first-reaction method*, has been used [92]: for each spin of the chain, a random variable u_i from a uniform distribution is generating and the respective random times is evaluated as:

$$\tau_i = \frac{1}{\alpha_i(\sigma_i)} ln\left(\frac{1}{u_i}\right)$$

From the equation above, one may notice that such random times depends on the *action rates* of the relative spin, meaning that spins with higher $\alpha_i(\sigma_i)$ will generally have a smaller τ_i. Once the random times has been generated, the *firs-reaction* method provides that the spin with minimum τ_i will flip first and such change will be accepted with probability given by Equation 2.8. This mechanism allows to define an order on the sequence of spin-flips, still respecting the fact that only one variation is accepted at the time. However, the concept of time in this algorithm might be more clarified. One has to distinguish between the simulation step (simulation time) and what it is referred as *internal time*. The algorithm is characterized by the presence of a parameter dt that represent an interval of time after which the new state (new configuration $\boldsymbol{\sigma}$) is considered part of the chain. Thus, the parameter dt influences the correlation between consecutive states: the larger it is, the more the simulation will makes flips with the result that the final configuration, after that dt is elapsed, will be less correlated to the previous state. Setting a large value of dt has the disadvantage of making the simulation slower, however if one decrease its value, the risk is that consecutive states might be highly correlated. Thus, the *internal time* scans the flow of time until the value dt is reached, after which a new state will be added to the chain and the simulation time will be updated. In more details, the steps that the simulation follows during the interval dt are summarized in Algorithm 5: the spin with minimum time τ_i will flip its value if $p(\sigma_i \to -\sigma_i|\text{attempt}) > r$, with r a random variable sampled from an uniform distribution. The *internal time* will be updated by adding the time τ_i elapsed, while at the random times of the others spin, the value τ_i will be subtracted and a new τ_i for the spin i will be generated. The procedure repeats until the sum between internal time is lower than dt. When it ends, if the difference between the internal time and dt is different from zero, the random times of all the spins will be updated by subtracting to them the latter difference. Finally, a new configuration of the system will be obtained.
The whole *continuous algorithm* (CT) provides a *burn-in* time, as well as a *frame steps*, after which a configuration is obtained, over which energy and magnetzation are evaluated. The full procedure is summarized in Algorithm 6.

Algorithm 5 Advance step - Continuous time algorithm

while $i < L$ **do** ▷ L is the length of the chain.
  generate $u \sim U(0,1)$
  calculate τ_i
end while
$\bar{\tau}_k = min[(\tau_i)_{i=1,...L}]$
while internal time + $\bar{\tau}_k < dt$ **do** ▷ **Beginning advance**
  internal time = internal time + $\bar{\tau}_k$
  $(\tau_j)_{\substack{j=1,...,L \\ j\neq i}} = (\tau_j)_{\substack{j=1,...,L \\ j\neq i}} - \bar{\tau}_k$
  generate $r \sim U(0,1)$
  if $p(\sigma_k \to -\sigma_k|\text{attempt}) > r$ flip spin i ▷ $p(\sigma_i \to -\sigma_i|\text{attempt})$is given by Equation 2.8
  else do not flip
  generate new τ_k for spin k
  $\bar{\tau}_k = min[(\tau_i)_{i=1,...L}]$ ▷ Find the new spin with minimum τ
end while
$(\tau_i)_{i=1,...L} = (\tau_i)_{i=1,...L} - (\text{internal time} - dt)$ ▷ **End advance**

Algorithm 6 Continuous time Algorithm (CT) - Ising Chain

Initialize a random configuration $\boldsymbol{\sigma}_0$ ▷ $\boldsymbol{\sigma}_0$ is *state* of the chain
while $t < \tau_0$ **do** ▷ τ_0 is the *burn-in* time
  Make a step advance of Algorithm 5
end while
$\boldsymbol{\sigma}_0 \leftarrow \boldsymbol{\sigma}_{\tau_0}$
while $t < \tau$ **do**
  Make a step advance of Algorithm 5
  if t % $n = 0$ ▷ n is the frame step
    Store energy $H(\boldsymbol{\sigma}_t)$
    Store magnetization M
  end if
  $t \leftarrow t + 1$
end while

3.4 Algorithms of ensemble sampling

The algorithms introduced in the previous sections (Algorithm 3-4-6) evolve in time, starting from a random initial condition. However, when the length of the chain increases or, for example, the parameter *dt* in the discrete algorithm becomes smaller, the computational cost of such algorithms are quite high. To achieve better performance and in a faster time, a valid alternative solution relies on the *ensemble sampling algorithms*. Since two different quantities shall be analyzed, two different algorithms have been used in this work. The one referred as *burn-in algorithm* provides several different initial conditions, from each of which a simulation of length of *burn-in* time is started. At the end, each of these simulations will provide one configuration that will contribute to form a unique sample over which energy and magnetization will be evaluated. However, the *burn-in* time is set after that a simulation as in Algorithm 3-4-6 has been performed, on the basis of its autocorrelation function. The other approach (*average trajectories algorithm*) will start by generating different initial conditions as well, but for each of them a trajectory until time t will be created. In order to reduce the computational cost of such methods, the initial conditions are created through the *burn-in algorithm* so that the *burn-in* time of each trajectory can be set to a lower value, thus increasing the performance of the algorithm itself. At the end, a single trajectory will be obtained by averaging over all the trajectories. The latter algorithm will be used on the the response to a temperature perturbation.

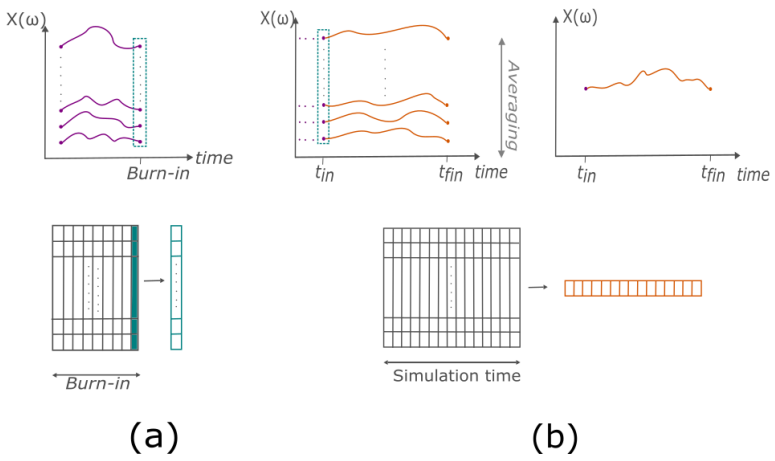

Figure 3.1: *Ensemble sampling algorithm.* (a) *Burn-in algorithm*: multiple simulations until *burn-in* time. The last state of each of them will be part of the final sample. (b) *Average trajectories algorithm.* The initial condition of all the trajectories are generated by algorithm (a). Then, simulations will run until t_{final} and a unique trajectory is obtained by averaging them.

3.5 Results

3.5.1 Observables: energy and magnetization

As it has been introduced in section section 2.3, one could be interested in evaluating macroscopic quantities of the system under analysis, which are called *observables*. In the case of the Ising model, such observables are the energy and the magnetization of the system, given by Equation 2.1-2.4. In the present work, these two quantities are evaluated by using the *ensemble sampling* algorithm (section 3.4), both for the *Metropolis Monte Carlo* (MMC), than the *discrete* (DT) and *continuous* (CT) time algorithms. This has been done in order to compare the results given by these two last methods, with the already well-tested Monte Carlo algorithms. For the cases in which the number of spins is not too large[1], rather than using only the results provided by the MMC, also theoretical quantities can be computed. More specifically, given an Ising chain with number of spins N, there will exist 2^N possible configurations $\boldsymbol{\sigma}$. Since different configurations may contribute to the realization of the same macroscopic quantity (energy or magnetization), which in general can assume different values, it is possible to theoretically derive the probability that certain configurations will realize a precise energy or magnetization level ($\bar{H}$ and $\bar{M}$ respectively):

$$\begin{aligned}
\mathbb{P}\Big(H(\boldsymbol{\sigma}) = \bar{H}\Big) &= \sum_{\boldsymbol{\sigma}} \mathbb{P}\Big(\boldsymbol{\sigma} | H(\boldsymbol{\sigma}) = \bar{H}\Big) = \\
&= \frac{\sum_{\boldsymbol{\sigma}} \mathrm{e}^{-\beta H(\boldsymbol{\sigma})} \mathbb{1}_{(\boldsymbol{\sigma}|H(\boldsymbol{\sigma})=\bar{H})}}{\sum_{\bar{H}} \sum_{\boldsymbol{\sigma}} \mathrm{e}^{-\beta H(\boldsymbol{\sigma})} \mathbb{1}_{(\boldsymbol{\sigma}|H(\boldsymbol{\sigma})=\bar{H})}} \\
\mathbb{P}\Big(M(\boldsymbol{\sigma}) = \bar{M}\Big) &= \sum_{\boldsymbol{\sigma}} \mathbb{P}\Big(\boldsymbol{\sigma} | M(\boldsymbol{\sigma}) = \bar{M}\Big) = \\
&= \frac{\sum_{\boldsymbol{\sigma}} \mathrm{e}^{-\beta H(\boldsymbol{\sigma})} \mathbb{1}_{(\boldsymbol{\sigma}|M(\boldsymbol{\sigma})=\bar{M})}}{\sum_{\bar{M}} \sum_{\boldsymbol{\sigma}} \mathrm{e}^{-\beta H(\boldsymbol{\sigma})} \mathbb{1}_{(\boldsymbol{\sigma}|M(\boldsymbol{\sigma})=\bar{M})}}
\end{aligned} \tag{3.3}$$

Thus, the probability of having a level $\bar{H}$ or $\bar{M}$ is given by the ratio between the sum of the weights relative to the configurations that give such level and a normalization factor, expressed by the sum, over all the possible $\bar{H}$ or $\bar{M}$, of the weights of the configurations realizing each of them. In Algorithm 7 is schematize how these probabilities are evaluated in the simulation.

[1] bigger than 80, for computational reasons

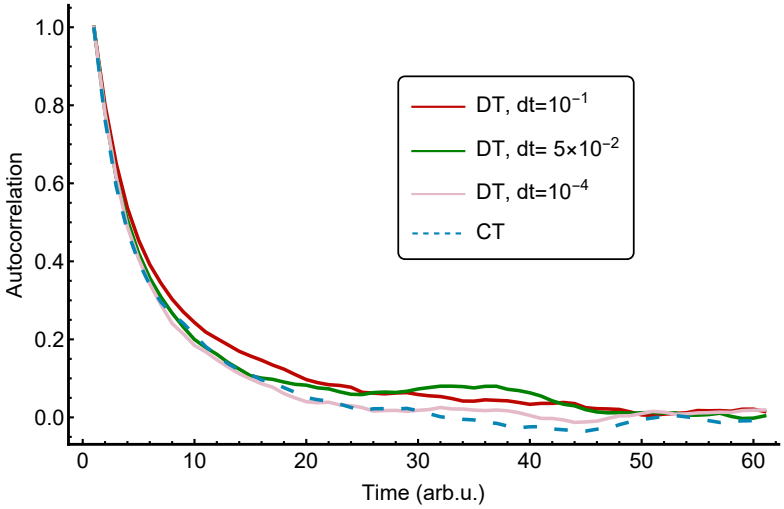

Figure 3.2: *Autocorrelation functions for choice of dt.* Sequential DT and CT algorithms are applied on an Ising chain with $N = 10$ spins and $\alpha_{2i} = 0.1, \alpha_{2i+1} = 0.3, k_BT = 2, J = 1, h = 0$. Different dt are used on the discrete algorithm. The best choice is $dt = 10^{-4}$ for the DT algorithm.

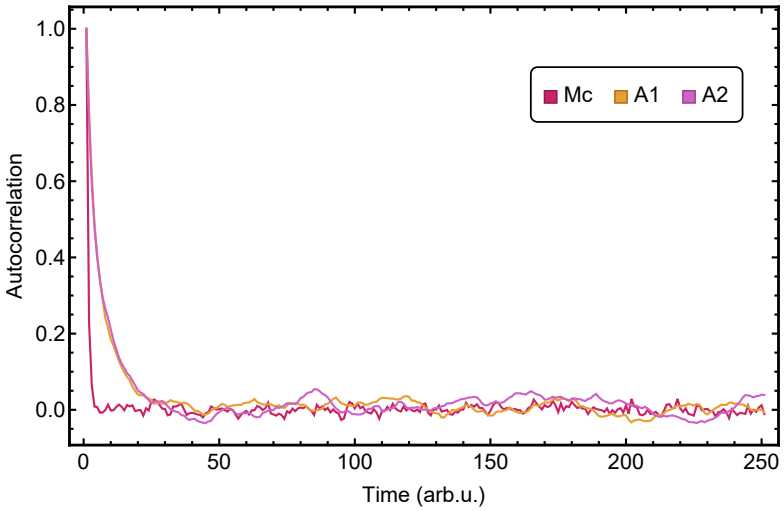

Figure 3.3: *Autocorrelation functions for choice of burn-in.* Sequential MMC, CT (with frame step $n = 1$) and DT with $dt = 10^{-4}$ algorithms are performed on an Ising chain with $N = 10$ spins and $\alpha_{2i} = 0.1, \alpha_{2i+1} = 0.3, k_BT = 2, J = 1, h = 0$. The *burn-in* are respectively equal to $100, 150 \cdot 10^4, 220$.

As it is pointed out in section 3.2-3.3, the main issue of dealing with different kinds of algorithms relies on the time-scale they are using. Thus, in order to make reliable comparisons between the results of the three different approaches, it is needed to find a method such that the time-scale is the same for all of them. For the CT and MMC algorithms it is sufficient to have same *frame step*[2], while more attention is required when dealing with the discrete time method. Indeed, as it is mentioned in section 3.2, the *autocorrelation functions* of the continuous and discrete time algorithms has been compared: since the parameter dt in the continuous algorithms represent the *internal time* (see section 3.3) *i.e.* an interval of time of the trajectory followed by system in which many flip events may occur, while dt of the discrete

[2]the dt in the CT algorithm is set to be equal to the frame step

approach is the small time during which only one spin can make an attempt, it results that, in principle, the time-scales of these two algorithms are different; to properly compare the results obtained by the DT and the CT method, the autocorrelation function, that exprimes a dependence in time, is useful to find the right time scales between the two algorithms (Figure 3.2). Once this purpose has been achieved, the *ensemble sampling* algorithms can be computed, where the choice of the *burn-in* time is made by looking at the autocorrelation functions of the three algorithms, performed using the sequential approach of Algorithm 3-4-6 (Figure 3.3). The barcharts of Figure 3.4-3.5 shows the results obtained for a chain made of $N = 10$ spins, where energy and magnetization level on the $x - axis$ indicates the different values of $\bar{H}$ and $\bar{M}$, while the counts are the number of samples that have a precise value of $\bar{H}$ and $\bar{M}$.

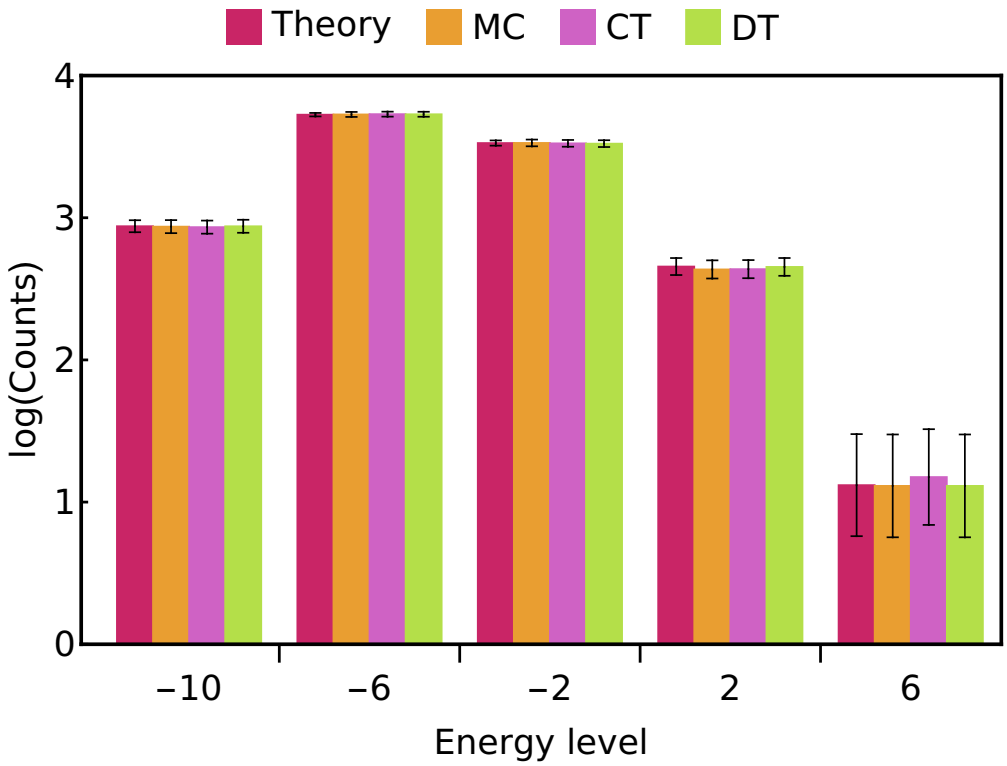

Figure 3.4: *Barchart for energy samples using ensemble sampling algorithms.* Probability distribution for energy of an Ising chain ($N = 10$ spins) in the canonical equilibrium ensemble at temperature $k_B T = 2, J = 1, h = 0$ (arb.u.). In the DT and CT models, the action rates (arb.u.) are $\alpha_i = 0.1$ for odd indices and $\alpha_i = 0.3$ for the even. Error bars are given by 3 standard deviations; each sample contains a total of 10^4 counts.

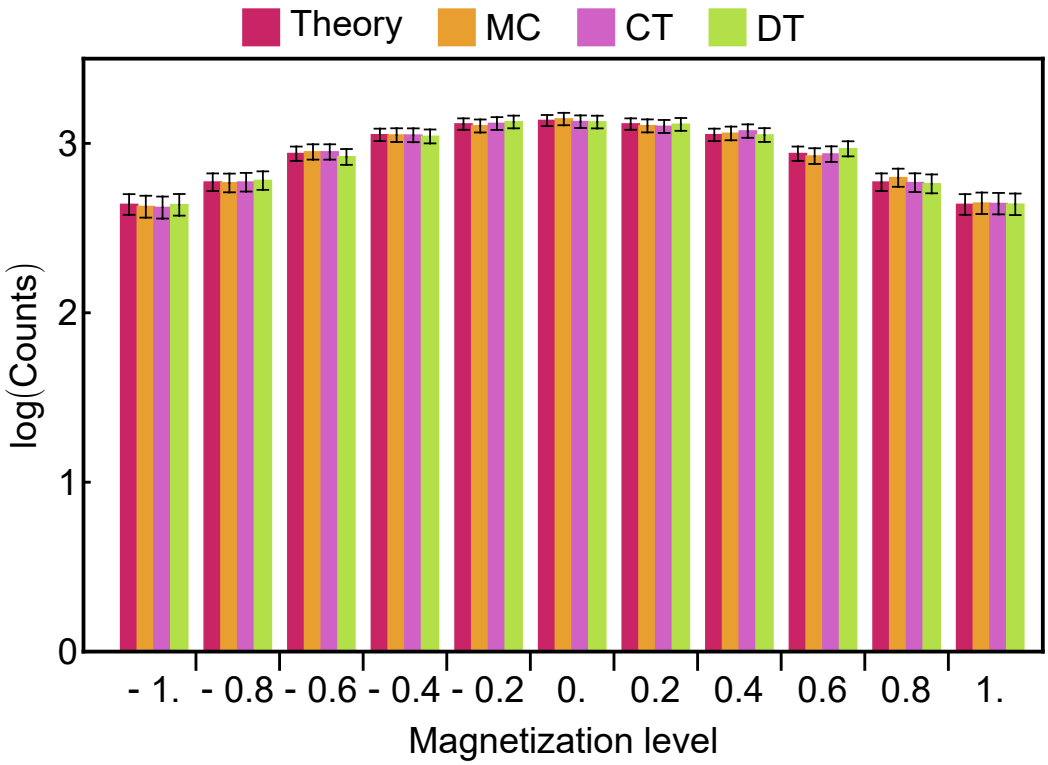

Figure 3.5: *Barchart for magnetization samples using ensemble sampling algorithms.* Probability distribution for magnetization of an Ising chain ($N = 10$ spins) in the canonical equilibrium ensemble at temperature $k_BT = 2, J = 1, h = 0$ (arb.u.). In the DT and CT models, the action rates (arb.u.) are $\alpha_i = 0.1$ for odd indices and $\alpha_i = 0.3$ for the even. Error bars are given by 3 standard deviations; each sample contains a total of 10^4 counts.

Both Figure 3.4-3.5 show the accordance on the outcome between the three algorithm, as well as with the theory. Besides these qualitative results, one should also evaluate if the approaches are quantitatively the same. In order to do so, a one sample *Likelihood ratio* statistical test with *William's correction* [93, 94] (Appendix D) has been performed and of which the *null hypothesis* consists in supposing that energy and magnetization samples of the three algorithms come from the same distribution of the theoretical one, where the latter is a multinomial distribution $\mathcal{M}(n, k, \boldsymbol{p})$ with n being the total number of samples, k the different energy/magnetizaton levels the system can account for and $\boldsymbol{p} = (p_1, \dots p_k)$ being the theoretical probability of the system to belong to a level $i = 1, \dots, k$ (Equation 3.3). The results are shown in Table 3.1.

	Energy pvalue	Magnetization pvalue
MMC	0.986	0.735
DT	0.996	0.591
CT	0.966	0.801

Table 3.1: *Likelihood ratio test - pvalues.* Results on the pvalues of the test both for energy and magnetization samples. *Null hypothesis* H_0 : energy and magnetization samples of the algorithms come from the same distribution of the theoretical ones.

Algorithm 7 Theoretical quantities - Ising Chain

Initialize empty dictionary H
Initialize empty dictionary M
Generate 2^N configurations $\boldsymbol{\sigma}$ ▷ N is the number of spins
for each configuration $\boldsymbol{\sigma}$
  evaluate energy level h
  evaluate magnetization level m
  Set key of H equal to h
  H[key $= h$] $+=$ $\mathrm{e}^{-h/T}$ ▷ $\mathrm{e}^{-h/T}$ is the weight
  Set key of M equal to m
  M[key $= m$] $+=$ $\mathrm{e}^{-h/T}$ ▷ $\mathrm{e}^{-h/T}$ is the weight
end for
Initialize $Z_h = 0$
Initialize $Z_m = 0$
for each different key h
  $Z_h = Z_h +$ number of different $\boldsymbol{\sigma}$ giving h
end for
Normalize weights of H by Z_h ▷ obtaining probabilities

for each different key m
  $Z_m = Z_m +$ number of different $\boldsymbol{\sigma}$ giving m
end for
Normalize weights of M by Z_m ▷ obtaining probabilities

Simulations for different values of the parameters and with number of spins $N > 80$ [3] are shown in Appendix E.

[3]For $N > 80$ is computationally to expensive obtaining the theoretical distributions thus,

3.5.2 Response to temperature perturbation

Once the observables have been obtained, it is possible to try evaluating how they vary when one or more parameters of the system change. In the present work, it will be analyzed how the energy of the Ising chain will respond when a sudden change on the temperature will happen. At time $\bar{t}$, the temperature will pass from a value T_0 to a value T with a step-function behavior and, if $\Delta T = T - T_0$ is relative small, one may apply the linear response formalism of subsection 2.3.1. From a computational point of view, the time evolution of the system has been obtained by using a simulation based on a combination of both the *burn-in* and the *average trajectories* algorithms (section 3.4). The idea is to create a final trajectory given by the mean of the different ones of which initial states are obtained by using the *ensemble sampling* algorithm. In Figure 3.6 it is shown the trajectory followed by the system of an Ising Chain with $N = 10$ spins[4]. Such trajectory is the results of the average of 10^4 trajectories. At simulation time $\bar{t} = 10$ the temperature suddenly change from $T_0 = 1.8$ to $T = 2$ and in the MMC algorithms, as well as the DT and the CT ones, the system relaxes to the new equilibrium state following an exponential behaviour. Since the Ising chain is composed of $N = 10$ spins, it is possible to evaluate the theoretical average energy of the system at both temperatures T_0 and T (straight line in Figure 3.6). The simulations of all the three methods are in accordance with the theoretical averages, however it exist a main difference between the classical *Metropolis Monte Carlo* algorithm and the discrete, as well as the continuous time approach; since the last two methods make use of the *action rates*, when these parameters change, it is possible to see a different relaxation behavior of the system to the new equilibrium state. Such effect is not possible in the case of an MMC simulation because it does not have any parameters able to control how fast or slower the dynamic of the system can be. Indeed, for generally lower $\alpha_i(\sigma_i)$, the curves are smoother, while when the $\alpha_i(\sigma_i)$ increase, the system will go rapidly to the new equilibrium state.

different statistical test and graphical techniques will be used.

[4]Results with $N \neq 10$ are shown in Appendix E.

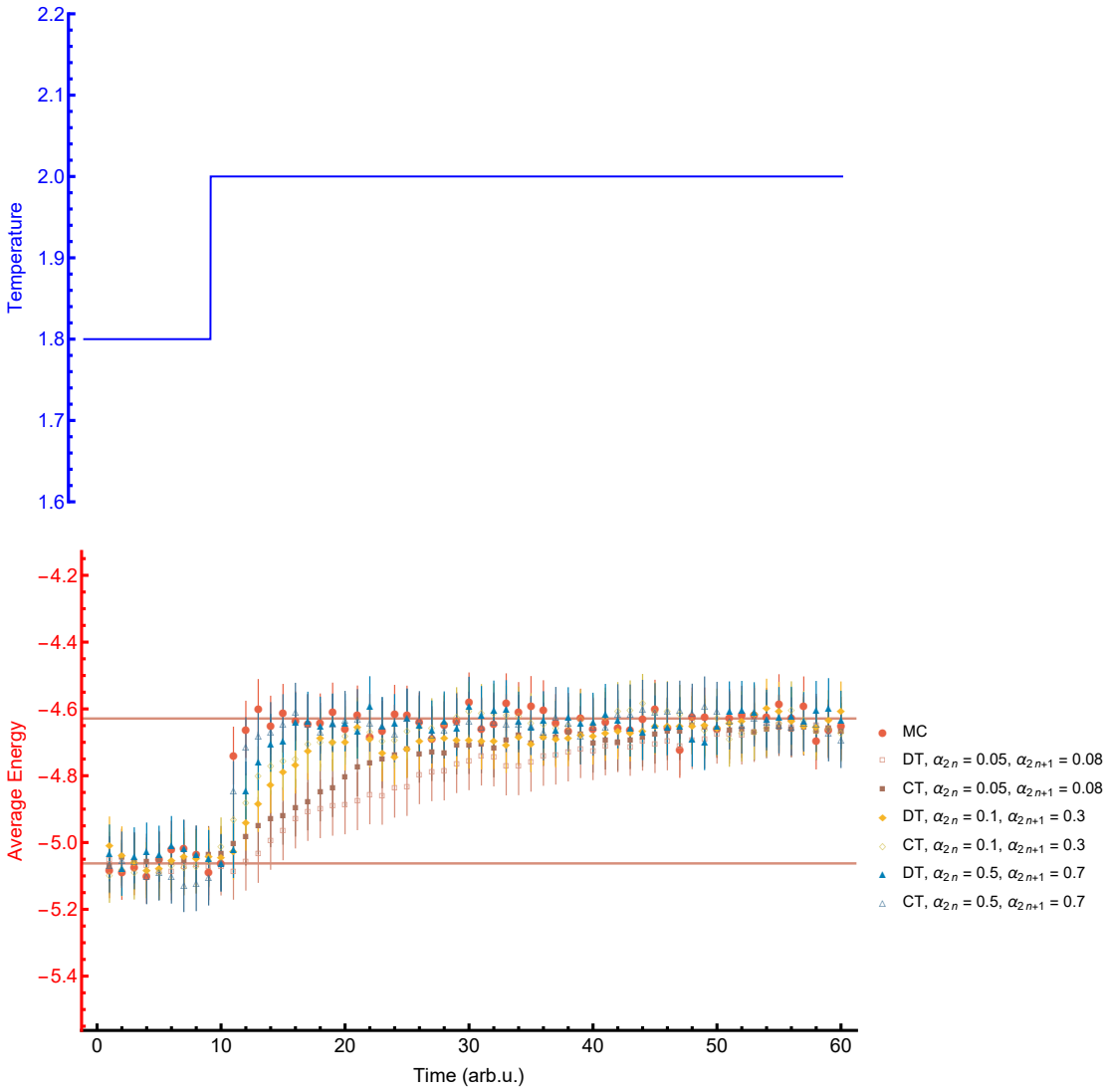

Figure 3.6: *Linear response of energy due to a temperature perturbation.* The *average trajectories* algorithm, combined with the *burn-in* algorithm, averages 10^4 trajectories over the interval of time $I = [0, 60]$. At time $\bar{t} = 10$, the temperature of the system change and $\Delta T = 0.2$. The DT algorithm is implemented with $dt = 10^{-4}$. The CT and DT algorithms are evaluated with different combination of $\alpha_i(\sigma_i)$. Straight lines indicate the theoretical average energies. Results of the three algorithm agree within 3 standard deviation.

Chapter 4

Dynamic Cellular Potts Model

4.1 Dynamic Cellular Potts

One of the first attempt to explain the mechanism behind tissue morphogenesis relies on the *differential adhesion hypothesis* (DAH), a thermodynamic interpretation stating that the movement made by the cells to self-organize, is dictated by the minimization of their interfacial free energy [49]. However, such thermodynamic view is concerning only about equilibrium configurations and not about the kinetics. Instead, Glazier and Graner have shown, in the context of cell sorting, the key role played by membrane fluctuations [4]; experimentally it is possible to introduce drugs able to block membrane fluctuations and thus inhibit cell sorting. Nevertheless, such drugs act also at the cytoskeleton level, making impossible to distinguish if the failure to observe sorting is due to absence of membrane fluctuations or changes in cell-cell adhesivity, in response to the changes of the cytoskeleton. Through Glazier and Graner simulations it has been possible to show that the loss of membrane fluctuations is actually deterministic on preventing cell sorting [95]. Despite of being of thermal nature, membrane fluctuations are generally caused by cellular activity [96] and its mechanical properties highly influence cell motility [97]. In the CPM the temperature parameter resembles cellular activity, thus cell motility is implemented in function of T and it manifests itself through the movement of the cells' center of mass. Such method lacks on describing mechanical proprieties of the cell membrane influencing motility, therefore a more realistic kinetic is worthy of attention and the *Dynamic Cellular Potts* model aims to provide different kinetics rules resembling properties of the cells, on the basis of what it has been done concerning transport properties of composite materials [81].

4.1.1 Cell Sorting in the development of mammals

Cell sorting is the process leading the segregation of heterotypic cell aggregates and, in the present work, the *Dynamic Cellular Potts* is used for simulating cell sorting in the development of a mammal, as described in [11]. The early embryogenesis process starts with the formation of the *blastocyst* in which it is possible to distinguish between the outer layer of cells, called *trophectoderm* (TE) and the inner collection of cells referred as *inner cell mass* (ICM). The latter is located in one side of the blastocyst so that it is present a cavity filled of fluid, denominated *blastocoel*. The trophectoderm will develop into structures that help the implant of the embryo in the uterus, while the ICM will differentiate into *epiblast* (EPI) that will form the fetus and the *primitive endoderm* (PrE). The differentiation of these two cells has been shown to happen at stage E3.75 (where one must refers to them as pEPI and pPrE respectively), while the lineage sorting is verified at stage E4.75 in which the EPI are incapsulated between the trophectoderm and the layer of PrE (Figure 4.1).

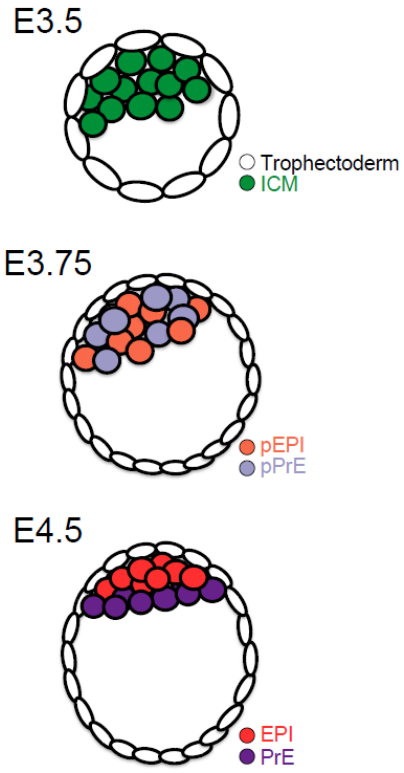

Figure 4.1: *Cell sorting [11].* At stage E3.5 ICM and TE are formed. The differentiation between EPI and PrE cells takes place at E3.75, while the sorting of the two types of cells is completed at stage E4.5

4.1.2 Microscopic Stochastic Kinetics

The cellular sorting described in subsection 4.1.1 presents two types of cells that organize in an environment filled of a fluid, scenario that can be properly modelled through a CPM approach. Indeed, as a modified version of the CPM, the *Dynamic Cellular Potts* (DCPM) assigns at the two kinds of cells (EPI and PrE) a type represented through a natural number, while the medium is indicated with value zero. Furthermore, the DCPM is coupled with a microscopic stochastic kinetics that, at equilibrium, can be described as following: each lattice site which can indicate either a cell of type EPI or PrE, as well as the medium, can make an attempt to change its value with an *action rate* that generally depends on the cell type and usually indicated as $\alpha(\sigma_E)$, $\alpha(\sigma_P)$ or $\alpha(\sigma_M)$ respectively. In each attempt, the site has a probability to change its value or to keep it, proportional to a *directing function*. More precisely:

$$\mathbb{P}(\sigma_E \to \sigma_P|\text{attempt}) \propto \mathrm{e}^{L(\sigma_P)} \qquad \mathbb{P}(\sigma_{PrE} \to \sigma_E|\text{attempt}) \propto \mathrm{e}^{L(\sigma_E)}$$
$$\mathbb{P}(\sigma_M \to \sigma_E|\text{attempt}) \propto \mathrm{e}^{L(\sigma_E)} \qquad \mathbb{P}(\sigma_M \to \sigma_P|\text{attempt}) \propto \mathrm{e}^{L(\sigma_P)}$$

It is worth noticing that, when non-equilibrium processes (such as the death of the cell) are not present, it does not exist a spontaneous transition from an EPI or PrE state to a medium (M) state. Instead, it is possible that a site indicated the medium changes its value in EPI or PrE, thus simulating the expansion of such cells types to an other lattice site. Therefore, the unconditional probabilities of making a change can be expressed as:

$$\mathbb{P}(\sigma_E \to \sigma_P) = \alpha(\sigma_E)dt\frac{\mathrm{e}^{L(\sigma_P)}}{Z}$$

$$\mathbb{P}(\sigma_P \to \sigma_E) = \alpha(\sigma_P)dt\frac{\mathrm{e}^{L(\sigma_E)}}{Z}$$

$$\mathbb{P}(\sigma_M \to \sigma_E) = \alpha(\sigma_M)dt\frac{\mathrm{e}^{L(\sigma_E)}}{Z}$$

$$\mathbb{P}(\sigma_M \to \sigma_P) = \alpha(\sigma_M)dt\frac{\mathrm{e}^{L(\sigma_P)}}{Z}$$

with Z being a normalization constant.

Supposing the feasibility for a change of a value site in terms of connectivity (Figure 1.8) and that the system is in equilibrium, one can derive the expression for the variation of the directing functions by using detailed balance:

$$\mathbb{P}(\sigma_E)\mathbb{P}(\sigma_E \to \sigma_P) = \mathbb{P}(\sigma_P)\mathbb{P}(\sigma_P \to \sigma_E)$$

$$\mathrm{e}^{-\beta H(\sigma_E)}\alpha(\sigma_E)\mathrm{e}^{L(\sigma_P)} = \mathrm{e}^{-\beta H(\sigma_P)}\alpha(\sigma_P)\mathrm{e}^{L(\sigma_E)}$$

$$\mathrm{e}^{\underbrace{L(\sigma_P) - L(\sigma_E)}_{\Delta L(E\to P)}} = \frac{\alpha(\sigma_P)}{\alpha(\sigma_E)}\mathrm{e}^{-\beta[\underbrace{H(\sigma_P) - H(\sigma_E)}_{\Delta H(E\to P)}]}$$

$$\Rightarrow \mathrm{e}^{\Delta L(E\to P)} = w_E = \frac{\alpha(\sigma_P)}{\alpha(\sigma_E)}\mathrm{e}^{-\beta\Delta H(E\to P)} \tag{4.1}$$

Likewise, for the other possible changes, one can write:

$$\mathrm{e}^{\Delta L(P\to E)} = w_P = \frac{\alpha(\sigma_E)}{\alpha(\sigma_P)}\mathrm{e}^{-\beta\Delta H(P\to E)}$$

$$\mathrm{e}^{\Delta L(M\to E)} = w_{ME} = \frac{\alpha(\sigma_E)}{\alpha(\sigma_M)}\mathrm{e}^{-\beta\Delta H(M\to E)} \tag{4.2}$$

$$\mathrm{e}^{\Delta L(M\to P)} = w_{MP} = \frac{\alpha(\sigma_P)}{\alpha(\sigma_M)}\mathrm{e}^{-\beta\Delta(M\to P)}$$

4.1.3 The Algorithm

The *Dynamic Cellular Potts* model has been simulated in three dimension, thus the unit of the lattice is a cube, usually called *voxel*, as it is shown in Figure 2.1(c). Therefore, a cell is made of voxels with the same *index* and that have the same *type* (Figure 4.2). Besides its type, the cell is characterized also by its *age, target volume* and *division volume*. The latter is randomly sampled from a division volume distribution, obtained experimentally, while the target/preferred volume, at initial time, is set to be equal to half of the mean of the possible division volumes, but it changes during the simulation according to a *growth rate*, set a priori and which may vary with the type EPI or PrE. Thus, the algorithm is capable of simulating *cell growth*, as well as other non-equilibrium processes, like *division* and *death*. Indeed, the first step of the algorithm consists in checking, for each cell in the simulation lattice, if the latter will die or divide; if the death probability is larger than a random value sampled from a uniform distribution, the cell will be killed *i.e.* each of its voxel will become medium, while the division will occur when the cell volume reaches the division one. In the latter case, the mother cell will be divided along its long axis in two cells with same type of the parent cell and of volume equal to half of the volume of the latter. Furthermore, the age, the preferred and the division volume of the daughters cells will be set and their center of mass will be computed as well. Besides their structural properties and according to the kinetics rules described in the previous section, at each voxel of a cell is associated an *action rate* which express the tendency of the voxel to modify its type. Indeed, after the death and division check, the algorithm will evaluate the probability of a value change of each voxel in the simulation lattice. Firstly, the set of *target neighborhood* relative to the current voxel site is computed, considering it as a Von Neuomann neighborhood in three dimension (Figure 4.3(a)). The voxel will try to change its value if its *action probability* is larger than a random value sampled from a uniform distribution, otherwise it will not even make the attempt. The time *dt* in which an attempt is made, is taken so small that only one change is allowed at each step. If the voxel succeeds to make the attempt, an energy base is evaluated according to the expression of Equation 1.1, considering the current index and type of the voxels

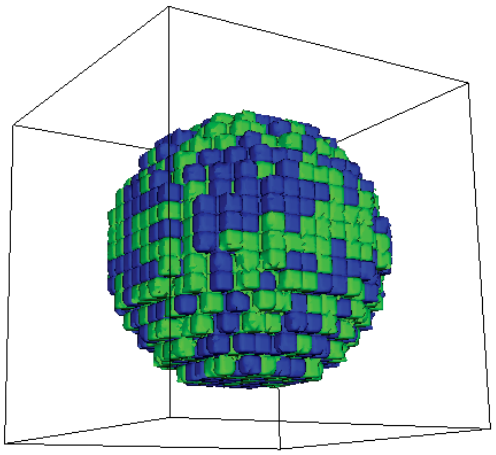

Figure 4.2: *CPM in 3D [98].* Typical simulation of a CPM with cells in the three-dimensional lattice.

being the lattice site x and composing the cell γ. At the energy base will be added another energy term, still of the type of Equation 1.1, but with index and voxel type corresponding respectively to the ones of the target site the current voxel may change to. In each of these energy terms, the part corresponding to the interface interaction between cells is evaluating considering a *coupling neighborhood* of order II (Moore) in three dimension (Figure 4.3(b)). At the end of this process, at each voxel that has tried to change, correspond a vector of length equal to the number of its target neighbours, filled with the weights given by Equation 4.1-4.2, according to the type of the voxel taken into account. In order to prevent fragmentations, before allowing a voxel to change its type, it must be verified if the target sites respects the notion of connectivity of [55], already introduced in subsection 1.2.2. With this check, the possibilities of the current voxel to make a change may be reduced to those of which the target value respects connectivity. The latter control allows to compute the normalization factor Z, given by the sum of all the weights that respect the connectivity requirement. Given the value of Z, it is possible to evaluate the probabilities and the voxel type and index will change to the one of the target site in correspondence of which the sum of such probabilities is larger than a certain threshold. Once the algorithm has computed these steps, for each voxel of the three-dimensional lattice, all the cells are let to grow according to their *growth rates*, their ages are incremented and, at the end, the simulation time is updated. A scheme of the present algorithm is shown in Algorithm 8.

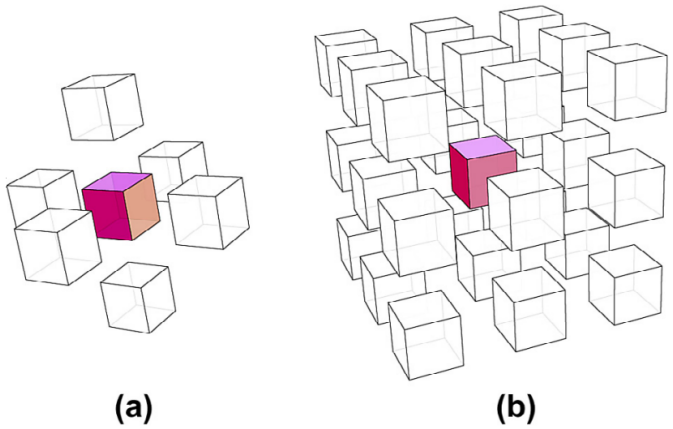

Figure 4.3: *Neighborhood in 3D [99].* (a) Von Neumann in three dimension. (b) Moore neighborhood in three dimension.

Algorithm 8 Dynamic Cellular Potts Algorithm (DCPM)

Initialize a starting configuration $\boldsymbol{\sigma}_0$ ▷ $\boldsymbol{\sigma}_0$ refers to all the cells in the 3D simulation lattice
while $t < \tau$ **do** ▷ τ is the total simulation time
  for cell **in** lattice:
    Check death and division of the cell
  end for
  for voxel **in** lattice:
    Compute *target neighborhood* N_T
    Store target voxel in V_T
    if length of V_T is 1 **exit**
    Compute *action probability* α ▷ α depends on the type of the voxel
    if $\alpha < u$, $u \sim U(0,1)$ **exit**
    Evaluate *energy_base* H_b ▷ H_b is evaluated with Equation 1.1 using voxel
    for target voxel in V_T
      Evaluate $H = H_b + H_t$ ▷ H_t is evaluated with Equation 1.1 using target voxels
      Compute weights $\boldsymbol{w}$ ▷ $\boldsymbol{w}$ are evaluated using Equation 4.1-4.2
      Store $\boldsymbol{w}$ in *buffer*
    end for

    Check connectivity of voxel in N_T ▷ the connectivity refers to [55]
    Discard from V_T target voxels not respecting connectivity
    Keep the weights on $\boldsymbol{w}$ of voxels in V_T
    $Z = \sum_i \boldsymbol{w}_i$ ▷ Z is the normalization factor
    Compute probabilities $\boldsymbol{p} = \boldsymbol{w}/Z$ ▷ $\boldsymbol{p}$ is a vector whose indices correspond to indices of V_T
    Set a threshold s
    Initialize $P = 0$
    for i in $\boldsymbol{p}$
      $P = P + i$
      if $P > s$ voxel $= (V_T)_i$ **exit** ▷ Change the current voxel to one of its allowed target
    end for
  end for

  for cell **in** lattice:
    Compute growth of the cell
    Update age of the cell
  end for
  t = t + 1
end while

4.1.4 Results

The cell sorting phenomena has been simulated in a three-dimensional lattice of which elementary units are *voxels* (Figure 4.4). Therefore, the first step of the simulation is creating the elementary voxels, where the ones with same cell indexes compose a cell. In Figure 4.5 is shown the output of a simulation carried for a time $t = 5040$ that creates 81 different cells. By increases the simulation time, the number of cells generated grow.

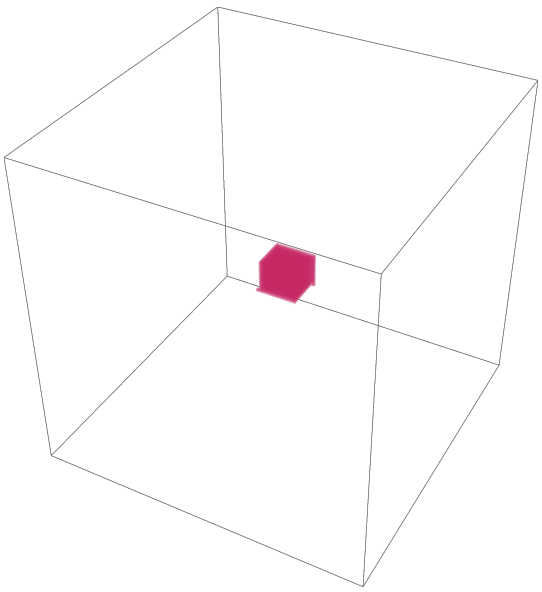

Figure 4.4: *Cell sorting simulation in 3D.* The simulation lattice is a cube and the elementary unit is a voxel.

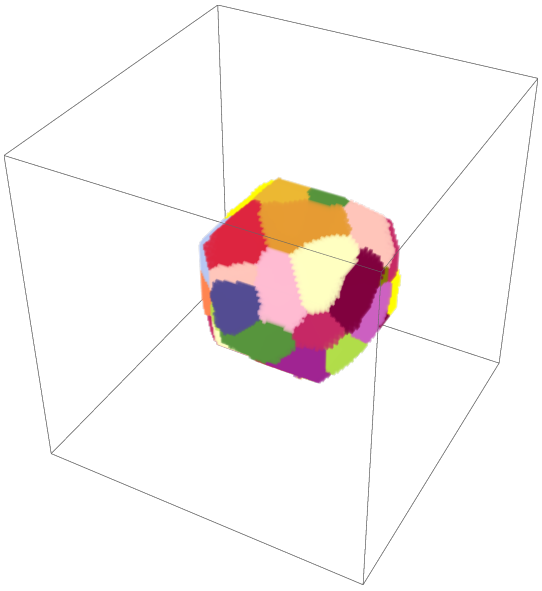

Figure 4.5: *Cell sorting simulation in 3D.* The voxel with same indeces compose a cell. The different color indicates different cells.

Given all the different cells, at each of them is randomly assigned a type (Figure 4.6). The physical parameters such as the surface tension values between different types of cells, as well as the growth and division rate are defined for the different kind of cells. Moreover, the *action probabilities* for the *medium, epiblast* and the *primitive endoderm* are set. A simultation of total time $t = 1440$ is performed and the final sorting is shown in Figure 4.7. The organized cluster of cells is correctly reproduced; the PRE cells (green colors) occupies the outer layer which covers the EPI cells (blue) that indeed are located between the *trophectoerm* and the PRE cells.

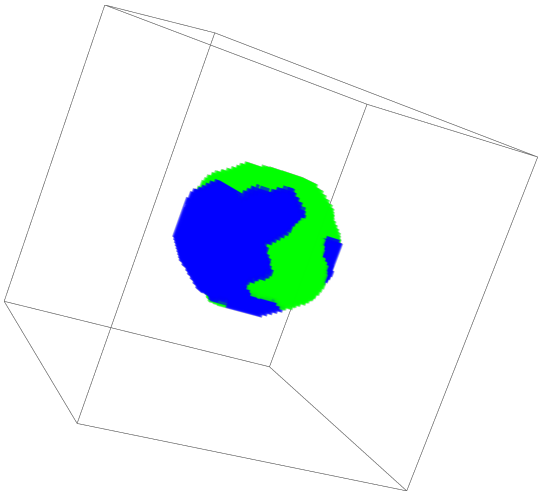

Figure 4.6: *Cell sorting simulation in 3D.* Each cell has a type, distinguished by colors. The green cells are PRE cells, while the blue ones are EPI. The action probabilities are $\alpha(\sigma_M) = 0.1, \alpha(\sigma_{EPI}) = 0.5\alpha(\sigma_{PRE}) = 0.2$

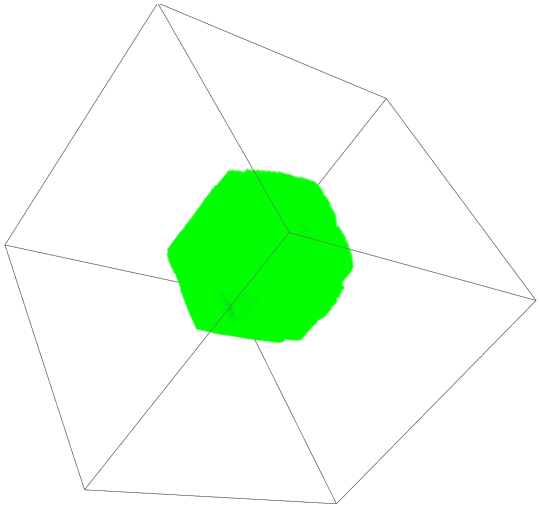

Figure 4.7: *Cell sorting simulation in 3D.* The simulation reproduces the cell sorting phenomena of subsection 4.1.1. The outer PRE cells (green) incorporate an inner cluster of EPI cells (blue).

Chapter 5

Conclusion and future research

The present work introduces a novel approach to modeling dynamics of discrete-state systems, which relies on recent developments in the stochastic thermodynamics. An application of the framework is demonstrated with a *Cellular Potts Model* of cell sorting in mouse embryogenesis—a subject of active research in biology. By using the paradigmatic example of Ising chain, it has been examined in more detail the theoretical foundations of the approach and verified it numerically.

The new formulation of Cellular Potts Models provides an immediate physical interpretation of the model parameters describing cell sorting mechanism, in continuous and discrete time, removes shortcomings of the modified Monte-Carlo Metropolis algorithm adopted in the traditional schemes and offers a finer control of the system's kinetic properties. Such properties can be interpreted as intrinsic characteristics of cells and determine their motility. Furthermore, straightforward computational improvements of the CPM can be sought. For instance, the discrete-time algorithm admits a simpler parallelization scheme than the traditional Monte-Carlo calculations.

The example of the Ising chain conspicuously shows that the above kinetic properties affect only *frenesy*—the time-symmetric part of the stochastic action associated with the possible trajectories of the system. The time-symmetric counterpart—entropy production—remains independent of these properties. Therefore, the new approach reproduces the distribution of the system's states determined by the Hamiltonian in the canonical equilibrium with a heat bath at temperature T, as confirmed by numerical simulations.

The new theoretical framework allows to consistently reproduce, qualitatively and quantitatively, the results both in the Ising simulations, than in the CPM case (used for the lineage sorting of EPI and PrE cells), with respect to the traditional methods used.

Appendix A

Given $\Gamma = 0,1,\ldots,n$ the set of cell indexes and S the lattice, the space configuration is defined as Γ^S.

Definition. The set of *absorbing* states A is given by all the possible constant-u configurations C_u, with $u \in \Gamma$, where all the sites $x \in S$ have cell index u

$$A := \bigcup_{u \in \Gamma} C_u$$

The set A is called absorbing (or trap) because if the chain starts in A, there is no way to get out of it.
Definition. The *return time* T_y is a random variable expressing how many steps are needed to visit y if the chain starts in y. Therefore, the probability of returning to y in a finite number of steps can be expressed as:

$$p_{y,y} = \mathbb{P}_y(T_y < \infty)$$

Definition A state y is called *transient* if $p_{y,y} < 1$.

Definition A state y is called *recurrent* if $p_{y,y} = 1$.

The transience and the recurrence are *class* properties. By the definition of *absorbing* set is possible to conclude that the states in A are recurrent.

In the case of a Markov chain, the transition probabilities can be summarized in the *transition matrix* P

$$P = \begin{pmatrix} I_A & 0_{A,T} \\ P_{T,A} & P_{T,T} \end{pmatrix}$$

where $P_{T,T}$ is a substochastic matrix containing the transition probabilities between transient states, instead the entries of the $P_{T,A}$ matrix are the probabilities to go from transient states in the set T to absorbing states in A. Since, once the chain is in A, it cannot escape from the set A, the null matrix 0_A indicates the impossibility on going from the set A to the set T.
Now, for the absorbing property, it is valid that, if the chain starts in A, it will remain in A. However, supposing that the chain starts in a state in T, one should show that the chain will eventually reach the set A. Firstly, it is needed to show that the chain will get in A, almost surely *i.e.* that, for any initial distribution over the states, it holds that:

$$\lim_{k\to\infty} \mathbb{P}(X_k \in A) = 1$$

Indeed, supposing that to get from the set T to the set A, k steps are need, one can define the transition probabilities in k steps as entries of the $k-th$ power of the transition matrix, P^k. Indicating by $\boldsymbol{\pi}_0$ the initial distribution over the states and by $\boldsymbol{\pi}_k$ the distribution at time k, it holds that $\boldsymbol{\pi}_k = \boldsymbol{\pi}_0 P^k$ and that:

$$\begin{aligned}\mathbb{P}(X_k \in A) &= \boldsymbol{\pi}_k(A) = \\ &= 1 - \boldsymbol{\pi}_k(T) = 1 - \sum_{y\in T} \boldsymbol{\pi}_k(y) = \\ &= 1 - \sum_{y\in T}\sum_{z\in T} \boldsymbol{\pi}_0(z) P^k_{T,T}(z,y)\end{aligned}$$

And taking the limit $k \to \infty$:

$$\begin{aligned}\lim_{k\to\infty} \mathbb{P}(X_k \in A) &= \lim_{k\to\infty} \left(1 - \sum_{y\in T}\sum_{z\in T} \boldsymbol{\pi}_0(z) P^k_{T,T}(z,y)\right) = \\ &= 1 - \sum_{y\in T}\sum_{z\in T} \boldsymbol{\pi}_0(z) \left(\lim_{k\to\infty} P^k_{T,T}(z,y)\right) = \\ &= 1\end{aligned}$$

where the last equality holds because $P_{T,T}$ is substochastic.

More precisely, transition probabilities from T to A in k steps, entries of the matrix $P_{T,A}$, can be derived as following:

$$P_{(T,A)_k} = \left(\sum_{j=0}^{k-1} P_{T,T}^j \right) P_{T,A}$$

and for large k:

$$\begin{aligned} \lim_{k\to\infty} P_{(T,A)_k} &= \left(\lim_{k\to\infty} \sum_{j=0}^{k-1} P_{T,T}^j \right) P_{T,A} = \\ &= (I_T - P_{T,T})^{-1} P_{T,A} \end{aligned}$$

where the last equality holds because:

$$\begin{aligned} (I_T - P_{T,T}) \left(\sum_{j=0}^{k-1} P_{T,T}^j \right) &= (I_T - P_{T,T})(I_T + P_{T,T} + P_{T,T}^2 + \dots P_{T,T}^{k-1}) = \\ &= I_T - P_{T,T} + P_{T,T} - P_{T,T}^2 + P_{T,T}^2 + .. - P_{T,T}^{k-1} + P_{T,T}^{k-1} - P_{T,T}^k \end{aligned}$$

and for $k \to \infty$:

$$\begin{aligned} (I_T - P_{T,T}) \left(\lim_{k\to\infty} \sum_{j=0}^{k-1} P_{T,T}^j \right) &= I_T \\ \Rightarrow \lim_{k\to\infty} \sum_{j=0}^{k-1} P_{T,T}^j &= (I_T - P_{T,T})^{-1} \end{aligned}$$

Appendix B

In order to show that the one-dimensional Ising model does not show phase transition, it is useful to reformulate the Hamiltonian in Equation 2.2 by symmetrizing the field term:

$$H = -h\sum_{i=1}^{N-1}\frac{s_i + s_{i+1}}{2} - J\sum_{i=1}^{N} s_i s_{i+1} = \\ = \sum_{i=1}^{N-1} H_{nn}(s_i, s_{i+1})$$

where the last equality is due to the fact that is now possible to rewrite the Hamiltonian totally in function in s_i and s_{i+1}.
The partition function Z will be:

$$Z_N = \sum_{s_1}\sum_{s_2}\cdots\sum_{s_N}\exp[-\beta H_{nn}(s_1, s_2) - \beta H_{nn}(s_2, s_3)\cdots - \beta H_{nn}(s_N, s_1)] = \\ = \sum_{s_1}\sum_{s_2}\cdots\sum_{s_N} T(s_1, s_2)T(s_2, s_3)\ldots T(s_N, s_1)$$

where

$$T(s, s') = \exp[-\beta H(s, s')]$$

can be seen as an element of what is called *Transfer matrix* $\hat{T}$ *i.e.* $T(s, s') = \hat{T}_{s,s'}$.
The transfer matrix $\hat{T}$ is such that:

$$\hat{T} = \begin{bmatrix} e^{\beta(h+J)} & e^{-\beta J} \\ e^{-\beta J} & e^{\beta(-h+J)} \end{bmatrix}$$

since s, s' can only assume value ± 1.
The partition function can be thus rewritten as:

$$Z_N = \sum_{s_1}\sum_{s_2}\cdots\sum_{s_N}\hat{T}_{s_1,s_2}\hat{T}_{s_2,s_3}\ldots\hat{T}_{s_N,s_1} = \\ = \sum_{s_1=\pm 1}\hat{T}^N_{s_1,s_1} = Tr(\hat{T}^N) = \lambda_1^N + \lambda_2^N$$

since it holds that $\sum_{s_i=\pm 1} \hat{T}_{s_{i-1},s_i} \hat{T}_{s_i,s_{i+1}} = \hat{T}^2_{s_{i-1},s_i}$. The parameter λ_1^N and λ_2^N instead indicates the eigenvalues of $\hat{T}$, obtained by solving the characteristic equations

$$\lambda^2 - Tr(\hat{T}^N) + det(\hat{T}) = 0$$

which gives

$$\lambda_{1,2} = \mathrm{e}^{\beta J} cosh(\beta h) \pm \sqrt{sinh^2 \beta h + \mathrm{e}^{-4\beta J}}$$

The free energy density is:

$$\begin{aligned} F &= -k_B T ln Z_N = -k_B T ln(\lambda_1^N + \lambda_2^N) = \\ &= -k_B T ln \left[\lambda_1^N \left(1 + \left(\frac{\lambda_2}{\lambda_1} \right)^N \right) \right] = \\ &= -k_B T ln \lambda_1^N - k_B T ln \left[1 + \left(\frac{\lambda_2}{\lambda_1} \right)^N \right] \simeq -N k_B T ln \lambda_1 \end{aligned}$$

since in the thermodynamic limit $N \to \infty$, $\frac{\lambda_2}{\lambda_1} << 1$ Now, the magnetization density m is given by:

$$\begin{aligned} M &= -\frac{1}{N} \frac{\partial F}{\partial h} \overset{N \to \infty}{\simeq} -\frac{1}{N} \frac{\partial}{\partial h} \left[-N k_B T ln \lambda_1 \right] = \\ &= k_B T \frac{\partial ln \lambda_1}{\partial h} = k_B T \frac{\partial}{\partial h} \left\{ ln \left[\mathrm{e}^{\beta J} \left(cosh(\beta h) + \sqrt{sinh^2(\beta h) + \mathrm{e}^{-4\beta J}} \right) \right] \right\} \end{aligned}$$

And, by solving the last derivitive one obtain:

$$M = \frac{sinh(\beta h)}{\sqrt{sinh^2(\beta h) + \mathrm{e}^{-4\beta J}}}$$

So, it is immediate to notice that, for $h = 0$, it would always be $m = 0$ and so the model is not able to predict spontaneous magnetization at any temperature.

Appendix C

The system introduced in section 2.3 provides that a microstate Γ defines the positios and momenta of the atoms composing the systems. In the *canonical ensemble*, the system is in contact, through rigid walls, with an heat bath at constant temperature T. Indicating by E_B the the energy of the bath and by $H(\Gamma)$ the energy of the system (in terms of Hamiltonian since it describes the dynamic), one can say that the total energy is:

$$E_T = E_B + H(\Gamma)$$

Indicating by $\Omega'_B(\Gamma')$ the number of bath's microstates and by S'_B its entropy when the system is in microstate Γ', the probability that the system is in microstate Γ' can be thought as proportional to Ω'_B:

$$\mathbb{P}(\Gamma') \propto \Omega'_B = \mathrm{e}^{\frac{S'_B}{k_B}}$$

where the last equality is due to the relation $S = k_B ln\Omega$. If the system goes from Γ' to Γ'', the ratio of the probabilities to be in that states is:

$$\frac{\mathbb{P}(\Gamma'')}{\mathbb{P}(\Gamma')} = \mathrm{e}^{[S''_B - S'_B]/k_B}$$

and for the bath:

$$dS_B = \frac{1}{T_B}(dE_B + p_B dV_B - \mu_B dN_B) = \frac{1}{T_B} dE_B$$

where the last equality holds since there is no mechanical, neither chemical work. Integrating:

$$\Delta S_B = \frac{\Delta E_B}{T_B} = -\frac{H(\Gamma'') - H(\Gamma')}{T_B} = -\frac{H(\Gamma'') - H(\Gamma')}{T}$$

since the temperature T of the system coincides with the ones of the bath. At this point, it possible to rewrite:

$$\frac{\mathbb{P}(\Gamma'')}{\mathbb{P}(\Gamma')} = \mathrm{e}^{-[H(\Gamma'')-H(\Gamma')]/k_B T}$$
$$\frac{\mathbb{P}(\Gamma')}{\mathrm{e}^{-H(\Gamma')/k_B T}} = \frac{\mathbb{P}(\Gamma'')}{\mathrm{e}^{-H(\Gamma'')/k_B T}} \equiv \frac{1}{Z}$$

From where:

$$\mathbb{P}(\Gamma) = \frac{\mathrm{e}^{-H(\Gamma)/k_B T}}{Z}$$

Appendix D

The one-sample *likelihood ratio* test bases its idea on verify how the *likelihood* functions of a sample differs from the reference (theoretical) one. The *null hypothesis* H_0 states that the two samples come from the same distribution. The likelihood function expresses how likely the observed sample has been generated by a given set of parameter $\boldsymbol{\theta}$ so, given $\boldsymbol{\theta}$ and a sample $\boldsymbol{X}$ of n observation, the likelihood function is defined as:

$$\mathcal{L}(\boldsymbol{\theta}|\boldsymbol{X}) = \mathbb{P}_{\boldsymbol{\theta}}(\boldsymbol{X} = x_1, x_2, ..., x_n)$$

Thus, if H_0 is true, one would expect that the set of parameter of the theoretical distribution $\boldsymbol{\theta}$ and the ones relative to the observed distribution $\hat{\boldsymbol{\theta}}$ would give likelihoods that do not differ much. The statistic of such test is given by the formula:

$$\lambda_{LR} = -2[l(\boldsymbol{\theta}) - l(\hat{\boldsymbol{\theta}})]$$

where l indicates the logarithm of the likelihood function.
In the case of section 3.5 the set of parameters corresponds to the set of probabilities of the energy or magnetization level, so the test will compare the two *likelihoods*, one computed by using the theoretical probabilities as given by Equation 3.3 and the other by using the estimated ones. Given k levels and indicating with $\pi_{i,i=1,...k}$ the theoretical probabilities and by $p_i = \frac{x_i}{n}$ the observed probabilities, where n is the total number of observation and x_i the counts for the level i, it is possible to evaluate the likelihoods of the multinomial distribution[1] as:

$$\mathcal{L}_{theory} = n! \prod_{i=1}^{k} \frac{\pi_i^{x_i}}{x_i!}$$

$$\mathcal{L}_{estimated} = n! \prod_{i=1}^{k} \frac{p_i^{x_i}}{x_i!}$$

[1] the counts per level are distributed as a multinomial.

Now, the the statistic will be:

$$\begin{aligned}\lambda_{LR} &= -2\left[log\left(n!\prod_{i=1}^{k}\frac{\pi_i^{x_i}}{x_i!}\right) - log\left(n!\prod_{i=1}^{k}\frac{p_i^{x_i}}{x_i!}\right)\right] \\ &= -2\left[\sum_{i=1}^{k} x_i log\left(\frac{\pi_i}{p_i}\right)\right]\end{aligned}$$

If H_0 is true, as the number of observation n increases[2], the statistic distributes as a $\chi^2(k-1)$ and so the pvalue is given by the incomplete gamma $\Gamma(k-1, \lambda_{LR})$. However the statistic is usually modified with the factor of the Williams' correction [94].

[2]in the case of section 3.5 $n = 10^4$

Appendix E

Further results for a chain with $N = 10$ spins have been obtained by setting $k_B T = 2, h = 0.4, J = -1$ and $\alpha_{2i} = 0.1, \alpha_{2i+1} = 0.3$. The results are shown in the following:

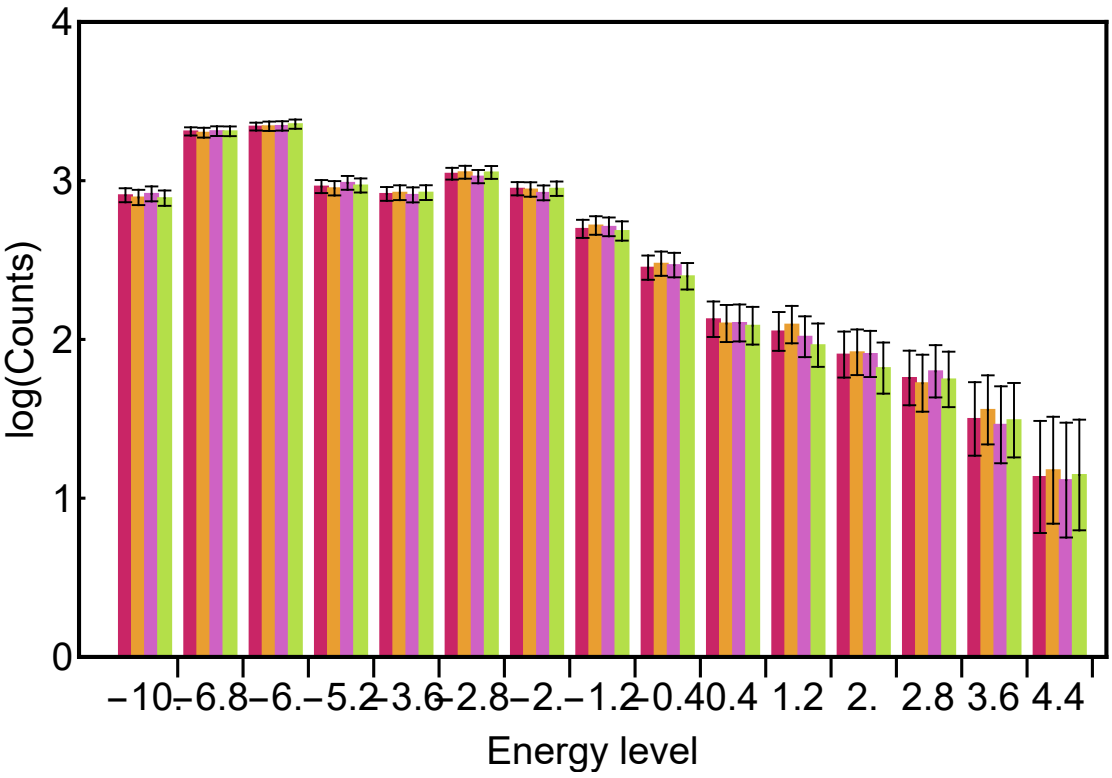

Figure E.1: *Barchart of energy, $N = 10$ spins.* Sample of 10^4 observation. In the DT algorithm the parameter $dt = 10^{-4}$.

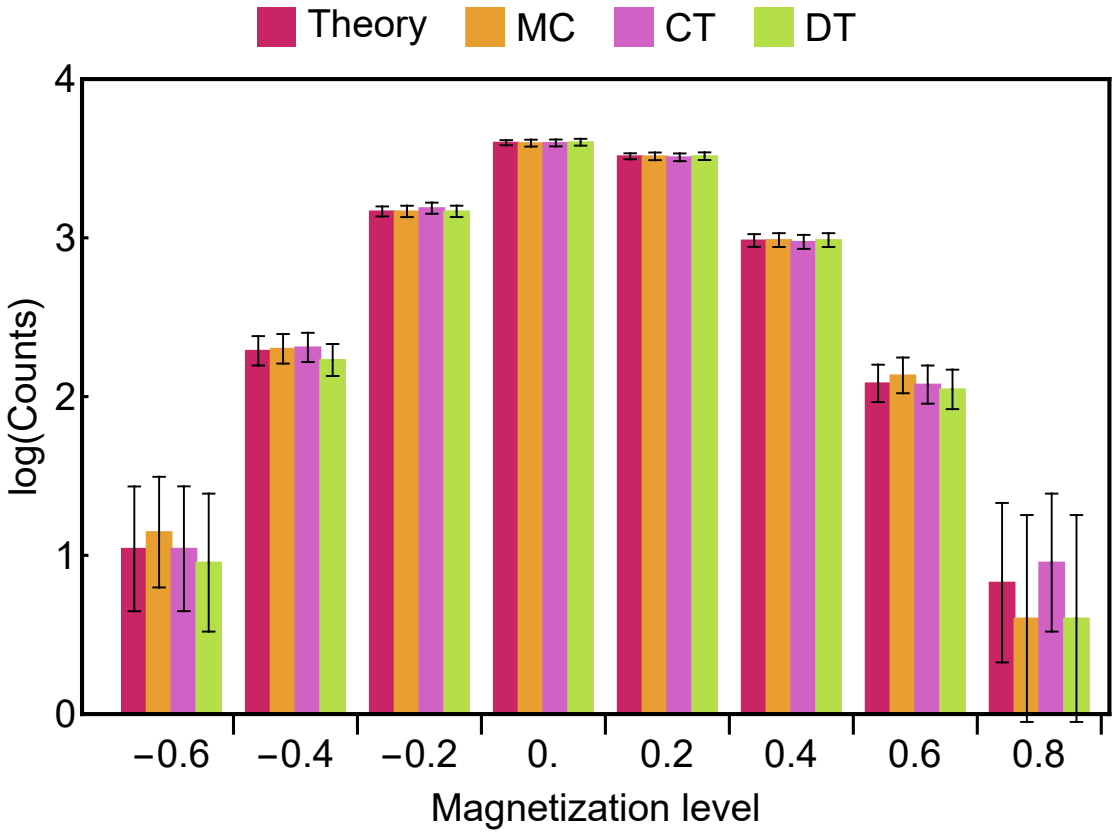

Figure E.2: *Barchart of magnetization,* $N = 10$ *spins.* Sample of 10^4 observation. In the *DT* algorithm the parameter $dt = 10^{-4}$.

	Energy pvalue	Magnetization pvalue
MMC	0.999	0.999
DT	0.999	0.999
CT	0.999	0.999

Table E.1: *Likelihood ratio test - pvalues.* Results on the pvalues of the test for energy and magnetization samples. Parameters: $k_B T = 2, h = 0.4, J = -1$ and $\alpha_{2i} = 0.1, \alpha_{2i+1} = 0.3$. *Null hypothesis* H_0 : energy and magnetization samples of the algorithms come from the same distribution of the theoretical ones.

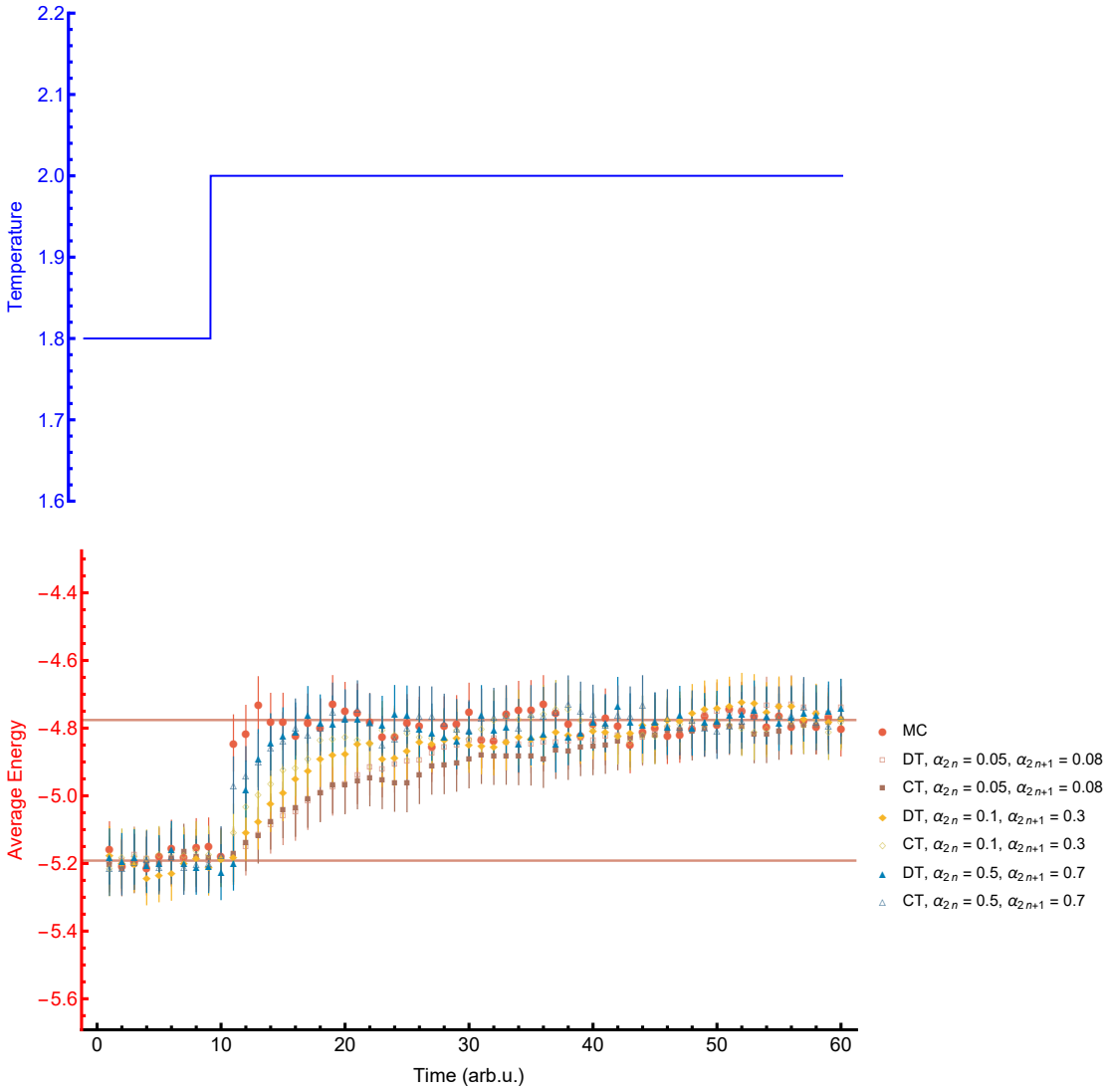

Figure E.3: *Linear response to temperature perturbation,* $N = 10$ *spins,* $h = 0.4, J = -1$

As mentioned in section 3.5, in the case of $N > 80$, obtaining theoretical probabilities is quite challenging, as well as getting the value of all the possible energy and magnetization levels. Nevertheless, the three algorithms will be performed as well, but the theoretical samples will not be generating. Thus, in order to compare the results, a *Kernel Density Estimation* (KDE) will be used to plot the probability density function of energy and magnetization. Instead, in order to get quantitatively meaning for the agreements of such samples, the χ^2 two-samples test [100] will be applied. The statistic of the test will be computed as following:

$$t_{\chi^2} = \sum_{i=1}^{k} \frac{(R_i - S_i)^2}{R_i + S_i}$$

where k is the number of different energy/magnetization levels, while R_i and S_i are the number of samples in level i for the two algorithm being compered. By construction of the sampling, the sum of R_i and S_i is the same, thus the number of degree of freedoms of the χ^2 is equal to $k-1$. One shall observe that, if there are no data neither in R_i or S_i, the degree of freedoms of the statistic will be subtracted by one.
In this case will be shown the results for an Ising chain with $N = 100$ spins, at temperature $k_B T = 2$, $h = 0, J = 1$ and action rates $\alpha_{2i} = 0.1, \alpha_{2i+1} = 0.3$.

	Energy pvalue	Magnetization pvalue
DT	0.855	0.793
CT	0.982	0.910

Table E.2: χ^2 *test - pvalues.* Results on the pvalues of the test both for energy and magnetization samples. *Null hypothesis* H_0 : energy and magnetization samples of the CT and DT algorithms come from the same distribution of the MMC one.

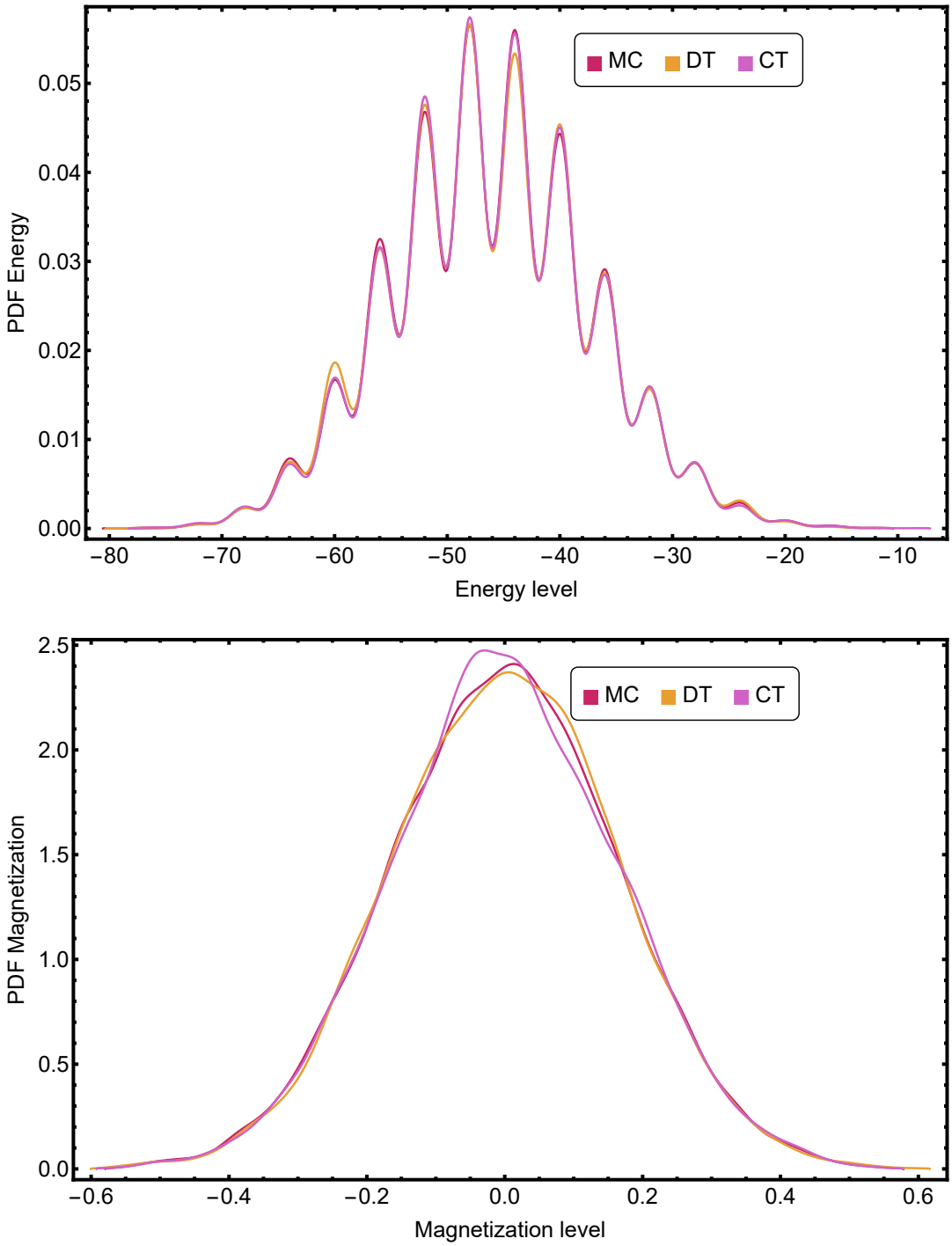

Figure E.4: *KDE of energy and magnetization,* $N = 100$ *spins.* KDE performed on samples of 10^4 observation. In the *DT* algorithm the parameter $dt = 10^{-1}$.

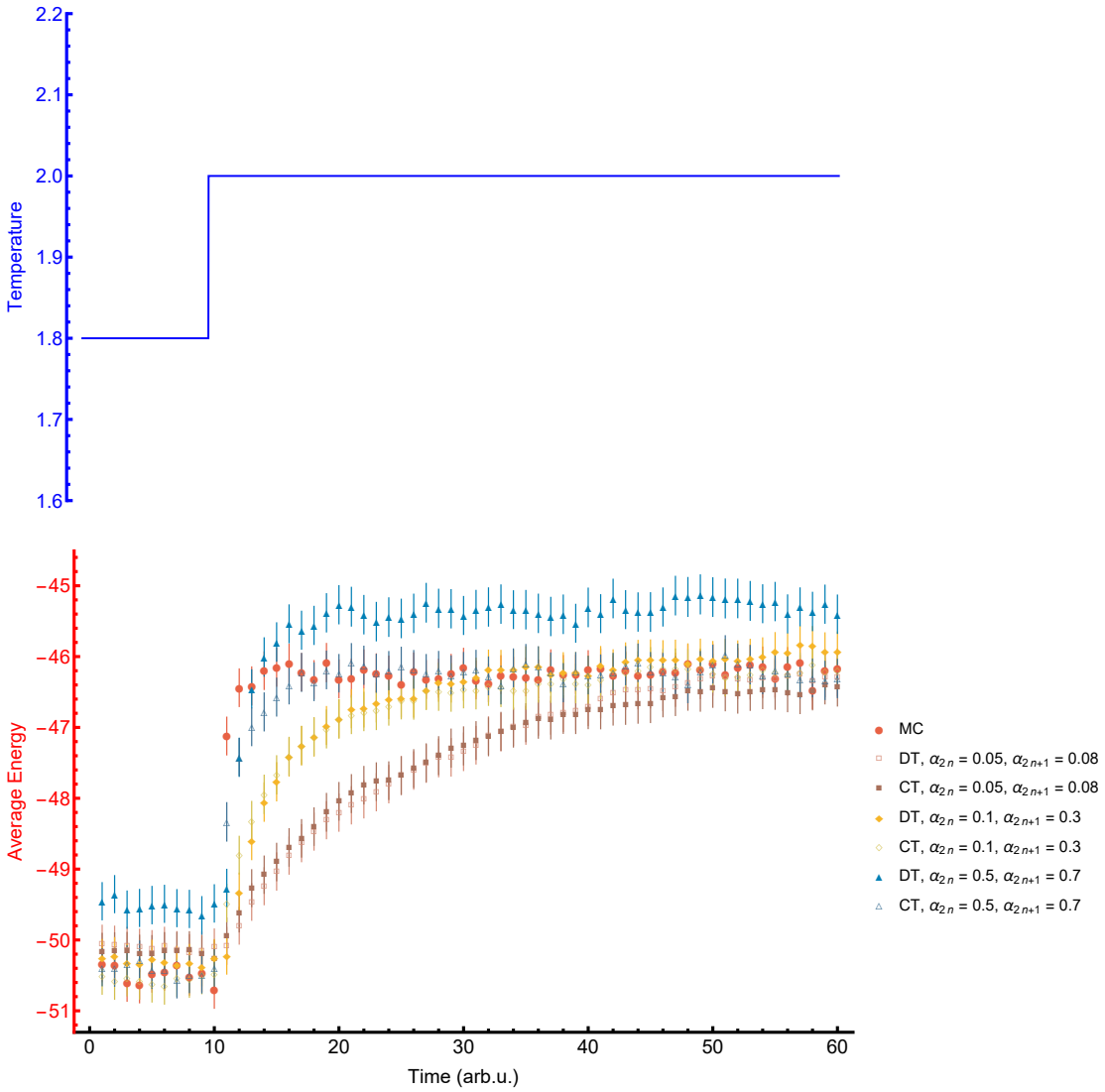

Figure E.5: *Linear response to temperature perturbation,* $N = 100$ *spins.*

Bibliography

[1] Eric Karsenti. «Self-Organization In Cell Biology: A Brief History». In: *Nature reviews. Molecular cell biology* 9 (Apr. 2008), pp. 255–62. DOI: 10.1038/nrm2357 (cit. on p. ii).

[2] Qi Chen, Junchao Shi, yi Tao, and Magdalena Zernicka-Goetz. «Tracing the origin of heterogeneity and symmetry breaking in the early mammalian embryo». In: *Nature Communications* 9 (May 2018). DOI: 10.1038/s41467-018-04155-2 (cit. on p. ii).

[3] Fran çois Graner and James A. Glazier. «Simulation of biological cell sorting using a two-dimensional extended Potts model». In: *Phys. Rev. Lett.* 69 (13 Sept. 1992), pp. 2013–2016. DOI: 10.1103/PhysRevLett.69.2013. URL: https://link.aps.org/doi/10.1103/PhysRevLett.69.2013 (cit. on pp. ii, 3, 4).

[4] James A. Glazier and Fran çois Graner. «Simulation of the differential adhesion driven rearrangement of biological cells». In: *Phys. Rev. E* 47 (3 Mar. 1993), pp. 2128–2154. DOI: 10.1103/PhysRevE.47.2128. URL: https://link.aps.org/doi/10.1103/PhysRevE.47.2128 (cit. on pp. ii, 57).

[5] M. Scianna and L. Preziosi. «Multiscale Developments of the Cellular Potts Model». In: *Multiscale Modeling & Simulation* 10.2 (2012), pp. 342–382. DOI: 10.1137/100812951. eprint: https://doi.org/10.1137/100812951. URL: https://doi.org/10.1137/100812951 (cit. on pp. ii, 11).

[6] Satoru Okuda, Yasuhiro Inoue, and Taiji Adachi. «Three-dimensional vertex model for simulating multicellular morphogenesis». In: *Biophysics and Physicobiology* 12 (Aug. 2015), pp. 13–20. DOI: 10.2142/biophysico.12.0_13 (cit. on p. ii).

[7] Benedetta Cerruti et al. «Polarity, cell division, and out-of-equilibrium dynamics control the growth of epithelial structures». In: *Journal of Cell Biology* 203.2 (Oct. 2013), pp. 359–372. ISSN: 0021-9525. DOI: 10.1083/jcb.201305044. eprint: https://rupress.org/jcb/article-pdf/203/2/359/

1362760/jcb_201305044.pdf. URL: https://doi.org/10.1083/jcb.201305044 (cit. on p. ii).

[8] Elisabeth G. Rens and Leah Edelstein-Keshet. «From energy to cellular forces in the Cellular Potts Model: An algorithmic approach». In: *PLOS Computational Biology* 15.12 (Dec. 2019), pp. 1–23. DOI: 10.1371/journal.pcbi.1007459. URL: https://doi.org/10.1371/journal.pcbi.1007459 (cit. on p. ii).

[9] Christian Maes. «Frenesy: Time-symmetric dynamical activity in nonequilibria». In: *Physics Reports* 850 (Mar. 2020), pp. 1–33. DOI: 10.1016/j.physrep.2020.01.002. URL: https://doi.org/10.1016%2Fj.physrep.2020.01.002 (cit. on pp. ii, 23).

[10] Luca Peliti and Simone Pigolotti. *Stochastic Thermodynamics: An Introduction*. Princeton University Press, July 2021. ISBN: 978-0-691-20177-1 (cit. on p. ii).

[11] Ayaka Yanagida et al. «Cell surface fluctuations regulate early embryonic lineage sorting». In: *bioRxiv* (2020). DOI: 10.1101/2020.08.16.250084. eprint: https://www.biorxiv.org/content/early/2020/08/16/2020.08.16.250084.full.pdf. URL: https://www.biorxiv.org/content/early/2020/08/16/2020.08.16.250084 (cit. on pp. ii, 58).

[12] D'Arcy Wentworth Thompson. *On Growth and Form*. Ed. by John TylerEditor Bonner. Canto. Cambridge University Press, 1992. DOI: 10.1017/CBO9781107325852 (cit. on p. 1).

[13] Thomas Iskratsch, Haguy Wolfenson, and Michael Sheetz. «Appreciating force and shape - the rise of mechanotransduction in cell biology». In: *Nature reviews. Molecular cell biology* 15 (Oct. 2014). DOI: 10.1038/nrm3903 (cit. on p. 1).

[14] Bidisha Sinha et al. «Cells Respond to Mechanical Stress by Rapid Disassembly of Caveolae». In: *Cell* 144 (Feb. 2011), pp. 402–413. DOI: 10.1016/j.cell.2010.12.031 (cit. on p. 1).

[15] W. H. Goldmann. «Mechanotransduction and Focal Adhesions». In: *Cell Biol Int* (2012). URL: Goldmann%20Cell%20Biol%20Int%202012_2.pdf (cit. on p. 1).

[16] Irena L. Ivanovska, Joe Swift, Takamasa Harada, John David Pajerowski, and Dennis E. Discher. «Physical plasticity of the nucleus and its manipulation.» In: *Methods in cell biology* 98 (2010), pp. 207–20 (cit. on p. 1).

[17] Yunfei Cai and Michael P Sheetz. «Force propagation across cells: mechanical coherence of dynamic cytoskeletons». In: *Current Opinion in Cell Biology* 21.1 (2009). Cell structure and dynamics, pp. 47–50. ISSN: 0955-0674. DOI: https://doi.org/10.1016/j.ceb.2009.01.020. URL: https://www.sciencedirect.com/science/article/pii/S0955067409000325 (cit. on p. 1).

[18] Christopher S. Chen. «Mechanotransduction – a field pulling together?» In: *Journal of Cell Science* 121.20 (Oct. 2008), pp. 3285–3292. ISSN: 0021-9533. DOI: 10.1242/jcs.023507. eprint: https://journals.biologists.com/jcs/article-pdf/121/20/3285/1504174/3285.pdf. URL: https://doi.org/10.1242/jcs.023507 (cit. on p. 1).

[19] Farshid Guilak, Daniel Cohen, Bradley Estes, Jeffrey Gimble, Wolfgang Liedtke, and Christopher Chen. «Control of Stem Cell Fate by Physical Interactions with the Extracellular Matrix». In: *Cell stem cell* 5 (Aug. 2009), pp. 17–26. DOI: 10.1016/j.stem.2009.06.016 (cit. on p. 1).

[20] Ewa Paluch and Carl-Philipp Heisenberg. «Biology and Physics of Cell Shape Changes in Development». In: *Current biology : CB* 19 (Sept. 2009), R790–9. DOI: 10.1016/j.cub.2009.07.029 (cit. on p. 1).

[21] Xavier Trepat, Michael R. Wasserman, Thomas E. Angelini, Emil Millet, David A Weitz, James P. Butler, and Jeffrey J. Fredberg. «Physical forces during collective cell migration». In: *Nature Physics* 5 (2009), pp. 426–430. URL: https://www.nature.com/articles/nphys1269 (cit. on p. 1).

[22] Gang Cheng, Janet Tse, Rakesh K. Jain, and Lance L. Munn. «Micro-Environmental Mechanical Stress Controls Tumor Spheroid Size and Morphology by Suppressing Proliferation and Inducing Apoptosis in Cancer Cells». In: *PLOS ONE* 4.2 (Feb. 2009), pp. 1–11. DOI: 10.1371/journal.pone.0004632. URL: https://doi.org/10.1371/journal.pone.0004632 (cit. on p. 1).

[23] Shalini Menon and Karen A. Beningo. «Cancer Cell Invasion Is Enhanced by Applied Mechanical Stimulation». In: *PLOS ONE* 6.2 (Feb. 2011), pp. 1–11. DOI: 10.1371/journal.pone.0017277. URL: https://doi.org/10.1371/journal.pone.0017277 (cit. on p. 1).

[24] Rodney J. Baxter. *Exactly solved models in statistical mechanics*. Canto. Academic Press, Inc., 1982 (cit. on p. 2).

[25] Sara Checa and Patrick Prendergast. «A Mechanobiological Model for Tissue Differentiation that Includes Angiogenesis: A Lattice-Based Modeling Approach». In: *Annals of biomedical engineering* 37 (Dec. 2008), pp. 129–45. DOI: 10.1007/s10439-008-9594-9 (cit. on p. 2).

[26] Hanifeh Khayyeri, Sara Checa, Magnus Tagil, and Patrick Prendergast. «Corroboration of Mechanobiological Simulations of Tissue Differentiation in an In Vivo Bone Chamber Using a Lattice-Modeling Approach». In: *Journal of orthopaedic research : official publication of the Orthopaedic Research Society* 27 (Dec. 2009), pp. 1659–66. DOI: 10.1002/jor.20926 (cit. on p. 2).

[27] P. Van Liedekerke, M. M. Palm, N. Jagiella, and D. Drasdo. «Simulating tissue mechanics with agent-based models: concepts, perspectives and some novel results». In: *Computational Particle Mechanics* 2.4 (Dec. 2015), pp. 401–444. DOI: 10.1007/s40571-015-0082-3 (cit. on p. 2).

[28] Philipp J. Albert and Ulrich S. Schwarz. «Dynamics of Cell Shape and Forces on Micropatterned Substrates Predicted by a Cellular Potts Model». In: *Biophysical Journal* 106.11 (2014), pp. 2340–2352. ISSN: 0006-3495. DOI: https://doi.org/10.1016/j.bpj.2014.04.036. URL: https://www.sciencedirect.com/science/article/pii/S0006349514004548 (cit. on p. 2).

[29] Philipp J. Albert and Ulrich S. Schwarz. «Dynamics of Cell Ensembles on Adhesive Micropatterns: Bridging the Gap between Single Cell Spreading and Collective Cell Migration». In: *PLOS Computational Biology* 12.4 (Apr. 2016), pp. 1–34. DOI: 10.1371/journal.pcbi.1004863. URL: https://doi.org/10.1371/journal.pcbi.1004863 (cit. on p. 2).

[30] Alexander G. Fletcher, Miriam Osterfield, Ruth E. Baker, and Stanislav Y. Shvartsman. «Vertex Models of Epithelial Morphogenesis». In: *Biophysical Journal* 106.11 (2014), pp. 2291–2304. ISSN: 0006-3495. DOI: https://doi.org/10.1016/j.bpj.2013.11.4498. URL: https://www.sciencedirect.com/science/article/pii/S0006349513057949 (cit. on p. 2).

[31] Silvanus Alt, Poulami Ganguly, and Guillaume Salbreux. «Vertex models: from cell mechanics to tissue morphogenesis». In: *Philosophical Transactions of the Royal Society B: Biological Sciences* 372.1720 (2017), p. 20150520. DOI: 10.1098/rstb.2015.0520. eprint: https://royalsocietypublishing.org/doi/pdf/10.1098/rstb.2015.0520. URL: https://royalsocietypublishing.org/doi/abs/10.1098/rstb.2015.0520 (cit. on p. 2).

[32] Reza Farhadifar, Jens-Christian Röper, Benoit Aigouy, Suzanne Eaton, and Frank Jülicher. «The influence of cell mechanics, cell-cell interactions, and proliferation on epithelial packing». In: *Current biology : CB* 17.24 (Dec. 2007), pp. 2095–2104. ISSN: 0960-9822. DOI: 10.1016/j.cub.2007.11.049. URL: https://doi.org/10.1016/j.cub.2007.11.049 (cit. on p. 2).

[33] Jos Käfer, Takashi Hayashi, Athanasius F. M. Marée, Richard W. Carthew, and François Graner. «Cell adhesion and cortex contractility determine cell patterning in the Drosophilaretina». In: *Proceedings of the National Academy of Sciences* 104.47 (2007), pp. 18549–18554. DOI: 10.1073/pnas.0704235104. eprint: https://www.pnas.org/doi/pdf/10.1073/pnas.0704235104. URL: https://www.pnas.org/doi/abs/10.1073/pnas.0704235104 (cit. on p. 3).

[34] Ismael Fortuna, Gilberto L. Thomas, Rita M. C. de Almeida, and Fran çois Graner. «Growth Laws and Self-Similar Growth Regimes of Coarsening Two-Dimensional Foams: Transition from Dry to Wet Limits». In: *Phys. Rev. Lett.* 108 (24 June 2012), p. 248301. DOI: 10.1103/PhysRevLett.108.248301. URL: https://link.aps.org/doi/10.1103/PhysRevLett.108.248301 (cit. on p. 3).

[35] Andrew C. Oates, Nicole Gorfinkiel, Marcos Gonzalez-Gaitan, and C. P. Heisenberg. «Quantitative approaches in developmental biology». In: *Nature Reviews Genetics* 10 (2009), pp. 517–530 (cit. on p. 3).

[36] Florian Thüroff, Andriy Goychuk, Matthias Reiter, and Erwin Frey. «Bridging the gap between single-cell migration and collective dynamics». In: *eLife* 8 (Dec. 2019). Ed. by Naama Barkai, Pierre Sens, and Igor S Aranson, e46842. ISSN: 2050-084X. DOI: 10.7554/eLife.46842. URL: https://doi.org/10.7554/eLife.46842 (cit. on p. 3).

[37] A Szabó, K Varga, T Garay, B Hegedűs, and A Czirók. «Invasion from a cell aggregate—the roles of active cell motion and mechanical equilibrium». In: *Physical Biology* 9.1 (Feb. 2012), p. 016010. DOI: 10.1088/1478-3975/9/1/016010. URL: https://doi.org/10.1088/1478-3975/9/1/016010 (cit. on p. 3).

[38] Alexandre J. Kabla. «Collective cell migration: leadership, invasion and segregation». In: *Journal of The Royal Society Interface* 9.77 (2012), pp. 3268–3278. DOI: 10.1098/rsif.2012.0448. eprint: https://royalsocietypublishing.org/doi/pdf/10.1098/rsif.2012.0448. URL: https://royalsocietypublishing.org/doi/abs/10.1098/rsif.2012.0448 (cit. on p. 3).

[39] Kevin Doxzen, Sri Ram Krishna Vedula, Man Chun Leong, Hiroaki Hirata, Nir S. Gov, Alexandre J. Kabla, Benoit Ladoux, and Chwee Teck Lim. «Guidance of collective cell migration by substrate geometry». In: *Integrative Biology* 5.8 (June 2013), pp. 1026–1035. ISSN: 1757-9708. DOI: 10.1039/c3ib40054a. eprint: https://academic.oup.com/ib/article-pdf/5/8/1026/27302155/c3ib40054a.pdf. URL: https://doi.org/10.1039/c3ib40054a (cit. on p. 3).

[40] Julio M. Belmonte, Sherry G. Clendenon, Guilherme M. Oliveira, Maciej H. Swat, Evan V. Greene, Srividhya Jeyaraman, James A. Glazier, and Robert L. Bacallao. «Virtual-tissue computer simulations define the roles of cell adhesion and proliferation in the onset of kidney cystic disease». In: *Molecular Biology of the Cell* 27.22 (2016). PMID: 27193300, pp. 3673–3685. DOI: 10.1091/mbc.E16-01-0059. eprint: https://doi.org/10.1091/mbc.E16-01-0059. URL: https://doi.org/10.1091/mbc.E16-01-0059 (cit. on p. 3).

[41] STEPHEN TURNER and JONATHAN A. SHERRATT. «Intercellular Adhesion and Cancer Invasion: A Discrete Simulation Using the Extended Potts Model». In: *Journal of Theoretical Biology* 216.1 (2002), pp. 85–100. ISSN: 0022-5193. DOI: https://doi.org/10.1006/jtbi.2001.2522. URL: https://www.sciencedirect.com/science/article/pii/S0022519301925226 (cit. on p. 3).

[42] Brenda M. Rubenstein and Laura J. Kaufman. «The role of extracellular matrix in glioma invasion: a cellular Potts model approach.» In: *Biophysical journal* 95 12 (2008), pp. 5661–80 (cit. on p. 3).

[43] Abbas Shirinifard, J. Scott Gens, Benjamin L. Zaitlen, Nikodem J. Popławski, Maciej Swat, and James A. Glazier. «3D Multi-Cell Simulation of Tumor Growth and Angiogenesis». In: *PLOS ONE* 4.10 (Oct. 2009), pp. 1–11. DOI: 10.1371/journal.pone.0007190. URL: https://doi.org/10.1371/journal.pone.0007190 (cit. on p. 3).

[44] Eline Boghaert, Derek C. Radisky, and Celeste M. Nelson. «Lattice-Based Model of Ductal Carcinoma In Situ Suggests Rules for Breast Cancer Progression to an Invasive State». In: *PLOS Computational Biology* 10.12 (Dec. 2014), pp. 1–14. DOI: 10.1371/journal.pcbi.1003997. URL: https://doi.org/10.1371/journal.pcbi.1003997 (cit. on p. 3).

[45] András Szabó and Roeland M. Merks. «Cellular Potts Modeling of Tumor Growth, Tumor Invasion, and Tumor Evolution». In: *Frontiers in Oncology* 3 (2013). ISSN: 2234-943X. DOI: 10.3389/fonc.2013.00087. URL: https://www.frontiersin.org/articles/10.3389/fonc.2013.00087 (cit. on p. 3).

[46] Jonathan F. Li and John Lowengrub. «The effects of cell compressibility, motility and contact inhibition on the growth of tumor cell clusters using the Cellular Potts Model». In: *Journal of Theoretical Biology* 343 (2014), pp. 79–91. ISSN: 0022-5193. DOI: https://doi.org/10.1016/j.jtbi.2013.10.008. URL: https://www.sciencedirect.com/science/article/pii/S0022519313005006 (cit. on p. 3).

[47] Philipp J. Albert and Ulrich S. Schwarz. «Modeling cell shape and dynamics on micropatterns». In: *Cell Adhesion & Migration* 10.5 (2016). PMID: 26838278, pp. 516–528. DOI: 10.1080/19336918.2016.1148864. eprint: https://doi.org/10.1080/19336918.2016.1148864. URL: https://doi.org/10.1080/19336918.2016.1148864 (cit. on p. 3).

[48] F. Y. Wu. «The Potts model». In: *Rev. Mod. Phys.* 54 (1 Jan. 1982), pp. 235–268. DOI: 10.1103/RevModPhys.54.235. URL: https://link.aps.org/doi/10.1103/RevModPhys.54.235 (cit. on p. 3).

[49] Malcolm S. Steinberg. «Reconstruction of Tissues by Dissociated Cells». In: *Science* 141.3579 (1963), pp. 401–408. DOI: 10.1126/science.141.3579.401. eprint: https://www.science.org/doi/pdf/10.1126/science.141.3579.401. URL: https://www.science.org/doi/abs/10.1126/science.141.3579.401 (cit. on pp. 4, 57).

[50] Leoncini Emanuele. «Applied mathematics to biology and medicine». PhD thesis. Nowhere: INRIA, 2010 (cit. on p. 6).

[51] Anja Voss-Böhme. «Multi-Scale Modeling in Morphogenesis: A Critical Analysis of the Cellular Potts Model». In: *PLOS ONE* 7.9 (Sept. 2012), pp. 1–14. DOI: 10.1371/journal.pone.0042852. URL: https://doi.org/10.1371/journal.pone.0042852 (cit. on p. 7).

[52] José C. M. Mombach and James A. Glazier. «Single Cell Motion in Aggregates of Embryonic Cells». In: *Phys. Rev. Lett.* 76 (16 Apr. 1996), pp. 3032–3035. DOI: 10.1103/PhysRevLett.76.3032. URL: https://link.aps.org/doi/10.1103/PhysRevLett.76.3032 (cit. on pp. 7, 10).

[53] Anja Voss-Böhme. «Multi-Scale Modeling in Morphogenesis: A Critical Analysis of the Cellular Potts Model». In: *PLOS ONE* 7.9 (Sept. 2012), pp. 1–14. DOI: 10.1371/journal.pone.0042852. URL: https://doi.org/10.1371/journal.pone.0042852 (cit. on pp. 7, 8).

[54] Ariel Balter, Roeland Merks, NJ Popławski, Maciej Swat, James Glazier, KA Rejniak, ARA Anderson, and MAJ Chaplain. «The Glazier–Graner–Hogeweg Model: Extensions, future directions, and opportunities for further study». In: *Single-Cell-Based Models in Biology and Medicine* (Jan. 2007), pp. 151–167 (cit. on pp. 8, 14).

[55] Marc Durand and Etienne Guesnet. «An efficient Cellular Potts Model algorithm that forbids cell fragmentation». In: *Computer Physics Communications* 208 (2016), pp. 54–63. ISSN: 0010-4655. DOI: https://doi.org/10.1016/j.cpc.2016.07.030. URL: https://www.sciencedirect.com/science/article/pii/S0010465516302284 (cit. on pp. 9, 12, 62, 63).

[56] L. Wolpert, J. C. Smith, Dirk Dormann, Bakhtier Vasiev, and Cornelis J. Weijer. «The control of chemotactic cell movement during Dictyostelium morphogenesis». In: *Philosophical Transactions of the Royal Society of London. Series B: Biological Sciences* 355.1399 (2000), pp. 983–991. DOI: 10.1098/rstb.2000.0634. eprint: https://royalsocietypublishing.org/doi/pdf/10.1098/rstb.2000.0634. URL: https://royalsocietypublishing.org/doi/abs/10.1098/rstb.2000.0634 (cit. on p. 11).

[57] Nicholas J. Savill and Paulien Hogeweg. «Modelling Morphogenesis: From Single Cells to Crawling Slugs». In: *Journal of Theoretical Biology* 184.3 (1997), pp. 229–235. ISSN: 0022-5193. DOI: https://doi.org/10.1006/jtbi.1996.0237. URL: https://www.sciencedirect.com/science/article/pii/S0022519396902374 (cit. on p. 11).

[58] R Chaturvedi et al. «On multiscale approaches to three-dimensional modelling of morphogenesis». In: *Journal of The Royal Society Interface* 2.3 (2005), pp. 237–253. DOI: 10.1098/rsif.2005.0033. eprint: https://royalsocietypublishing.org/doi/pdf/10.1098/rsif.2005.0033. URL: https://royalsocietypublishing.org/doi/abs/10.1098/rsif.2005.0033 (cit. on p. 11).

[59] Zhiliang Xu, Nan Chen, Shawn C. Shadden, Jerrold E. Marsden, Malgorzata M. Kamocka, Elliot D. Rosen, and Mark Alber. «Study of blood flow impact on growth of thrombi using a multiscale model». In: *Soft Matter* 5 (4 2009), pp. 769–779. DOI: 10.1039/B812429A. URL: http://dx.doi.org/10.1039/B812429A (cit. on p. 11).

[60] James M. Osborne. «Multiscale Model of Colorectal Cancer Using the Cellular Potts Framework». In: *Cancer Informatics* 14 (2015), pp. 83–93 (cit. on p. 11).

[61] Marco Scianna, Luca Munaron, and Luigi Preziosi. «A multiscale hybrid approach for vasculogenesis and related potential blocking therapies». In: *Progress in Biophysics and Molecular Biology* 106.2 (2011). Systems Biology and Cancer, pp. 450–462. ISSN: 0079-6107. DOI: https://doi.org/10.1016/j.pbiomolbio.2011.01.004. URL: https://www.sciencedirect.com/science/article/pii/S0079610711000174 (cit. on p. 11).

[62] Nan Chen, James A. Glazier, Jesús A. Izaguirre, and Mark S. Alber. «A parallel implementation of the Cellular Potts Model for simulation of cell-based morphogenesis». In: *Computer Physics Communications* 176.11 (2007), pp. 670–681. ISSN: 0010-4655. DOI: https://doi.org/10.1016/j.cpc.2007.03.007. URL: https://www.sciencedirect.com/science/article/pii/S0010465507002044 (cit. on p. 12).

[63] José Juan Tapia and Roshan M. D'Souza. «Parallelizing the Cellular Potts Model on graphics processing units». In: *Computer Physics Communications* 182.4 (2011), pp. 857–865. ISSN: 0010-4655. DOI: https://doi.org/10.1016/j.cpc.2010.12.011. URL: https://www.sciencedirect.com/science/article/pii/S001046551000490X (cit. on p. 12).

[64] Antonio J. Tomeu and Alberto G. Salguero. «A Lock Free Approach To Parallelize The Cellular Potts Model: Application To Ductal Carcinoma In Situ». In: *Journal of Integrative Bioinformatics* 17.1 (2020), p. 20190070. DOI: doi:10.1515/jib-2019-0070. URL: https://doi.org/10.1515/jib-2019-0070 (cit. on p. 12).

[65] Kejing He, Yi Jiang, and Shoubin Dong. «A Hybrid Parallel Framework for the Cellular Potts Model Simulations». In: (2009), pp. 624–631. DOI: 10.1109/ICPADS.2009.131 (cit. on p. 12).

[66] Fernando Cercato, José Carlos Mombach, and Gerson Cavalheiro. «High Performance Simulations of the Cellular Potts Model». In: *20th International Symposium on High-Performance Computing in an Advanced Collaborative Environment, 2006. HPCS 2006* (Jan. 2006), p. 28. DOI: 10.1109/HPCS.2006.28 (cit. on p. 12).

[67] Marco Berghoff, Jakob Rosenbauer, Felix Hoffmann, and Alexander Schug. «Cells in Silico – introducing a high-performance framework for large-scale tissue modeling». In: *BMC Bioinformatics* 21 (Oct. 2020), p. 436. DOI: 10.1186/s12859-020-03728-7 (cit. on p. 12).

[68] Daniel A Fletcher and Julie A Theriot. «An introduction to cell motility for the physical scientist». In: *Physical Biology* 1.1 (Feb. 2004), T1–T10. DOI: 10.1088/1478-3967/1/1/t01. URL: https://doi.org/10.1088/1478-3967/1/1/t01 (cit. on p. 14).

[69] Trenis D. Palmer, William J. Ashby, John D. Lewis, and Andries Zijlstra. «Targeting tumor cell motility to prevent metastasis». In: *Advanced Drug Delivery Reviews* 63.8 (2011). Target Cell Movement in Tumor and Cardiovascular Diseases, pp. 568–581. ISSN: 0169-409X. DOI: https://doi.org/10.1016/j.addr.2011.04.008. URL: https://www.sciencedirect.com/science/article/pii/S0169409X11001335 (cit. on p. 14).

[70] Gary Meyer and Eva L. Feldman. «Signaling mechanisms that regulate actin-based motility processes in the nervous system». In: *Journal of Neurochemistry* 83.3 (2002), pp. 490–503. DOI: https://doi.org/10.1046/j.1471-4159.2002.01185.x. eprint: https://onlinelibrary.wiley.com/doi/pdf/10.1046/j.1471-4159.2002.01185.x. URL: https://onlinelibrary.wiley.com/doi/abs/10.1046/j.1471-4159.2002.01185.x (cit. on p. 14).

[71] H. A. Kramers and G. H. Wannier. «Statistics of the Two-Dimensional Ferromagnet. Part I». In: *Phys. Rev.* 60 (3 Aug. 1941), pp. 252–262. DOI: 10.1103/PhysRev.60.252. URL: https://link.aps.org/doi/10.1103/PhysRev.60.252 (cit. on p. 17).

[72] H. A. Kramers and G. H. Wannier. «Statistics of the Two-Dimensional Ferromagnet. Part II». In: *Phys. Rev.* 60 (3 Aug. 1941), pp. 263–276. DOI: 10.1103/PhysRev.60.263. URL: https://link.aps.org/doi/10.1103/PhysRev.60.263 (cit. on p. 17).

[73] Lars Onsager. «Crystal Statistics. I. A Two-Dimensional Model with an Order-Disorder Transition». In: *Phys. Rev.* 65 (3-4 Feb. 1944), pp. 117–149. DOI: 10.1103/PhysRev.65.117. URL: https://link.aps.org/doi/10.1103/PhysRev.65.117 (cit. on p. 17).

[74] R. Peierls. «On Ising's model of ferromagnetism». In: *Mathematical Proceedings of the Cambridge Philosophical Society* 32.3 (1936), pp. 477–481. DOI: 10.1017/S0305004100019174 (cit. on p. 17).

[75] P. G. J. van Dongen and D. Vollhardt. «Exact mean-field Hamiltonian for fermionic lattice models in high dimensions». In: *Phys. Rev. Lett.* 65 (13 Sept. 1990), pp. 1663–1666. DOI: 10.1103/PhysRevLett.65.1663. URL: https://link.aps.org/doi/10.1103/PhysRevLett.65.1663 (cit. on p. 17).

[76] Shinichiro Akiyama, Yoshinobu Kuramashi, Takumi Yamashita, and Yusuke Yoshimura. «Phase transition of four-dimensional Ising model with higher-order tensor renormalization group». In: *Phys. Rev. D* 100 (5 Sept. 2019), p. 054510. DOI: 10.1103/PhysRevD.100.054510. URL: https://link.aps.org/doi/10.1103/PhysRevD.100.054510 (cit. on p. 17).

[77] Marco Zamparo, Donatella Valdembri, Guido Serini, Igor V. Kolokolov, Vladimir V. Lebedev, Luca Dall'Asta, and Andrea Gamba. «Optimality in Self-Organized Molecular Sorting». In: *Phys. Rev. Lett.* 126 (8 Feb. 2021), p. 088101. DOI: 10.1103/PhysRevLett.126.088101. URL: https://link.aps.org/doi/10.1103/PhysRevLett.126.088101 (cit. on p. 18).

[78] Nicoletta I. Petridou, Bernat Corominas-Murtra, Carl-Philipp Heisenberg, and Edouard Hannezo. «Rigidity percolation uncovers a structural basis for embryonic tissue phase transitions». In: *Cell* 184.7 (2021), 1914–1928.e19. ISSN: 0092-8674. DOI: https://doi.org/10.1016/j.cell.2021.02.017. URL: https://www.sciencedirect.com/science/article/pii/S0092867421001677 (cit. on p. 18).

[79] Edouard Hannezo and Carl-Philipp Heisenberg. «Rigidity transitions in development and disease». In: *Trends in Cell Biology* 32.5 (2022), pp. 433–444. ISSN: 0962-8924. DOI: https://doi.org/10.1016/j.tcb.2021.12.006. URL: https://www.sciencedirect.com/science/article/pii/S0962892421002658 (cit. on p. 18).

[80] Avinash B. Patel et al. «A Liquid-to-Solid Phase Transition of the ALS Protein FUS Accelerated by Disease Mutation». In: *Cell* 162 (2015), pp. 1066–1077 (cit. on p. 18).

[81] Roman Belousov, Ali Hassanali, and É dgar Roldán. «Statistical physics of inhomogeneous transport: Unification of diffusion laws and inference from first-passage statistics». In: *Physical Review E* 106.1 (July 2022). DOI: 10.1103/physreve.106.014103. URL: https://doi.org/10.1103 (cit. on pp. 20, 57).

[82] Xiaona Fang, Karsten Kruse, Ting Lu, and Jin Wang. «Nonequilibrium physics in biology». In: *Rev. Mod. Phys.* 91 (4 Dec. 2019), p. 045004. DOI: 10.1103/RevModPhys.91.045004. URL: https://link.aps.org/doi/10.1103/RevModPhys.91.045004 (cit. on p. 22).

[83] Xiaona Fang and Jin Wang. «Nonequilibrium Thermodynamics in Cell Biology: Extending Equilibrium Formalism to Cover Living Systems». In: *Annual Review of Biophysics* 49.1 (). DOI: 10.1146/annurev-biophys-121219-081656. URL: https://par.nsf.gov/biblio/10170794 (cit. on p. 22).

[84] S. Dal Conte et al. «Ultrafast valley relaxation dynamics in monolayer MoS_2 probed by nonequilibrium optical techniques». In: *Phys. Rev. B* 92 (23 Dec. 2015), p. 235425. DOI: 10.1103/PhysRevB.92.235425. URL: https://link.aps.org/doi/10.1103/PhysRevB.92.235425 (cit. on p. 22).

[85] Y. Song, B. D. Peng, G. Z. Song, Z. Q. Yue, B. K. Li, J. M. Ma, L. Sheng, B. J. Duan, and H. X. Wang. «Investigating non-equilibrium carrier lifetimes in nitrogen-doped and boron-doped single crystal HPHT diamonds with an optical method». In: *Applied Physics Letters* 112.2 (2018), p. 022103. DOI: 10.1063/1.5019587. eprint: https://doi.org/10.1063/1.5019587. URL: https://doi.org/10.1063/1.5019587 (cit. on p. 22).

[86] Joyeux D Coppalle A. «An optical technique for measuring mean and fluctuating values of particle concentrations in round jets». In: (Feb. 1994). DOI: 10.1007/BF00206549. URL: https://doi.org/10.1007/BF00206549 (cit. on p. 22).

[87] Aymeric Delteil, Wei-bo Gao, Parisa Fallahi, Javier Miguel-Sanchez, and Atac Imamo ğlu. «Observation of Quantum Jumps of a Single Quantum Dot Spin Using Submicrosecond Single-Shot Optical Readout». In: *Phys. Rev. Lett.* 112 (11 Mar. 2014), p. 116802. DOI: 10.1103/PhysRevLett.112.116802. URL: https://link.aps.org/doi/10.1103/PhysRevLett.112.116802 (cit. on p. 22).

[88] Herbert B Callen. *Thermodynamics and an introduction to thermostatistics; 2nd ed.* New York, NY: Wiley, 1985. URL: https://cds.cern.ch/record/450289 (cit. on p. 37).

[89] Lamberto Rondoni. «Introduction to Nonequilibrium Statistical Physics and Its Foundations». In: Jan. 2021, pp. 1–82. ISBN: 978-981-15-9296-6. DOI: 10.1007/978-981-15-9297-3_1 (cit. on p. 38).

[90] Paolo Adamo, Roman Belousov, and Lamberto Rondoni. «Fluctuation-Dissipation and Fluctuation Relations: From Equilibrium to Nonequilibrium and Back». In: *Lecture Notes in Physics* 885 (Jan. 2014), pp. 93–133. DOI: 10.1007/978-3-642-54251-0__4 (cit. on p. 38).

[91] Nicholas Metropolis, Arianna W. Rosenbluth, Marshall N. Rosenbluth, Augusta H. Teller, and Edward Teller. «Equation of State Calculations by Fast Computing Machines». In: *The Journal of Chemical Physics* 21.6 (1953), pp. 1087–1092. DOI: 10.1063/1.1699114. eprint: https://doi.org/10.1063/1.1699114. URL: https://doi.org/10.1063/1.1699114 (cit. on p. 41).

[92] Daniel T. Gillespie. «Stochastic Simulation of Chemical Kinetics». In: *Annual Review of Physical Chemistry* 58.1 (2007). PMID: 17037977, pp. 35–55. DOI: 10.1146/annurev.physchem.58.032806.104637. eprint: https://doi.org/10.1146/annurev.physchem.58.032806.104637. URL: https://doi.org/10.1146/annurev.physchem.58.032806.104637 (cit. on p. 46).

[93] D. N. Lawley. «A General Method for Approximating to the Distribution of Likelihood Ratio Criteria». In: *Biometrika* 43.3/4 (1956), pp. 295–303. ISSN: 00063444. URL: http://www.jstor.org/stable/2332908 (visited on 09/08/2022) (cit. on p. 53).

[94] D. A. Williams. «Improved Likelihood Ratio Tests for Complete Contingency Tables». In: *Biometrika* 63.1 (1976), pp. 33–37. ISSN: 00063444. URL: http://www.jstor.org/stable/2335081 (visited on 09/08/2022) (cit. on pp. 53, 76).

[95] James Glazier, Ariel Balter, and Nikodem Popławski. «Magnetization to Morphogenesis: A Brief History of the Glazier-Graner-Hogeweg Model». In: Jan. 2007, pp. 79–106. ISBN: 978-3-7643-8101-1. DOI: 10.1007/978-3-7643-8123-3_4 (cit. on p. 57).

[96] C Monzel and K Sengupta. «Measuring shape fluctuations in biological membranes». In: *Journal of Physics D: Applied Physics* 49.24 (May 2016), p. 243002. DOI: 10.1088/0022-3727/49/24/243002. URL: https://doi.org/10.1088/0022-3727/49/24/243002 (cit. on p. 57).

[97] Kinneret Keren. «Cell motility: the integrating role of the plasma membrane». English. In: *European Biophysics Journal* 40.9 (2011). Winner of 2011 EBSA young investigator medal., pp. 1013–1027. DOI: 10.1007/s00249-011-0741-0 (cit. on p. 57).

[98] Dagmar Iber, Simon Tanaka, Patrick Fried, Philipp Germann, and Denis Menshykau. «Simulating Tissue Morphogenesis and Signaling». In: vol. 1189. Oct. 2014. ISBN: 1493911635. DOI: 10.1007/978-1-4939-1164-6_21 (cit. on p. 61).

[99] Ángel Rey. «A multi-secret sharing scheme for 3D solid objects». In: *Expert Systems with Applications* 42 (Oct. 2014). DOI: 10.1016/j.eswa.2014.10.035 (cit. on p. 62).

[100] William H. Press, Saul A. Teukolsky, William T. Vetterling, and Brian P. Flannery. *Numerical Recipes 3rd Edition: The Art of Scientific Computing*. 3rd ed. Cambridge University Press, 2007. ISBN: 0521880688. URL: http://www.amazon.com/Numerical-Recipes-3rd-Scientific-Computing/dp/0521880688/ref=sr_1_1?ie=UTF8&s=books&qid=1280322496&sr=8-1 (cit. on p. 80).